



TURKGEO

TURKISH JOURNAL OF GEOSCIENCES

e-ISSN 2717-7696

OPEN ACCESS



dergipark.org.tr/tr/pub/turkgeo
turkgeosciences@gmail.com

TURKGEO, December/2021
Volume: 2 - Issue: 2

About The Journal

Turkish Journal of Geosciences is a multi-disciplinary open-access journal aimed to publish peer-reviewed original research and review articles covering all aspects of geosciences. The journal includes a wide scope of information on scientific and technical advances in all areas related to geosciences and indexed in international indices and databases that publish studies on earth sciences.

Aim and Scope

TURKGEO Journal has the following aim and scopes;

Aim of TURKGEO

- TURKGEO aims to promote the theory and practice from the integration of instruments, methodologies, and technologies and their respective uses in the environmental and other natural sciences.
- TURKGEO aims to provide a widely accessible discussion environment that will strengthen and accelerate the exchange of knowledge and experience among scientists, researchers, engineers and other implementers involved in the subject directly or indirectly.

Scope of TURKGEO

- Earth and Environmental Sciences Applications
- Geographic Information Systems
- Remote Sensing
- Photogrammetry
- Geostatistics
- GPS/GNSS
- RADAR/SAR/LIDAR and Laser Scanning
- Spatial Data Infrastructure
- Spatial Decision Support Systems
- Climate Change
- Geology
- Geomorphology
- Hydrogeology
- Geophysics
- Hydrology and Water Resources
- Oceanography

Publishing Frequency

2 issues per year (June-December)

ISSN

2717-7696

WEB

<https://dergipark.org.tr/tr/pub/turkgeo>

Contact

sefa.bilgilioglu@gmail.com / osmanorhan44@gmail.com

EDITOR

Assist. Prof. Dr. Süleyman Sefa BİLGİLİOĞLU

Aksaray University, Faculty of Engineering, Department of Geomatics Engineering /Aksaray/Turkey

ASSOCIATE EDITOR

Assist. Prof. Dr. Osman ORHAN

Mersin University, Institute of Science, Remote Sensing and GIS /Mersin /Turkey

Dr. Cemil GEZGİN

Aksaray University, Faculty of Engineering, Department of Geomatics Engineering /Aksaray/Turkey

SECTION EDITORS

Assoc. Prof. Dr. Emine BAŞTÜRK, Aksaray University

Assist. Prof. Dr. Bahattin GÜLLÜ, Aksaray University

Dr. Mehmet MESUTOĞLU, Konya Technical University

Dr. Mustafa Haydar TERZİ, Aksaray University

EDITORIAL BOARD

Prof. Dr. Abdurrahman EYMEN, Erciyes University

Prof. Dr. Alper BABA, İzmir Institute of Technology

Prof. Dr. C. Serdar BAYARI, Hacettepe University

Prof. Dr. Fatih İŞCAN, Konya Technical University

Prof. Dr. Fatih POYRAZ, Cumhuriyet University

Prof. Dr. Fevzi KARSLI, Karadeniz Technical University

Prof. Dr. Füsün BALIK ŞANLI, Yıldız Technical University

Prof. Dr. Hakan KARABÖRK, Konya Technical University

Prof. Dr. Hediye ERDOĞAN, Aksaray University

Prof. Dr. Himmet KARAMAN, Istanbul Technical University

Prof. Dr. İbrahim TIRYAKIOĞLU, Afyon Kocatepe University

Prof. Dr. Mehmet ÇELİK, Ankara University

Prof. Dr. Murat YAKAR, Mersin University

Prof. Dr. Mustafa YANALAK, Istanbul Technical University

Prof. Dr. Nebiye MUSAOĞLU, Istanbul Technical University

Prof. Dr. Niyazi ARSLAN, Cukurova University

Prof. Dr. Orhan AKYILMAZ, Istanbul Technical University

Prof. Dr. Reha Metin ALKAN, Istanbul Technical University

Prof. Dr. Tolga ÇAN, Cukurova University

Assoc. Prof. Dr. Ahmet MERT, Isparta University of Applied Sciences

Assoc. Prof. Dr. Emine BAŞTÜRK, Aksaray University

Assoc. Prof. Dr. Hakan YAVAŞOĞLU, Istanbul Technical University

Assoc. Prof. Dr. Hüseyin KARAKUŞ, Dumlupınar University

Assoc. Prof. Dr. Mustafa EL-RAWY, Shaqra University

Assoc. Prof. Dr. Sefa YALVAÇ, Gumushane University

Assoc. Prof. Dr. Selçuk ALEMDAĞ, Gumushane University

Assoc. Prof. Dr. Serkan DOĞANALP, Konya Technical University

Assoc. Prof. Dr. Tekin SUSAM, Gazi Osman Pasa University

Assoc. Prof. Dr. Uğur AVDAN, Eskisehir Technical University

Assoc. Prof. Dr. Zaide DURAN, Istanbul Technical University

Assist. Prof. Dr. Ahmet ÇİLEK, Cukurova University

Assist. Prof. Dr. Aydan YAMAN, Aksaray University

Assist. Prof. Dr. Bahattin GÜLLÜ, Aksaray University

Assist. Prof. Dr. Can İBAN, Mersin University

Assist. Prof. Dr. Erkan YILMAZER, Aksaray University

Assist. Prof. Dr. Esra GÜRBÜZ, Aksaray University

Assist. Prof. Dr. Kamil KARATAŞ, Aksaray University

Assist. Prof. Dr. Nizar POLAT, Harran University

Assist. Prof. Dr. Özlem GÜLLÜ, Aksaray University

Assist. Prof. Dr. Resul ÇÖMERT, Gumushane University

Assist. Prof. Dr. Senem TEKİN, Adıyaman University

Assist. Prof. Dr. Zehra YİĞİT AVDAN, Eskisehir Technical University

Dr. Burak Ömer SARAÇOĞLU

Dr. Fabiana CALO, CNR IREA

Dr. Homayoun MOGHIMI, Payame Noor University

Dr. Kaan KALKAN, TUBITAK-UZAY Space Technologies Research Institute

Dr. Mert MUTLU, Aksaray University

Dr. Müge ÜNAL ÇİLEK, Cukurova University

Dr. Syed Mobasher AFTAB, University of Balochistan

ADVISORY BOARD

Prof. Dr. Bahadır AKTUÇ, Ankara University

Prof. Dr. Dursun Zafer ŞEKER, Istanbul Technical University

Prof. Dr. Hacı Murat YILMAZ, Aksaray University

Prof. Dr. Haluk ÖZENER, Bogazici University

Prof. Dr. Hatim ELHATİP, Aksaray University

Prof. Dr. Mustafa AFŞİN, Aksaray University

Prof. Dr. Mustafa IŞIK, Aksaray University

Prof. Dr. Yusuf Kağan KADIOĞLU, Ankara University

TECHNICAL STAFF

Ahmet Tarık TORUN, Aksaray University

Burhan Baha BİLGİLİOĞLU, Gumushane University

Halil İbrahim GÜNDÜZ, Aksaray University

Ozan ÖZTÜRK, ISTANBUL Technical University

Contents

Research Articles;

Page	Article Titles and Authors
1-	<i>The lahars of the South-East slope of Mount Cameroon: geological study, economic interest and impacts of their exploitation on the environment</i> Joseph Legrand Tchop, Victor Metang, Jacques Dili-Rake, Gaele Vanessa Nana, Pauline Wokwenmendam Nguet, Bernard Tassongwa, Benjamin Ntieche
13-	<i>Investigation of 3D models acquired with UAV oblique images</i> Hasan Bilgehan Makineci, Lütfiye Karasaka
21-	<i>Monitoring of continuous GNSS stations in Central Anatolia region</i> Abdulmalek Redhwan, Hediye Erdoğan, Osman Oktar, Cemil Gezgin
30-	<i>Classification and generation of the enclaves in Karapınar-Karacadağ volcanic rocks (Central Anatolia)</i> Gülin Gençoğlu Korkmaz, Hüseyin Kurt, Kürşad Asan
47-	<i>Modelling and assessing the impact of illegal water abstractions by upstream farmers on reservoir performance</i> Nura Jafar Shanono, John Ndiritu

The lahars of the South-East slope of Mount Cameroon: geological study, economic interest and impacts of their exploitation on the environment

Joseph Legrand Tchop¹, Victor Metang², Jacques Dili-Rake¹, Gaelle Vanessa Nana¹, Pauline Wokwenmendiam Nguet¹, Bernard Tassongwa³, Benjamin Ntieche⁴

¹Institute of Geological and Mining Research, Geophysical and Volcanological Research Unit, Buea, Cameroon

²University of Yaoundé 1, Faculty of Sciences, Department of Earth Sciences, Yaoundé, Cameroon

³University of Dschang, Faculty of Sciences, Department of Earth Sciences, Dschang, Cameroon

⁴University of Yaoundé 1, Higher Teacher Training College, Yaoundé, Cameroon

Keywords

Mount Cameroun
Explosive eruption
Lahars

ABSTRACT

Mount Cameroon is the site of explosive eruptions with the emission of ash, slag and lava flows. Mudflows, known as Lahars, can also be observed. These Lahars are mainly found in the lower part of the south-eastern slope. The outcrops observed on this flank show that these Lahars are very extensive and are avalanches of volcanic material, which flowed down the slopes of the volcano after the eruptions. The different outcrops observed are separated by pyroclastic products on which the lahars rest. The components of these lahars are generally black or grey basalts. The main granulometric characteristic of the deposits of these lahars is their heterometry. The size of the material varies from a few meters to the clay fraction. Large concentrations of mineable material are found in the watercourses. These materials are exploited in order to produce aggregates for civil engineering. This exploitation has consequences on the immediate environment. In addition to climatic factors, several parameters have influenced the mobilities and emplacement of the lahars on the south-eastern slope of Mount Cameroon: the slope, the volume and thickness of the deposits, the nature and physico-hydric characteristics of the deposits. The persistence of strombolian volcanic eruptions on Mount Cameroon and the particularly rainy context predispose it to other future episodes of lahar flow.

1. INTRODUCTION

In all geodynamic contexts, the magmas that reach the earth's surface generate volcanism. And the products (flows, fall out, projections, domes, etc.) accumulate in various ways. The volcanism can generate superficial phenomena such as landslides, mudflows or lahars and others (Dionne, 1991).

The term lahar, of Indonesian origin, refers to a mixture of water and debris of volcanic origin that collapse at high speed over a volcano and its foothills (Lavigne and Thouret, 2000; Huguet et al., 2001; Smith and Fritz, 1989). The phenomenon remobilizes ashes and blocks that have fallen on a volcano flank as a result of instability such as

earthquakes, landslides and meteoric causes (Lavigne et al., 2000).

Mount Cameroon (Figure 1) is the highest volcanic massif in Central and West Africa (4095m) in the intra plate continental domain characterized by alkaline volcanism (Déruelle and Kambou, 1987). Explosive eruptions emitted ash, slag and fluid lava flows. Besides these pyroclastic materials and lava flows, there are landslides (Lambi and Ngawana, 1991; Ayonghe et al., 2002; Ayonghe et al., 2004; Tytgat Nele, 2008) which are mudflows and intermingled rocks such as lahars (Figure 1). Lahars mostly outcrop in the lower zone of the south eastern flank in various localities Buea, Likomba, Ombe, Mutengene, Dibanda, Ekona and Bwenga.

* Corresponding Author

(joletech@yahoo.fr) ORCID ID 0000-0002-4103-494X
(metangvictor@yahoo.fr) ORCID ID 0000-0002-0911-6531
(dilirakejacques@yahoo.fr) ORCID ID 0000-0002-0540-1140
(vanessa.gaelle3@gmail.com) ORCID ID 0000-0001-6563-7027
(nguuetpauline@yahoo.fr) ORCID ID 0000-0002-3612-5222
(btassongwa2004@gmail.com) ORCID ID 0000-0002-2587-1553
(ntiechebenjo@yahoo.fr) ORCID ID 0000-0002-2952-8058

Cite this article

Tchop J.L., Metang V., Dilli-Rake J., Nana G.V., Nguet P.W., Tassongwa B. & Ntieche B. (2021). The lahars of the South-East slope of Mount Cameroon: geological study, economic interest and impacts of their exploitation on the environment. Turkish Journal of Geosciences 2(2), 1-12.

No detailed study has yet been carried out on these lahars though their exploitation for years for various uses. This exploitation is generally easy because of their great geotechnical qualities (Tchungouelieu et al., 2018).

The geological and geomorphological context of setting of lahars is mostly explained by the combination of internal geodynamic (mainly explosive strato-volcanoes) and external (meteorological, hydrological) factors (Lavigne and Thouret, 2000). Volcanoes located in tropical zones (prone to heavy and brutal precipitation) and glaciated volcanoes (Andes Cordillera) are the most concerned (Fisher and Schemincke, 1984; Rodolfo and Arguden, 1991; Thouret et al., 1995; Thouret et al., 1998; Corwin et al., 2017).

Most studies on Mount Cameroon focus on petrology, geochemistry (N'ni, 1984; Déruelle et al., 1987; Nkoumbou et al., 2001; Suh et al., 2003; Ngounouno et al., 2006; Tsafack et al., 2009; Wandji et al., 2009; Ngwa et al., 2019), seismology (Ateba

and Ntepe, 1997; Ateba et al., 2009), volcanism (Bardintzeff et al., 2000) and natural hazards such as landslides (Lambi and Ngawana, 1991; Ayonghe et al., 2002; Ayonghe et al., 2004; Tytgat Nele, 2008; Kervyn et al., 2014). Lahars on this south-eastern slope of the volcano have not been thoroughly studied, the reason of their current geological, geomorphological and economic interest.

Moreover, the site is one of the wettest areas in the world (Tsalefack et al., 2003) and Mount Cameroon is still an active volcano indicating that the lahar phenomenon is still pending. Thus, a geological study on Mount Cameroon lahars becomes a necessity.

They three main objectives in this study are:

- The setting mechanism, morphology, petrography and petrology;
- The guide for the prospecting of mineral materials;
- Identifying the environmental impacts of lahar expansion.

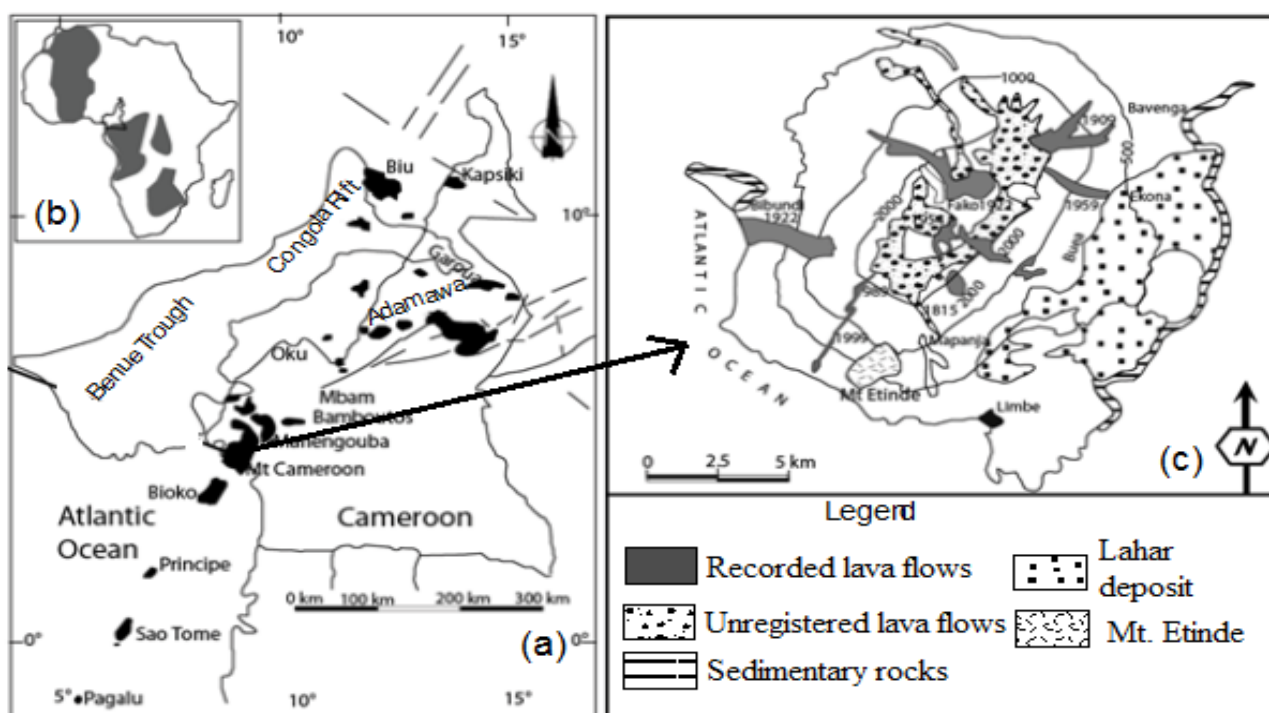


Figure 1. Location of the study area: (a) The Cameroon Volcanic Line; (b) Cratons after Deruelle et al. 1991 and (c) Location of Lahars on the South-East slope of Mount Cameroon

2. GEOLOGICAL SETTING

The Cameroon Volcanic Line, on which Mount Cameroon stands, is a volcano-tectonic megastructure oriented N30°E. It is one of the large intra-plate alkaline volcanic provinces, extending in the oceanic and continental domains (Fitton, 1987; Kagou Dongmo et al., 2001). It is an alignment of oceanic and continental volcanoes of Tertiary to present, from the volcanic island of Pagalu (Figure 1) in the Atlantic Ocean to Lake Chad (Déruelle et al., 1991). The most recent eruptions at Mount

Cameroon took place on 28 March-22 April 1999 and 28 May-19 June 2000 (Suh et al., 2003).

Morphologically, Mount Cameroon is a stratovolcano, located on a horst demarcated by faults expressed by slope breaks (Déruelle, 1982). The products issued are generally represented by Basaltic lavas and their pyroclastic products. Ngounouno et al. (2006) also described Camptonites, a type of lamprophyres made up of plagioclase and brown hornblende. In addition, enclaves (1-5 cm x 0.5-4 cm) of dunites, wehrlites and clinopyroxenites were found in basanites at Batoke in a Strombolian cone (Wandji et al., 2009).

Enclaves of wehrlites and clinopyroxenites were also found in basaltic tephra in a Strombolian cone (Deruelle et al., 2001).

From the fluidity of the magma, gas pressure and granulometry, there are ashes, bombs, slag, pumice, lapilli and blocks at Mount Cameroon.

3. METHODOLOGY

3.1. Fieldwork

Fieldwork is an essential step in any good geological study. Several field work enabled us to carry out macroscopic petrographic studies and make direct observations of lahar outcrops. They consist of:

1. Locating the different outcrops with a GPS and topographic maps;
2. Listing and describing the different types of formations observed;
3. Collecting samples for Thin section and granulometric analysis.

3.2 Laboratory Work

Thin sections on lavas and slags were made for petrographic study under the microscope. The granulometric analysis on lahars was carried out to

assess the frequency of elements. The method used is the sieve size analysis. It consists of washing with water, using a 63 μ sieve, 200 g of sample. The refusal is dried in an oven at 105°C for 24 hours, then weighed and sieved with a successive series of sieves of the AFNOR standard arranged from bottom to top (according to the dimensions of the square mesh): 63 μ , 125 μ , 160 μ , 500 μ , 1mm, 2 mm, 3 mm. The refusal of each sieve is weighed with a precision balance. Sieve analysis curves were made. Clay fraction was removed during washing.

4. RESULTS

4.1. Geological Characteristics of Lahars

They outcrop at Mutengene, Ombe and Likomba.

Mount Cameroon lahars are avalanches of volcanic material in large volumes that tumbled down the slopes after the eruptions. They look like conglomerates covering a large area (about 15 x 20 km², Figure 2 and 3). In the lower, gently sloping parts are volcanic cones still in the midst of lahar materials (Figure 4). Pyroclastic products separate different lahar outcrops. At places, there is a very thick pedological cover on pyroclastic products. These lahars are described according to their location, mode of outcropping and lithology.

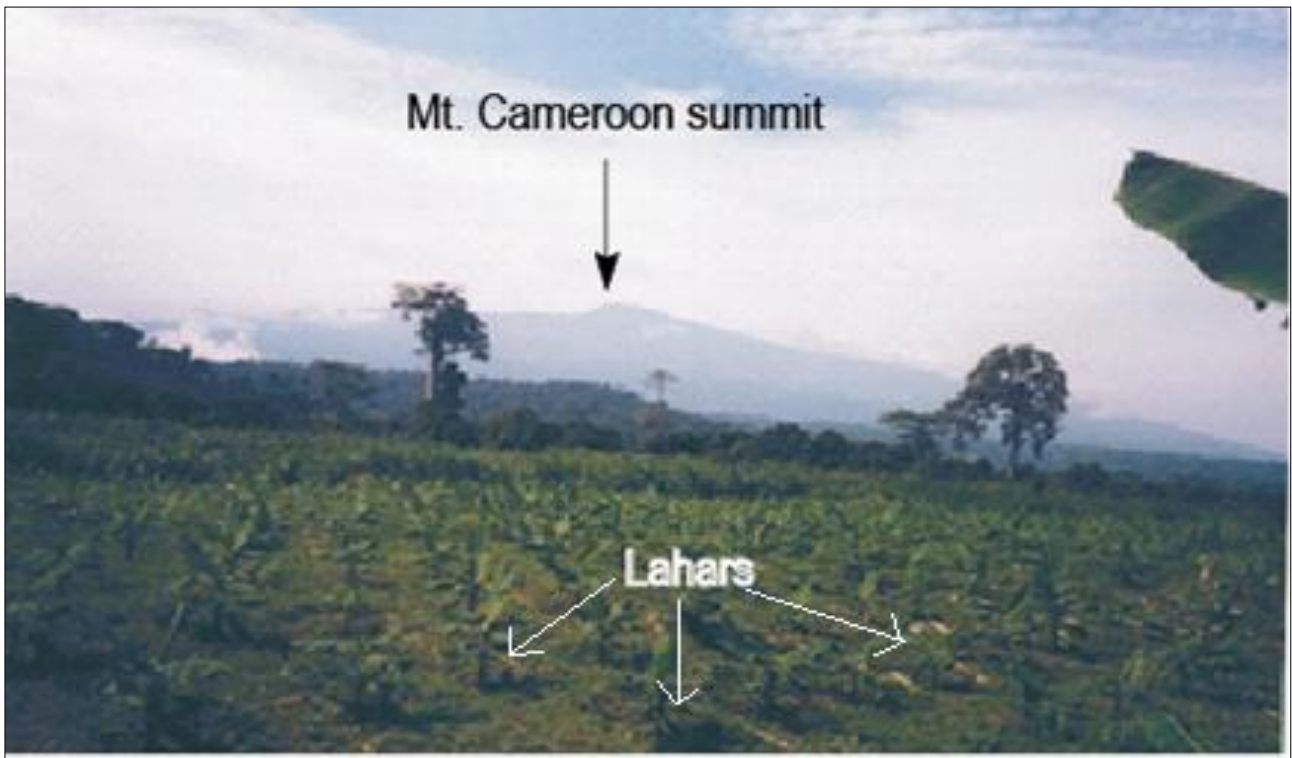


Figure 2. Extension of lahars flow, from the southern limit (Ombe) to the source (Mount Cameroon)

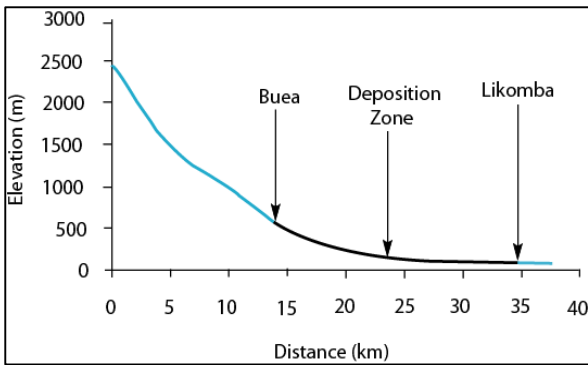


Figure 3. Longitudinal profile from the Mount Cameroon summit to downstream in the Tiko plain (Likomba)

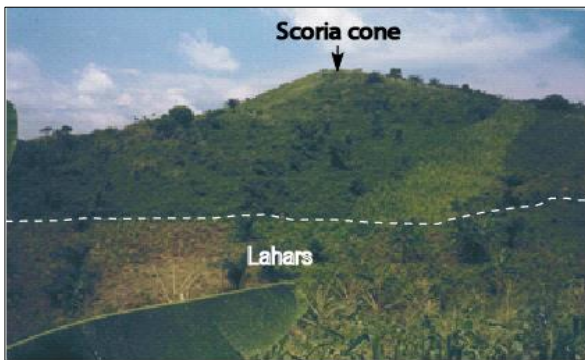


Figure 4. Photograph of the scoria cones emerging in the middle of lahars

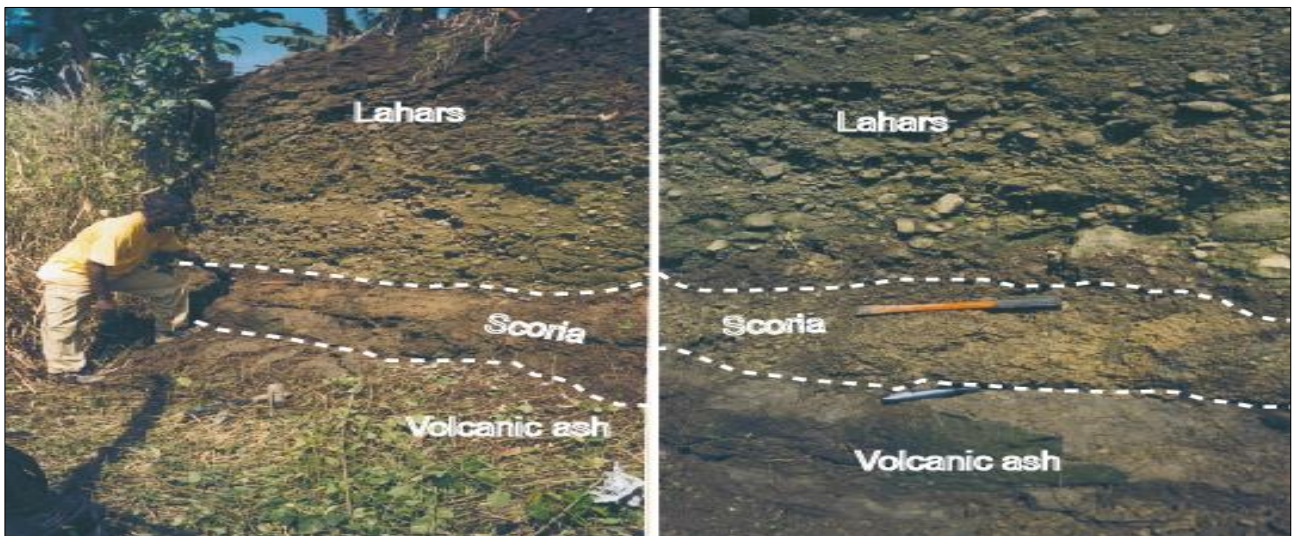


Figure 5. Contact between lahar blocks and the substratum (ash and slag) at its southern limit

4.1.2. Morphology of Tiko-Mutengene lahars

Tiko-Mutengene lahars offer a stepped topography comprising the Tiko unit (about 30m altitude), the Likomba unit (about 60m) and the Mutengene unit (150m). They mostly outcrop along rivers (Figure 8a) such as Essuke, Ndongo and Benoe. These lahars are strips several kilometers long, hundreds meters wide and 15 to 90 meters high. The vegetation is important.

4.1.1. Ombe outcrops

Lahar outcrops observed along the Ombe River extend continuously as far as Ombe-Native, almost 9 km south of Mutengene. They look like conglomerates in blocks of various sizes agglomerated by a sandstone matrix and covered by vegetation consisting of agro-industrial plantations of banana and palm trees. The topography at Ombe is relatively flat; but in detail, it presents interfluves and depressions where lahars partially mold hills of pyroclastic rocks (slag and ash, Figure 4). At road trenches and in incised valleys, the structures of lahars are maintained, with blocks well distributed.

Ombe River lahars; Lahars occupy most the river bed with generally identical elements and in descending order of importance, rounded blocks and pebbles.

-Rounded blocks of different sizes (from centimeters to several meters) witnessing a long transport. Their proportion reaches 80 to 90% in most places.

-Oval or flattened pebbles (≤ 3 cm in size) interspersed with gravel, sand and mud.

The Ombe River flows at the western limit of lahar deposits bear large boulders at bends and meanders. On its banks large slag slopes form the bedrock of lahars. These slags are friable or compact, about 8 m height (Figure 5).

4.1.3. Morphology of Tamben-Dibanda lahars

Tamben-Dibanda lahars outcrop to the north of Mutengene and stretch on slopes for more than 15 km right to mile 17 Buea. Blocks are light grey in color, larger (50 cm to ≥ 2 m in diameter) but smaller in size at mile 17 (10 to 40 cm in diameter). Vesicular blocks abound with millimeters to centimeters vacuoles.

4.1.4. Morphology of Bwenga lahars

Bwenga lahars outcrop in small blocks (≤ 30 cm) at the south-eastern end of all the studied lahars in a vast plain on stratified ashes. Textural and lithological features are similar to the others but with blocks lesser in size (Figure 8a).

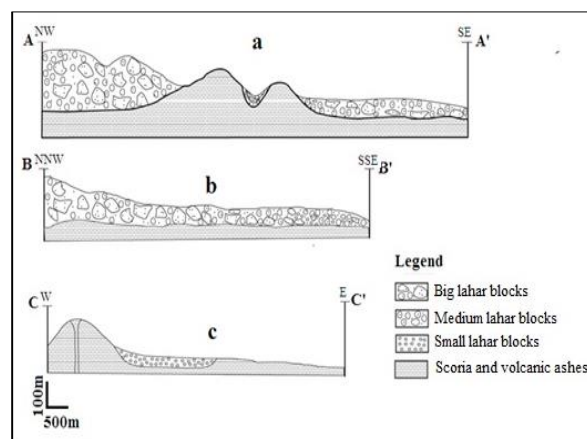


Figure 6. Geological profile showing the lateral and vertical structure of lahars

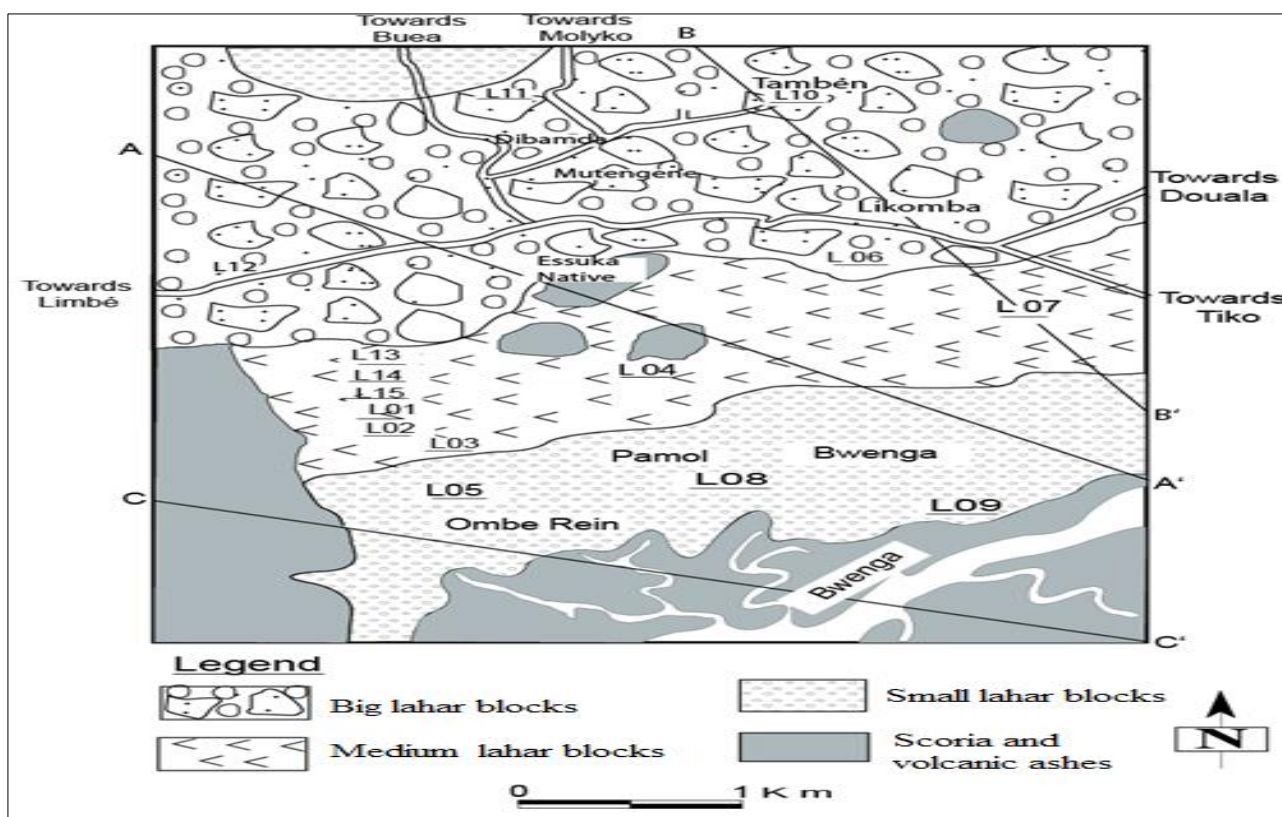


Figure 7. Map of lahar outcrops on the south-eastern flank of Mount Cameroon

4.2 Petrography

On the southeastern slope of Mount Cameroon lahars are basalts generally black or grey in color, compact or vesicular (Figure 8b). Vacuoles are rounded or elongated in the same direction. Blocks range from a few centimeters to a few meters (Figure 8a and 8b). The microscopic study reveals an aphyric microlitic or porphyritic microlitic texture with olivine, pyroxene and / or plagioclase phenocrysts (Figure 9).

Porphyritic basalts are rich in olivine phenocrysts (3-7 mm), pyroxene and plagioclase (10-25%) euhedral to subeuhedral, scattered or clustered. Olivine and pyroxene abound. Sub-

aphyric basalts show smaller size phenocrysts, below 2 mm. Aphyric basalts are finely crystallized with black or grey paste and no mineral is discernable to the naked eye (Figure 9a). Vacuolar blocks show almost the same features: less dense, spongy, very fine or developed vacuoles (rounded or elongated) with sizes up to several centimeters. Phenocrysts of olivine and/or pyroxene are present in some samples (Figure 9b).

Petrographic features of blocks in the studied lahars are identical in all the lavas resulting probably from various eruptions of Cameroun Mount; their elements result from several eruptions.

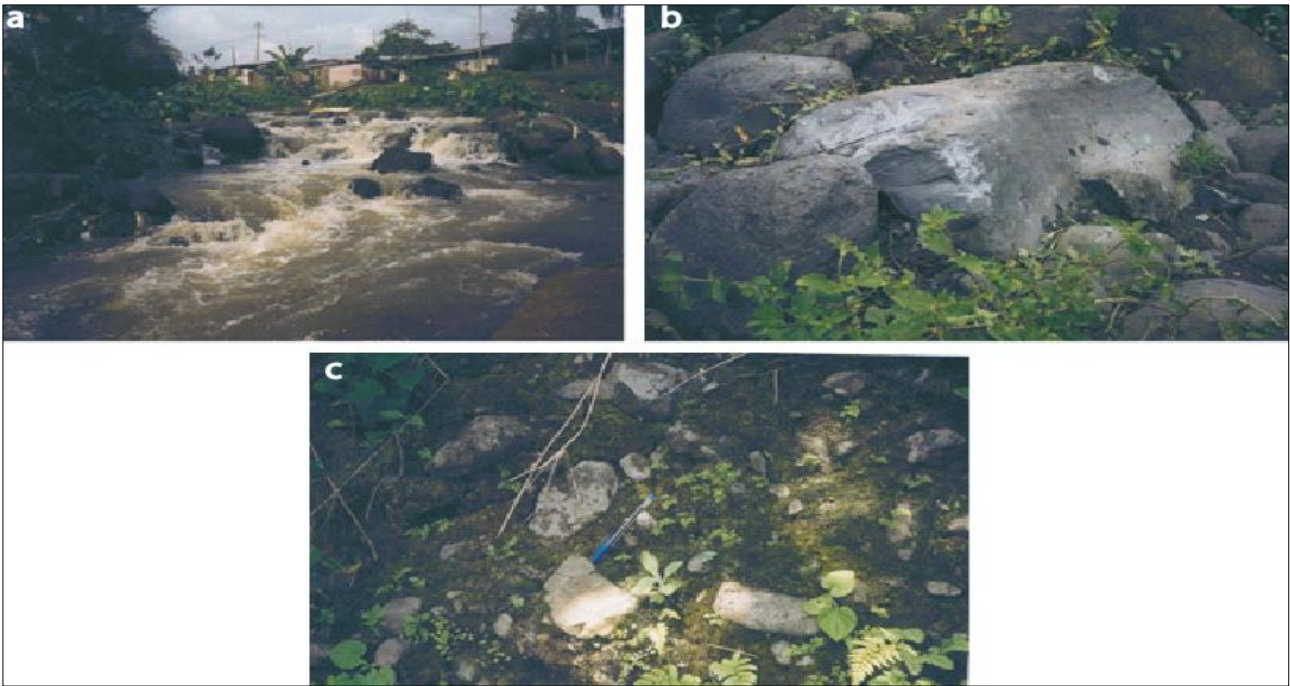


Figure 8. a) Metric blocks in the Benoe River (Mutengene); b) Porphyritic or aphyric blocks; c) Conglomeratic lahars (Mutengene-Ombe road)

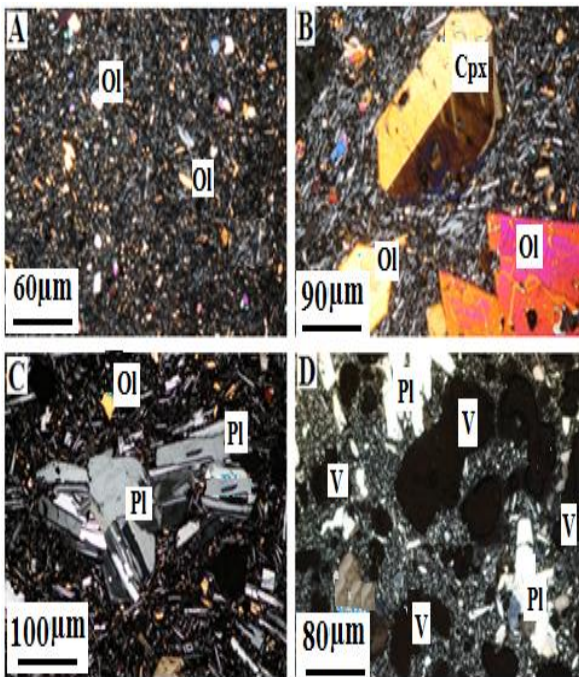


Figure 9. Textures of basalts on the SE slope of Mount Cameroon. A: Aphyric; B: Porphyritic; C: Microlitic with trachytic tendency; D: Vesicular. (Ol=Olivine; Cpx= clinopyroxene; Pl=plagioclase; V= Vesicula; according to Kretz, 1983)

4.3. Granulometric Analysis of the Fine Lahars

4.3.1. Elements size distribution

The elements in the studied lahars vary from clays to blocks and from one deposit to another (Figure 10). Heterometry is their main feature with rounded to sub-angular and very poorly sorted elements, compared with pyroclastic deposits beneath. Their deposition process conforms to the progressive aggregation model illustrated at Mont Rainier (Vallance and Scott, 1997).

4.3.2. Granulometric analysis

The particle size analysis concerns only fractions below 5 mm. It was carried out to determine the greater or lesser frequency of elements of different dimensions. The size of the materials varies from a few meters to clay fraction. Thus, the materials are poorly sorted. Tables 1, 2 and 3 show the concentration of fragments and clay. Moreover, the deposits are poly lithological, with mixed pyroclastic materials, lava and fragments from banks or the channel bed. The matrix is mainly sandy-gravel (Figure 11) (Scott et al., 1995).

Table 1. Particle size analysis results (Sample L13, Lithology: Lahar, Location OMBE, Fraction<63μ: 28.69, Dry start weight: 200g, Final dry weight: 171.31g)

Mesh size of sieves (mm)	Partial refusals (g)	Cumulative refusals (g)	Partial percentages (%)	Cumulative percentages (%)
PSD	200g			
4	60.23	60.23	30.115	30.115
3	57.99	118.22	28.995	59.11
2	11.79	130.01	5.895	65.005
1	15.32	145.33	7.66	72.665
0.5	12.60	157.93	6.3	78.965
0.25	5.22	163.15	2.61	81.575
0.16	3.48	166.63	1.74	83.315
0.125	1.71	168.34	0.855	84.17
0.063	2.97	171.31	1.485	85.655
Total	171.31		85.655	

Table 2. Particle size analysis results (Sample: L14, Lithology: Slags + Lapilli, Location: OMBE, Fraction < 63μ: 30,63, Dry start weight: 200g, Final dry weight: 169,37g)

Mesh size of sieves (mm)	Partial refusals (g)	Cumulative refusals (g)	Partial percentages (%)	Cumulative percentages (%)
PSD	200			
4	68.1	68.1	34.05	34.05
3	33.55	101.65	16.775	50.825
2	28.26	129.91	14.13	64.955
1	19.13	14,04	9.565	74.52
0.5	7.93	156.97	3.965	78.485
0.25	5.18	162.15	2.59	81.075
0.16	2.65	164.8	1.325	82.4
0.125	1.51	166.31	0.755	83.155
0.063	3.06	169.37	1.53	84.685
Total	169.32		84.66	

Table 3. Particle size analysis results (Sample: L15, Lithology: Volcanic ashes, Location: OMBE, Fraction < 63μ: 58.01, Dry start weight: 200g, Final dry weight: 141.99g)

Mesh size of sieves (mm)	Partial refusals (g)	Cumulative refusals (g)	Partial percentages (%)	Cumulative percentages (%)
PSD	200			
4	14.05	14.05	7.025	7.025
3	11.01	25.06	5.505	12.53
2	15.96	41.02	7.98	20.51
1	27.52	68.54	13.76	34.27
0.5	27.86	96.4	13.93	48.2
0.25	21.08	117.48	10.54	58.74
0.16	9.09	126.57	4.545	63.285
0.125	5.62	132.19	2.81	66.095
0.063	9.8	141.99	4.9	70.995
Total	141.99		70.995	

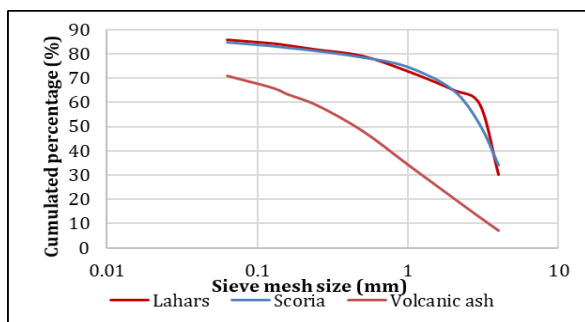


Figure 10. Particle size curves of lahars, scoria and volcanic ash of Mount Cameroon

4.4 Economic Interest and Impact of Their Exploitation on the Environment

Today, rocks are still the primary source of materials used by man for landscaping and major works. The development of the road network and the building boom in Cameroon require the opening of quarries near urban centers with high demand as Ombe. On the whole, quarries are opened in places where the material deposits are large and accessible. Their exploitation generates positive impacts (roads), and negative impacts (environment).

4.4.1. Prospecting of materials

The size and distribution of the studied lahars are related to geomorphology. The materials follow pre-existing valleys and sometimes interlayered with alluvium, colluvium and various pyroclasts, as is the case in Ombe and mutengene in our study site. They are thin on steep slopes and upstream, but thick downstream. Research carries out on significant concentrations of exploitable material, specific locations:

In waterways, there are abundant and highly concentrated materials in meanders of the Ombe River where lahar materials are exploited by several companies.

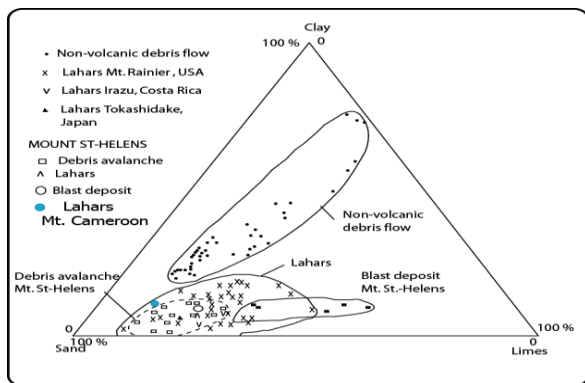


Figure 11. Position of Mount Cameroon lahars in the grain size distribution diagram of Lahars (Fisher and Schminke, 1984; Scott et al., 1995)

On slopes, the material is relatively less thick, but with a high concentration of large blocks ranging from 50 cm to 3 m in size at Dibanda and Tamben (especially upstream the Benoe River). Slope deposits are of a very good quality for deprived of fine particles, but steep slopes and difficult access hinder their exploitation.

In plains, the material is abundant in various sizes (fine to block) but scattered. Small size elements (≤ 30 cm) abound.

4.4.2. Use, exploitation and environmental impact

To produce aggregates for public works in general and road development in particular, several companies exploit Mount Cameroon lahars on the south-eastern flank. This open-cast exploitation affects the environment in various ways.

4.4.2.1. In civil engineering

Aggregates mainly used in road construction and others (bridges, houses,) with pozzuolanic properties can be used in the construction of treated subbases. The vesicular texture of materials is important. Their dry density is often relatively low, not leading to its rejection (due to their

porosity). The optimal moisture content is insignificant (CEBTP, 1984).

4.4.2.2. Exploitation

Basalt blocks are mined in the open air (Figure 12a) preceded by stripping the plant cover and the overburden that masks the deposit. Boulders are carried to the crushing station for physical transformation to gravel of granulometry 0/31.5, 15/25, 10/15, 5/10 and 0/5 mm. Besides is the large release rock dust. Aggregates are stored in heaps by granulometry (Figure 12b) and later loaded in trucks to various destinations.

4.4.2.3. Environmental impacts

The exploitation of quarries on Mount Cameroon lahars shows direct or indirect negative effects on the environment, the safety and health of local residents.

On the ground, clearing and earthwork during the opening of roads and the construction of structures expose the ground surface usually protected by vegetation to immediate erosion or compaction and sealing of surface layers. Leaking oil, grease and fuel from machines pollute the soil. This leads to the loss of productivity, destabilization of nature, reduction of agricultural land and shaping of topography.

On water resources: during extraction rivers become pasty due to enormous fine load or mud (Kuété, 1999). The water once drinkable and consumed by the populations becomes unusable. Some villages in the area change their water supply, but not the Ombe populations.

On air quality: extraction activities are a corollary of deterioration in air quality through the emission of fumes from machinery and trucks, dust and siliceous particles. This is a danger to the health of the workers and the populations of the surrounding villages.

Vegetation: as long as there are quarries, the regeneration of plants becomes difficult. Thick layers of dust particles on the vegetation hinder their growth. Siliceous dust particles cover the leaves of plants many kilometers round the site.

On wildlife: wild animals are no longer found in the area driven away by the noise of the machinery, the crushing of blocks and the destruction of their habitat.

4.5. Agricultural Interest of Soils Developed on Lahars

The soil provides plants with mineral nutrients that are absorbed by the roots. On the south-eastern flank of Mount Cameroon, soils developed on lahars show an abundant plant cover and high mineral reserves due to the proximity of the parent rock. They very well suit food crops, banana, cocoa and coffee, oil palm and rubber (Figure 13a and 13b).



Figure 12. a) Exploitation of lahar blocks. b) Crushing and storage of aggregates



Figure 13. Agricultural interest of lahars: a) fertile lahars soils in agro-industry; b) Industrial banana plantations

5. DISCUSSION

5.1. Interpretation of the Lahars

The studied lahars present large polygenic blocks of various sizes. Slopes of 50° played a major role in setting them up. Blocks covered nearly 25,000 m in the valleys at high speed as far as the Tiko plain. An enormous quantity of water also favored the formation of lahars from rain or ice. The distribution of rainfall at Mount Cameroon varies according to flanks (Figure 14). The SW flank shows the most rainfall but no lahars. But the SE flank shows average rainfall and thick and widespread lahars. Thus, rainfall is not the trigger factor for lahars. For their glacial origin Déruelle (1982) and Zogning (1988) describe two possibilities. Lahars result from solifluction flows related to periglacial freeze-thaw or sub-glacial eruption phenomena. Tricart and Cailleux (1965) and Maley (1983) suggest very important Quaternary climatic oscillations in Africa. Thick layers of ice covered some coastal regions (e.g. the Gulf of Guinea coast) during ice ages (Günz, Mindel, Riz and Würm) (Scaëtta, 1937; Moby Etia, 1979). For example, Kenya's glaciers descended to an altitude of 3300 m. However, Mount Cameroon peak is at 4100 m. In the end of Pleistocene between 20,000 and 15,000

years BP (at Würm) there was a strong phase of rapid erosion and sedimentation as shown by sediment analyses from Lake Barombi-Mbo near Mount Cameroon (Maley, 1996; Giresse et al., 1994). These erosions were probably melts from Pleistocene glaciers, explaining the origin of the water that generated the Mount Cameroon lahars, as in Nevada del Ruiz in Colombia (Thouret et al., 1995).

Mount Cameroon volcanism started in the Tertiary (Eocene) (Tsafack et al., 2009) by releasing basalts with Hawaiian to Strombolian dynamism. It continued in the Quaternary building hundreds Strombolian cones explained by the excellent conservation and freshness of rocks. For, these lahars comprise blocks of altered rock (probably of Tertiary age) and blocks of fresh rock, suggesting their formation in the Quaternary from the melting of glaciers, precisely in Pleistocene (20,000 - 15,000 years BP, würm) (Scaëtta, 1937). The size decrease of elements of lahar deposits on the SE slope result from a loss of water velocity (Lavigne and Thouret, 2000; Vallance and Iverson, 2015) leading to an abrupt stop of large elements. Fine elements settled farther (Figure 7). Thus, these are primary lahars of syn-eruptive type according to the classification of Lavigne (1998) resulting from a Strombolian dynamism during Quaternary glaciations.

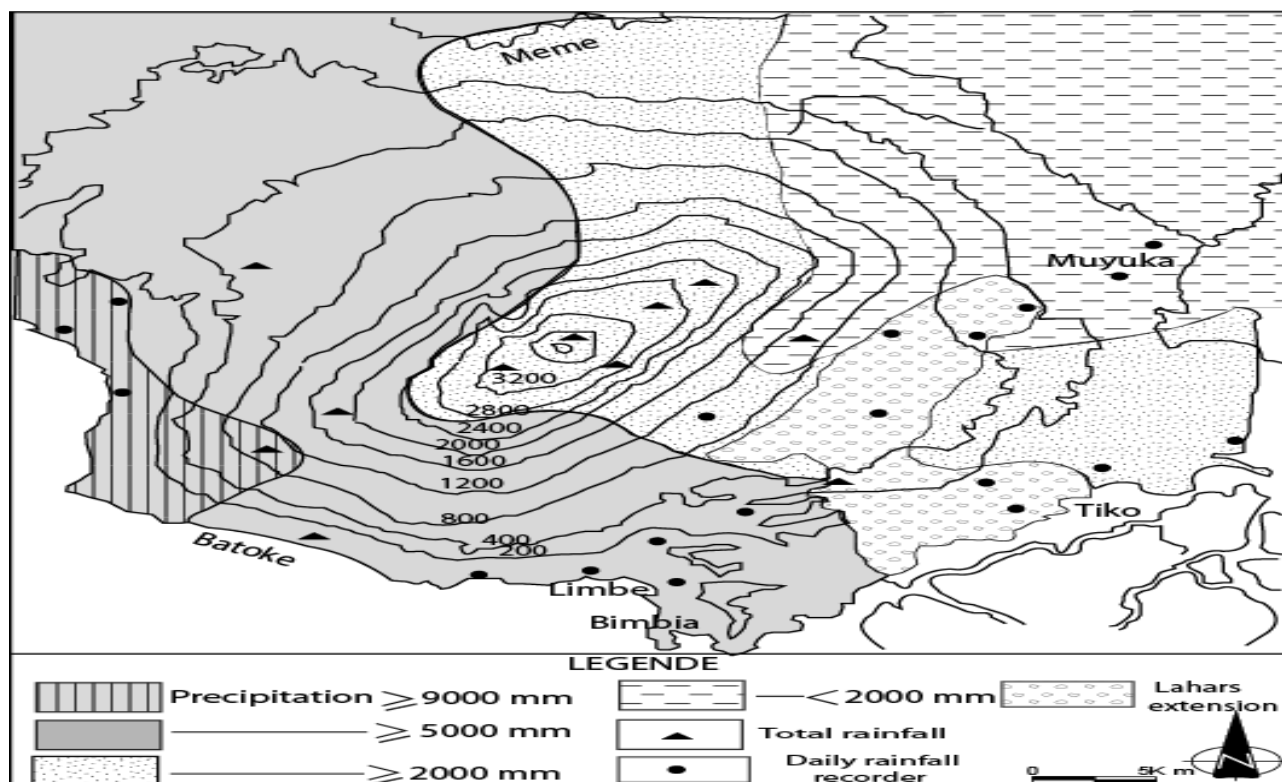


Figure 14. Distribution of rainfall and lahars on Mount Cameroon (Zogning, 1988)

6. CONCLUSION

Mount Cameroon lahars are deposits of large volumes of volcanic material that tumbled down the slopes of the volcano after eruptions. They are compact or vacuolar basalts in blocks of different sizes (centimeters to meters), pyroclasts (ash and slag) and carbonized wood. Rocks are aphyric or porphyritic with olivine, pyroxene or plagioclase phenocrysts.

Besides climatic factors, other parameters that influenced the release mobility and the setting up of lahars are slope, volume and thickness of remobilized deposits, nature and physico-hydraulic features of deposits. The material mostly in rivers (at meander bends) is exploited to produce aggregates for civil engineering. The exploitation affects the immediate environment, mainly the soil, vegetation, quality of water in rivers and health of the local population. Lahars soils are very fertile and suit for agriculture.

Acknowledgement

The authors would like to thank the Cameroon Geological and Mining Research Institute for all the facilities provided and also the Sedimentology Laboratory of the University of Yaoundé I for the granulometric analyses.

Author Contributions

Joseph Legrand Tchop: Collected the datasets and analyzed the data, Methodology, Validation. **Victor**

Metang: Investigation and data collection in the field. **Jacques Dili-Rake:** Making of figures **Gaelle Vanessa Nana:** Participation in field investigation. **Pauline Wokwenmendam Nguet:** Writing the manuscript-review and editing. **Bernard Tassongwa:** Writing the manuscript-review and editing. **Benjamin Ntieche:** Reviewing the manuscript before submission.

Conflicts of Interest

The authors declare no conflict of interest.

REFERENCES

- Ateba, B., Dorbath, C., Dorbath, L., Ntepe, N., Frogneux, M., Akja, F.T., Hell, J.V., Delmond, J.C., & Manguelle, D. (2009). Eruptive and earthquake activities related to the 2000 eruption of Mount Cameroon volcano (West Africa). *Journal of Volcanology and Geothermal Research*, 179, 206-216.
- Ateba, B., & Ntepe, N. (1997). Post-eruptive seismic activity of Mount Cameroon (Cameroon, West Africa): A statistical analysis. *Journal of Volcanology and Geothermal Research* 79 (1-2), 25-45.
- Ayonghe, S.N., Suh, C.E., Ntasin, E.B., Samalang, P., & Fantong, W. (2002). Hydrologically, seismically and tectonically triggered landslides along the Cameroon Volcanic Line, Cameroon. *Africa Geosciences Review*, 9(4), 325-336.

- Ayonghe, S.N., Ntasin, E.B., Samalang, P., & Suh, C.E. (2004). The June 27, 2001 landslide on volcanic cones in Limbe, Mount Cameroon, West Africa. *Journal of Africa Earth Science* 39(3-5), 435-439.
- Bardintzeff, J.M., Déruelles, B., Cheminée, J.L., Etame, J., Fosso, J., Hell, J.V., Lissom, J., Ngounouno, I., Nkouathio, D.G., Nkoumbou, C., Nni, J., & Nono, A. (2000). L'éruption de mars-avril 1999 du Mont Cameroun: dynamisme et premières données pétrologiques. *Cahier géologique*, 135, 1835-1837.
- Dionne, J.C. (1991). Campy, M et Macaire, JJ (1989), Géologie des formations superficielles (Géodynamique-faciès-utilisation). *Géographie physique et Quaternaire*, 45(1), 118-119.
- CEBTP, (1984). Guide pratique de dimensionnement des chaussées des pays tropicaux. Ministère de la coopération de la République Française (Eds).155 p.
- Corwin, K.A., Brand, B.D., Hubbard, M.L., & Johnston, D.M. (2017). Household preparedness motivation in lahar hazard zones: assessing the adoption of preparedness behaviors among laypeople and response professionals in communities downstream from Mount Baker and Glacier Peak (USA) volcanoes. *Journal of Applied Volcanology*, 6(1), 1-19.
- Déruelle, B. (1982). Risque volcanique au Mont Cameroun. *Revue de Géographie du Cameroun*, 3(1). 33-40.
- Déruelle, B., N'ni, J., & Kambou, R. (1987). Mont Cameroon: an active volcano of the Cameroon Line. *Journal of Africa Earth Sciences*, 6(2), 197-214.
- Déruelle, B., Moreau, C., Nkoumbou, C., Kambou, R., Lissom, J., Njonfang, E., ... & Nono, A. (1991). The Cameroon line: a review. *Magmatism in extensional structural settings*, 274-327.
- Fisher R.V., & Schemincke H.U. (1984). *Pyroclastic Rocks*, Springer-verlag. Berlin, Heidelberg, New York, Tokyo, 472.
- Fitton, J.G. (1987). The Cameroon line, West Africa: a comparison between oceanic and continental alkaline volcanism. *Geological Society, London, Special Publications*, 30(1), 273-291.
- Giresse, P., Maley, J., & Brenac, P. (1994). Late Quaternary palaeoenvironments in the Lake Barombi Mbo (West Cameroon) deduced from pollen and carbon isotopes of organic matter. *Palaeogeography, Palaeoclimatology, Palaeoecology*, 107(1-2), 65-78.
- Huguet, D., Thouret, J.C., Nehlig, P., Raffy, J., & Rochette, P. (2001). Les lahars du strato-volcan du Cantal (Massif Central, France): stratigraphie, modes de mise en place et implication paléo-géomorphologiques. *Bulletin de la Société Géologie de France*, 172(5), 573-585.
- Kagou Dongmo, A., Wandji, P., Pouclet, A., Vicat, J.P., Cheilletz, A., Nkouathio D.G., & Tchoua, F.M. (2001). Évolution volcanologique du mont Manengouba (Ligne du Cameroun); nouvelles données pétrographiques, géochimiques. géochronologiques. *Comptes Rendus Academie des Sciences-Series IIA-Earth and Planetary Science*. 333(3), 155-162.
- Kervyn, M.B. Van Wyk de Vries, B., Walter, T.R., Njome, M.S., Suh, C.E., & Ernst, G.G.J. (2014). Directional flank spreading at Mount Cameroon volcano: Evidence from analogue modeling, *Journal of Geophysic. Research. Solid Earth*, 119(10), 7542-7563.
- Kretz, R. (1983). Symbols for rock-forming minerals. *American mineralogist*, 68(1-2), 277-279.
- Kuété, M. (1999). Exploitation des ressources naturelles dans les environs de Dschang: Impact environnemental. *Géosciences au Cameroun, JP Vicat et P. Bilong, ed., Collection Géocam*, 47-54.
- Lambi, C.M., & Nwana, B.S. (1991). Human interference and environmental instability: the case of the Limbe landslide. *Revue de géographie du Cameroun*, 10(1), 44-52.
- Lavigne, F., & Thouret, J.C. (2000). Les lahars; depots, origines et dynamique. *Bulletin de la Société géologique de France*, 171(5), 545-557.
- Lavigne, F. (1998). Les lahars du volcan Merapi, Java central, Indonésie (Doctoral dissertation, Clermont-Ferrand 2).
- Lavigne, F., Thouret, J.C., Voight, B., Suwa, H., & Sumaryono, A. (2000). Lahars at Merapi volcano, Central Java: an overview. *Journal of volcanology and geothermal research*, 100(1-4), 423-456.
- Maley, J. (1983). Histoire de la végétation et du climat de l'Afrique nord-tropicale au Quaternaire récent. *Bothalia*, 14(3/4), 377-389.
- Moby Etia, P. (1979). Climats. In les Atlas Jeune Afrique, République Unie du Cameroun.

- N'NI, J. (1984). Le volcan actif du mont Cameroun (ligne du Cameroun): géologie et pétrologie du volcan (Doctoral dissertation).
- Ngounouno, I., Déruelle, B., Montigny, R., & Demaiffe, D. (2006). Les camptonites du mont Cameroun, Cameroun, Afrique. *Comptes Rendus Geoscience*, 338(8), 537-544.
- Ngwa, C.N., Lenhardt, N., Le Roux, P., & Mbassa, B.J. (2019). The subsurface magma eruptions: Geochemical constraints on the subsurface magma plumbing system. *Journal of Volcanology and Geothermal Research*, 384, 179-188.
- Nkoumbou, C., Nana, R., Eno Belinga, S., Vicat, J.P., & Tchoua, F. (2001). Les éruptions du Mont Cameroun de 1999: Etude volcanologique. Histoire Géologique du Cameroun. Eno Bélinga 117-123.
- Rodolfo, K.S., & Arguden, A.T. (1991). Rain-Lahars generation and sediment-delivery system at Mayon volcano.
- Scaëtta, H. (1937). Variations du climat pléistocène en Afrique Centrale. In *Annales de Géographie*, 46(260), 164-171.
- Scott, K.M., Vallance, J.W., & Pringle, P.T. (1995). Sedimentology, behavior and hazard of debris flows at Mount Rainier, Washington, *US Geological Survey*, 1547, 56.
- Smith, G.A., & Fritz, W.J. (1989). Volcanic influences on terrestrial sedimentation. *Geology*, 17(4), 375-376.
- Suh, C.E., Ayonghe, S.N., Sparks, R.S. J., Annen, C., Fitton, J.G., Nana, R., & Luckman, A. (2003). The 1999 and 2000 eruptions of Mount Cameroon: eruption behaviour and petrochemistry of lava. *Bulletin of Volcanology*, 65(4), 267-281.
- Tchungouelieu, H.W., Pizette, P., Wouatong, A.S.L., Abriak, N.E., Borrel, L.R., Razafimahatratra, N.F., Ngappue, & F, Guouillier, T. (2018). Effect of 0/5 basaltic aggregates on geotechnical properties of fine lateritic soils from Bafang (West-Cameroon) for road construction purposes. *National Geotechnical and Engineering Geology Days*.
- Thouret, J.C., Abdurachman, K.E., Bourdier, J.L., & Bronto, S. (1998). Origin, characteristics, and behaviour of subsequent lahars of the 1990 eruption at Kelud, East Java (Indonesia). *Bulletin of Volcanology*, 59, 460-480.
- Thouret, J.C., Vandemeulebrouck, J., Komorowsky, J. C., & Valla, F. (1995). Volcano-glacier interactions: field survey, remote sensing and modelling-a case study Nevado del Ruiz, Colombia. *Steepland geomorphology*, Sleymaker O., 63-88.
- Tricart, J., & Cailleux, A. (1965). Introduction à la géomorphologie climatique (Vol. 1). Société d'édition d'enseignement supérieur.
- Tsafack, J.P.F., Wandji, P., Bardintzeff, J.M., Bellon, H., & Guillou, H. (2009). The Mount Cameroon stratovolcano (Cameroon volcanic line, Central Africa): petrology, geochemistry, isotope and age data. *Geochemistry, mineralogy and Petrology*, 47, 65-78.
- Tsalefac, M., Ngoufo, R., Nkwambi, W., Tatsangue, E. D., & Fobissie, B.L. (2003). Fréquences et quantités des précipitations journalières sur le territoire camerounais. *Publ. AIC*, 15, 359-367.
- Tytgat Nele, J.L. (2008). Susceptibility analysis of the risk of small landslides on the southern slope of Mount Cameroon Volcano. Unpublished MSc thesis, Ghent University.
- Vallance, J.W., & Iverson, R.M. (2015). Lahars and their deposits. In *The encyclopedia of volcanoes* (649-664). Academic Press.
- Vallance, J.W., & Scott, K.M. (1997). The Osceola Mudflow from Mount Rainier: Sedimentology and hazard implications of a huge clay-rich debris flow. *Geological Society of America Bulletin*, 109(2), 143-163.
- Wandji, P., Tsafack, J.P.F., Bardintzeff, J.M., Nkouathio, D.G., Dongmo, A.K., Bellon, H., & Guillou, H. (2009). Xenoliths of dunites, wehrlites and clinopyroxenites in the basanites from Batoke volcanic cone (Mount Cameroon, Central Africa): petrogenetic implications. *Mineralogy and Petrology*, 96(1-2), 81-98.
- Zogning, A. (1988). Le Mont Cameroun, un volcan actif: contribution à l'étude de géographie physique appliquée (Doctoral dissertation, unpublished doctoral thesis, University of Yaounde, Cameroon).



Investigation of 3D models acquired with UAV oblique images

Hasan Bilgehan Makineci *¹, Lütfiye Karasaka*¹

¹Konya Technical University, Faculty of Engineering and Nature Sciences, Department of Geomatics Engineering, Konya, Turkey

Keywords

ANAFI
UAV
Oblique Image Acquisition
3D Model

ABSTRACT

The concept of oblique image acquisition entered the literature long after the overhead photogrammetric acquisition techniques. The oblique image acquisition technique is applied to model the edge surfaces of buildings that cannot be obtained with vertical (nadir) image acquisition and eliminate the problems that arise in the orthorectification of high-rise buildings in urban areas. Oblique image acquisition by Unmanned Aerial Vehicles (UAV) independent of aerial photogrammetry is considered possible with unique flight plans. How convenient oblique image acquisition with the help of UAVs is and how it affects the final product is a popular topic studied by researchers. In this study, oblique image acquisition was performed using a rotary-wing UAV (Parrot ANAFI) whose camera can move 180°. With the help of the 3D models obtained, the building was drawn in vector and evaluated to scale. As a result, it has been understood that almost all structural deficiencies in the final products can be eliminated by oblique images. However, it has been revealed that there is still a need for other methods for structures that do not have patterns, such as flat walls.

1. INTRODUCTION

The digital photogrammetry technique has been developing at a breathtaking movement since the 21st century when it was truly effective. Many factors such as the increase in the success of the GNSS technique in field works (in terms of Ground Sampling Distance -GSD-accuracy), the increase in the efficiency of flight planning software, the completion of pre-flight and post-flight processes in a quicker time, and the acceleration experienced in image acquisition systems have a part in this development (Yastikli and Özerdem, 2017). Despite all the development in this technique, frame-based aerial cameras are not considered sufficient in orthophoto map production in urban areas. Due to the nearby settlement of the building structures or the increase in very high-rise buildings in urban areas, problems arise in image acquisitions made from the nadir direction (vertical acquisition). Oblique image acquisition cameras introduced to solve this problem reveal actual results.

Aerial photogrammetry, which saves time and cost in large-scale map making (such as 1/1000 or 1/5000), is not considered economical at the same

level in very large-scale map works (such as 1/50 or 1/100). Today, Unmanned Aerial Vehicles (UAVs) are seen as the most crucial alternative in studies that can take a very long time with terrestrial methods, in very large-scale map production, in 3D modeling studies, and in almost all studies where humans may be under threat (Uysal et al., 2015). It is a technique used as another option for image acquisition with oblique aerial cameras (Erdönmez, 2018). Oblique image acquisition with UAV under certain conditions is essential to obtain acceptable results (Rossi et al., 2017; Vacca et al., 2017). However, sometimes using a single method in 3D modeling of an object/building may not be sufficient to reach a solution or meet expectations. For example, when creating a 3D model of a building, building facades can usually be modeled with close-up photogrammetry or terrestrial laser scanning method.

In contrast, the aerial photogrammetry method can provide the necessary perspective for building roofs (Aicardi et al., 2016). In such cases, where a single process is not sufficient for 3D modeling studies, it is necessary to solve it by combining the data obtained from different platforms and

* Corresponding Author

*(hbmakineci@ktun.edu.tr) ORCID ID 0000-0003-3627-5826
(lkarasaka@ktun.edu.tr) ORCID ID 0000-0002-2804-3219

Cite this article

Makineci H.B., & Karasaka L. (2021). Investigation of 3D models acquired with UAV oblique images. Turkish Journal of Geosciences 2(2), 13-20.

measurement methods. Today, UAV and Terrestrial Laser Scanner (TLS) methods are used in the documentation of buildings, historical artifacts, and archaeological sites in engineering applications (Achille et al., 2015; Toprak et al., 2019; Tuncer et al., 2018; Jo and Hong, 2019; Valenti and Paternò, 2019; Zeybek and Kaya, 2020).

Since it is challenging to use integrated cameras directly for oblique image acquire (it can be done with tilt motors only), it is possible to obtain accurate results in tilted images with the UAV only by paying attention to the fundamental issues in flight planning. It is a significant problem to determine the angle at which the camera will take the image and in which position it will record the image. This study aims to present acceptable and high-accuracy 3D models with oblique-angle images using accurate flight planning techniques. As for the purpose-oriented goals, it can be said that the acquisition, balancing, and modeling of oblique images without any problems. As a result, it is aimed to investigate the contribution and suitability of oblique images to the 3D model creation.

2. MATERIAL AND METHOD

In the study, Parrot ANAFI, a rotary-wing UAV with a compact RGB camera, whose camera can move 180°, was used. Meliha Ercan Patient Guesthouse, located in the Selçuk University Campus area, has been determined as the study area. Pix4Dcapture was preferred as flight planning software. With Dual Grid flight planning, which provides suitable planning conditions for 3D models, image acquisition was also performed at 1.50 cm/pix (GSD).

2.1. UAV Used in This Research

Parrot ANAFI compact UAV with the integrated camera is in the toy class in terms of weight (including 320 g battery weight) according to the General Directorate of Civil Aviation (SHGM) UAV Regulations (SHT-UAV). The current SHT-UAV valid in our country are classified as UAVs weighing 500 g (including) and above. For this reason, it does not require any legal license in terms of use. The manufacturer has documented its integrated camera with a field of view of 70° and a pixel size of 1.3 µm. The most defining aspect of this UAV is the 180° rotation of its integrated camera (Figure 1). It is possible to say that this feature is an excellent

opportunity to take an oblique image. Anafi camera specifications are as shown in Table 1.

Table 1. Anafi camera (Sony IMX230) specifications (Url-1)

Camera Type	Resolution	Focal Length	Pixel Size
Frame Based	5344x4016 pix.	7.5 mm	1.12x1.12 µm

The last valid regulation used for UAVs in our country, SHT-UAV (as revised on 14 July 2020), divides UAVs into four classes according to their maximum take-off weight. UAVs under 500 g take-off weight are not included in the instruction. Although the ANAFI UAV is not included in any UAV class due to its weight under 500 g, it has features that can also be used in photogrammetry and remote sensing studies (Table 1).

2.2. Study Area

Meliha Ercan Patient Guesthouse, which began its activities on May 17, 2018, is located on a total area of 4109 m². The guesthouse, situated in the Selçuk University Campus Area, is close to the border wall on the rear and side facades, as seen in Figure 2. Because of this closeness, images taken from the nadir direction with the UAV are not manageable to 3D modeling.

2.3. UAV Flight Planning Managed for Oblique Image Acquisition

UAV image acquisition plan was created with Pix4dcapture free UAV flight planning software. The design of the flight planning as a double-grid mission is because it allows the creation of horizontal and vertical columns. Figure 3 presents flight planning and considerations.

Pix4dcapture software was used to create the flight plan. Images were taken from a flight height of 39 m (1.5 cm/pixel GSD) to create a 3D model of the building. A total of 117 images were taken during this flight, which took 06:52 minutes in total. Seven GCPs were established around the study area before the flight. The coordinates of the GCPs were measured in epochs enduring 10 seconds at one time. Images and GCPs obtained from the field study were transferred to the computer.

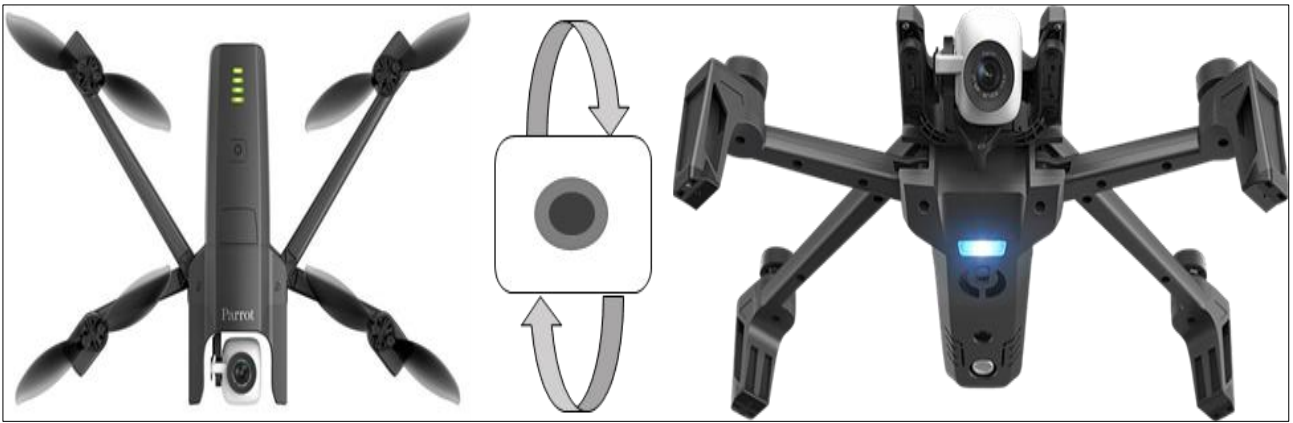


Figure 1. Parrot ANAFI UAV and 180° rotating integrated camera



Figure 2. Image of Guesthouse Facades (A-Left Front Facade and Lines Showing Closeness to the Border Wall, B- Left Rear Facade, C- Right Front Facade, D- Right Rear Facade)

Oblique images are taken from an aerial platform (airplane, helicopter, or UAV) with cameras at a unique angle of 35° to 45° from a nadir angle. Oblique images allow you to see every facade

of buildings and structures that cannot be seen in aerial images taken from a nadir angle, showing blind points (Halıcı and Aydın, 2019; Kun and Güler, 2019).

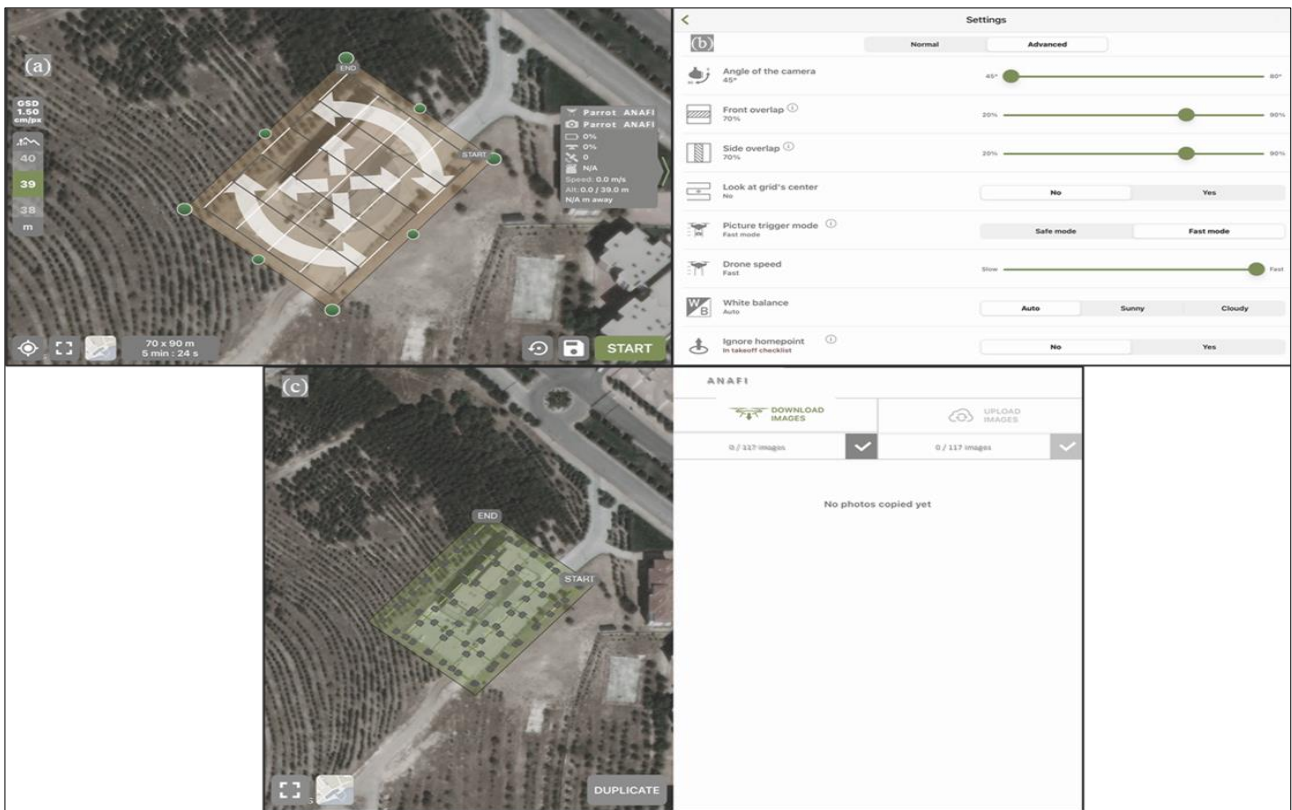


Figure 3. UAV Flight Planning Oblique Image Acquisition (A- Flight planning, B- Flight planning details, C- Post-flight details)

3. RESULTS

The aerial images acquisition by the UAV flight and the GCPs coordinates obtained from the field by GNSS were imported to the UAV image processing software and evaluated. As the first step, the images were matched each other. A sparse cloud point was produced by finding the matching points in the common areas between this process step and the aerial images. In addition, together with the sparse

point cloud, the camera's interior orientation parameters are automatically taken from the software library. Calibrating UAV cameras does not result in a huge increase in inaccuracy. Previous research shows that it would be appropriate to apply default camera parameters rather than calibrating the UAV Camera (Cramer et al., 2017; Przybilla et al., 2020). The camera's interior orientation parameters can be seen in the camera calibration report (Table 2).

Table 2. The camera's interior orientation parameters

	Value (px.)	Error	F	Cx	Cy	B ₁	B ₂	K ₁	K ₂	K ₃	K ₄	P ₁	P ₂
F	3683.58	0.15	1.00	0.04	-0.63	-0.24	-0.07	-0.20	0.24	-0.21	0.19	0.05	-0.60
Cx	-9.93684	0.15		1.00	-0.04	0.02	0.07	0.05	-0.03	0.02	-0.02	0.95	-0.05
Cy	12.9434	0.2			1.00	-0.08	0.01	-0.09	0.03	-0.03	0.03	-0.03	0.92
B ₁	-0.0132771	0.039				1.00	0.06	-0.06	0.03	-0.04	0.04	0.00	0.11
B ₂	0.779038	0.027					1.00	-0.02	-0.01	0.02	-0.02	0.03	0.01
K ₁	0.0201138	0.00022						1.00	-0.97	0.92	-0.87	0.03	-0.09
K ₂	-0.0784011	0.0011							1.00	-0.99	0.96	-0.02	0.04
K ₃	0.145407	0.0024								1.00	-0.99	0.01	-0.04
K ₄	-0.0903802	0.0016									1.00	-0.00	0.04
P ₁	-0.000301835	1.3×10 ⁻⁵										1.00	-0.05
P ₂	0.00037642	1.4×10 ⁻⁵											1.00

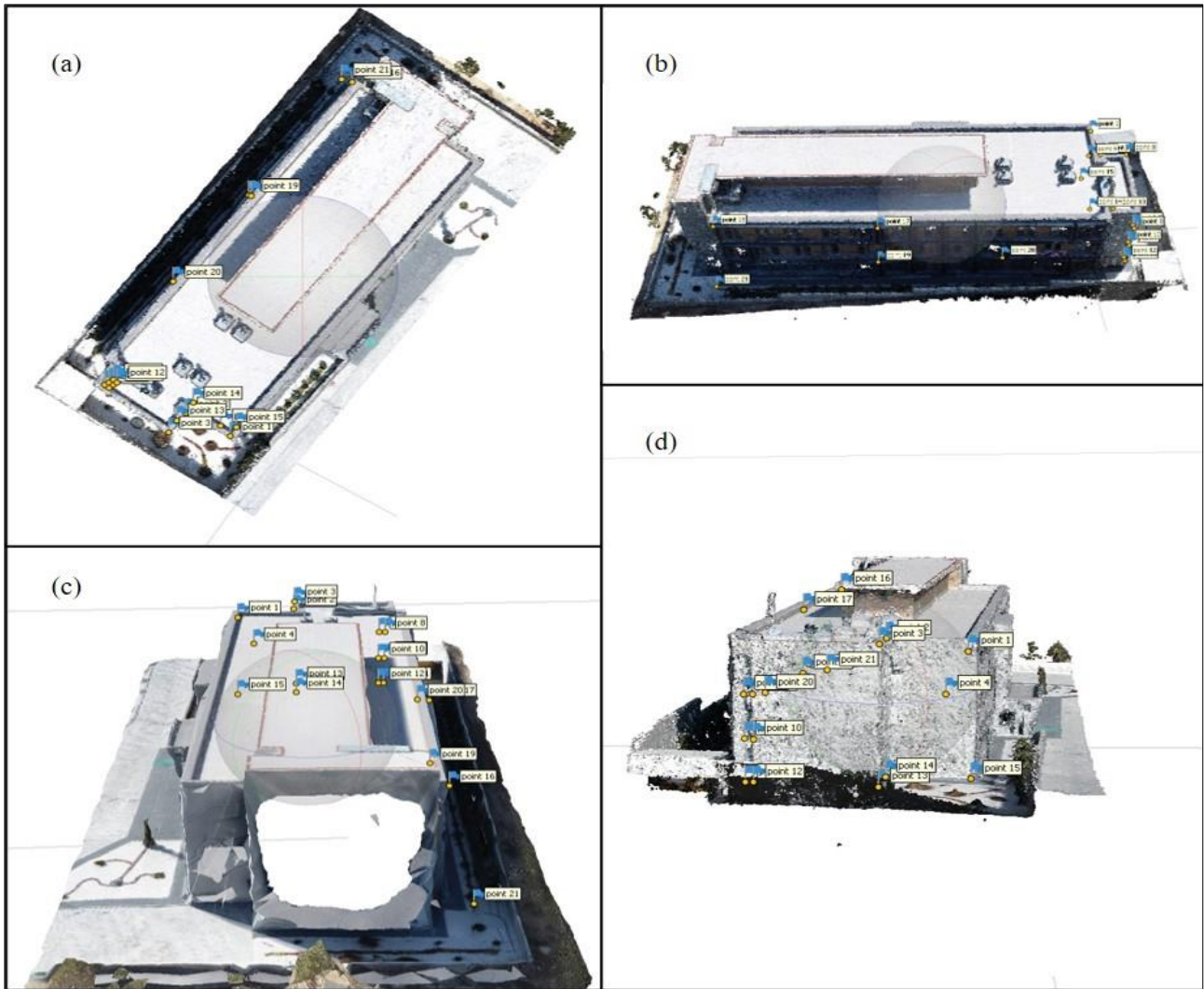


Figure 4. Dense point cloud data (A- Top View, B- Rear View, C- Right Side View, D- Left Side View)

As a next step, GCPs are defined for conversion and scaling to the field coordinate system. In the following step, a dense point cloud was created, in which the color information was also defined (Figure 4). The dense point cloud is based on the principle of compaction of optimal points by interpolation. After this step, where the software combines the depth information for each image acquisition point into a single set of dense points, the software creates the Triangulated Irregular Networks (TIN) by combining the dense point data with the color data (Figure 5). Then, the mesh model and texture model are produced using the TIN layer. The outcoming dense point clouds also form the basis for DEM and orthophoto.

The flights performed in the research caused some gaps in some parts of the 3D model of the building (especially the side facades and flat walls).

This problem is experienced for most of the objects that do not contain enough details in UAV photogrammetry. The point clouds (sparse and dense) generated by the software depend on the location of the acquisition centers of the images (appropriateness of the epipolar geometry) and the extraction of matchable detail in the images. When the error distributions of these produced points are reviewed, it is understood that the adjustment of coarsely faulted points is less than the mean faulty points. In addition, point distributions are proper to the aim of the study, except (right facade of the guesthouse) for a single facade.

As a scientific contribution, it can be said that oblique images can produce results such as rare images. This study shows that oblique images can provide a good alternative to situations where rare images are not likely to be very successful.

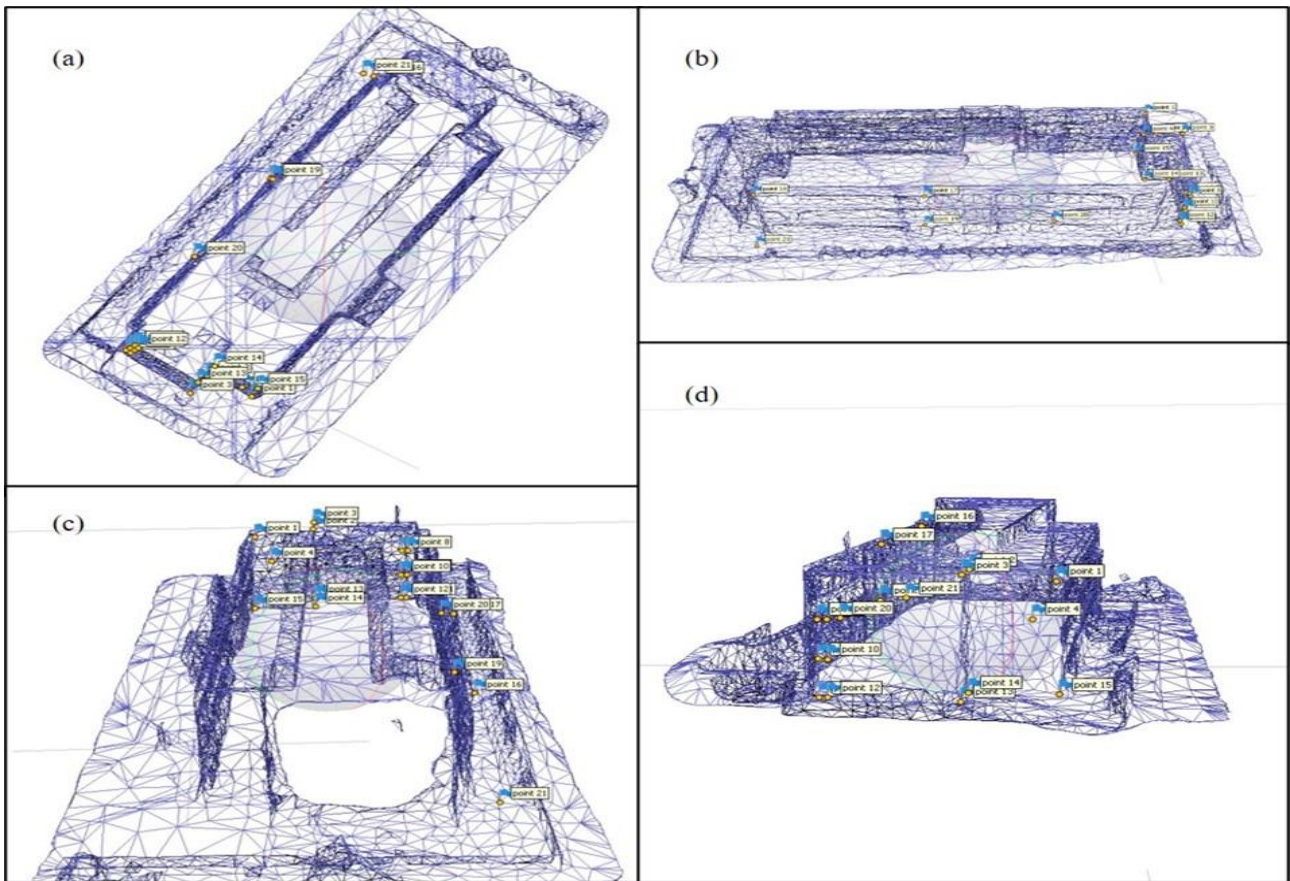


Figure 5. Triangulated Irregular Networks (A- Top View, B- Rear View, C- Right Side View, D- Left Side View)

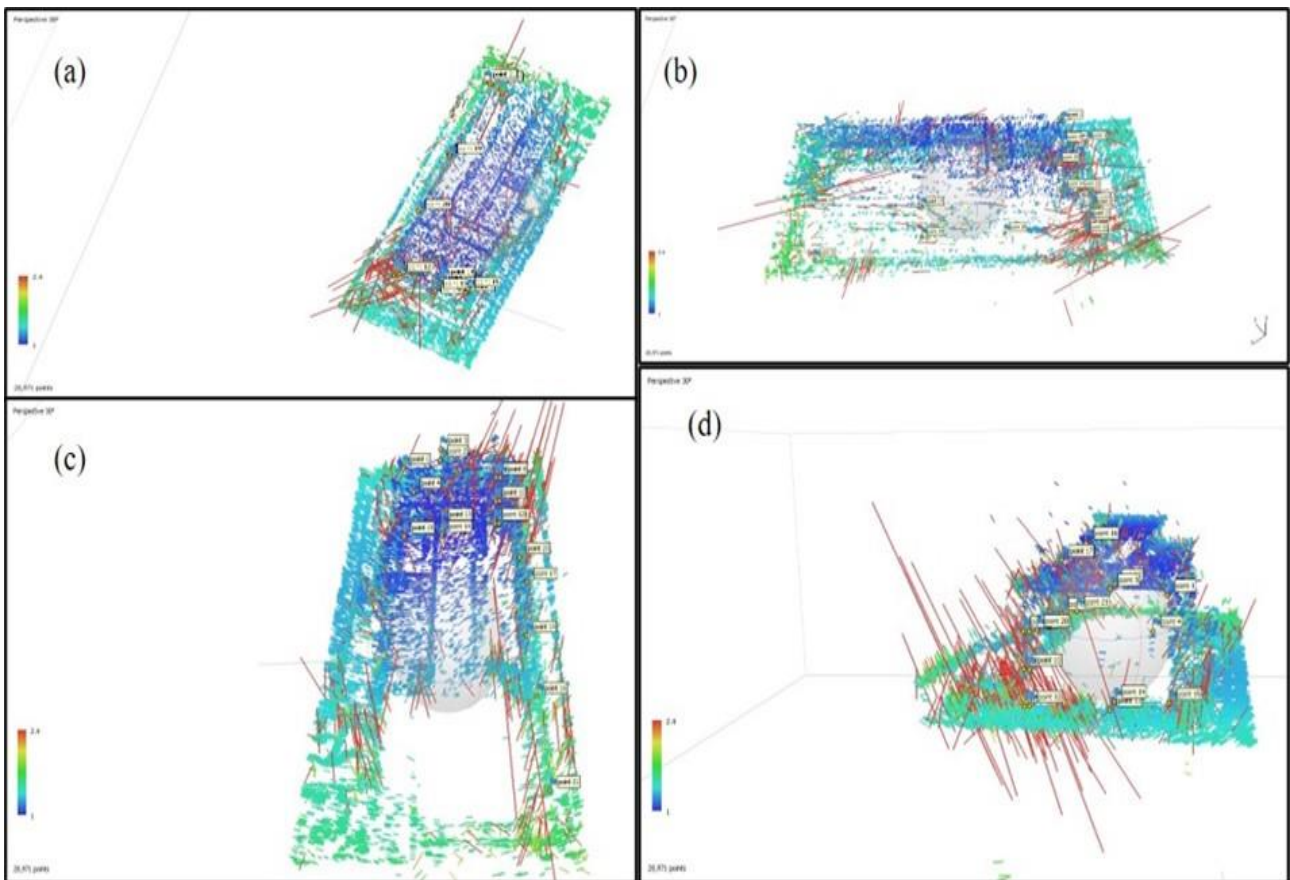


Figure 6. The error (pixel unit) of Points and their distribution to facades (A- Top View, B- Rear View, C- Right Side View, D- Left Side View)



Figure 7. Orthomosaic

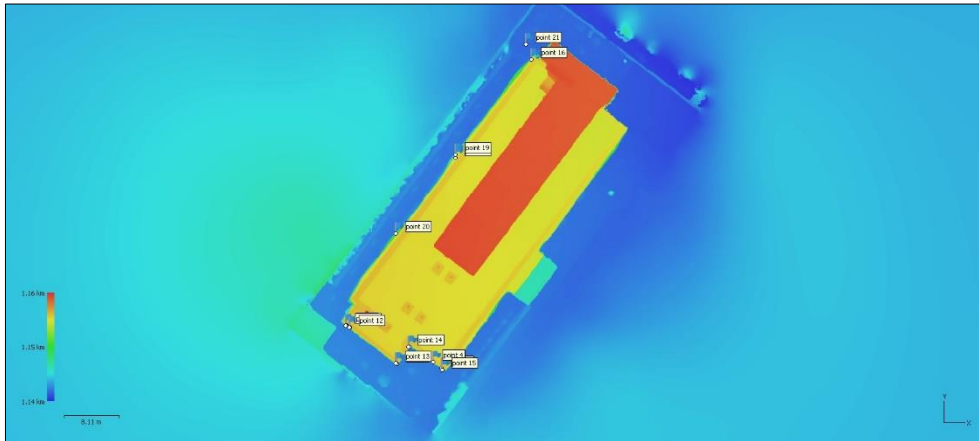


Figure 8. DEM

Oblique images were stuck together and obtained orthomosaic. This product is almost identical to the orthomosaic images taken with the nadir angle (Figure 7). In addition, DEM produced from oblique images allows a geometrically satisfactory result (Figure 8).

4. CONCLUSIONS

The orthomosaic and DEM obtained from oblique images are almost exactly the same as the orthomosaic and DEM produced from images taken in reality from the nadir angle. However, technical structures such as facade images, created TINs, meshes, and textures provide the results acquired with oblique images to be evaluated more efficiently. This research aimed to construct 3D models from oblique images and reduce the gaps in the outcomes acquired with the nadir direction 3D models.

It has been understood that almost all structural gaps in the final products can be closed by taking oblique images with the UAV. However, it has been determined that other methods are still needed for structures such as a plain wall without a pattern.

Acknowledgement

This work is supported by Konya Technical University Scientific Research Projects Coordinatorship with Project number 191005034.

Author Contributions

Hasan Bilgehan MAKİNEÇİ: Conceptualization, Data curation Methodology, Software, Writing-Original draft preparation. **Lütfiye KARASAKA:** Conceptualization, Methodology, Writing-Reviewing and Editing.

Conflicts of Interest

The authors declare no conflict of interest.

REFERENCES

- Achille, C., Adami, A., Chiarini, S., Cremonesi, S., Fassi, F., Fregonese, L., & Taffurelli, L. (2015). UAV-based photogrammetry and integrated technologies for architectural applications-Methodological strategies for the after-quake survey of vertical structures in Mantua (Italy). *Sensors*, 15 (7), 15520-15539.
- Aicardi, I., Chiabrando, F., Grasso, N., Lingua, A.M., Noardo, F., & Spanò, A. (2016). UAV photogrammetry with oblique images: first analysis on data acquisition and processing. *International Archives of the Photogrammetry, Remote Sensing & Spatial Information Sciences*, 41.
- Cramer, M., Przybilla, H.J., & Zurhorst, A. (2017). UAV cameras: Overview and geometric calibration benchmark. *The International Archives of Photogrammetry, Remote Sensing and Spatial Information Sciences*, 42, 85.
- Erdönmez, M. (2018). Application of oblique photogrammetry with the help of unmanned aerial vehicles in structured areas (Master's thesis). Necmettin Erbakan University, Konya, Turkey (in Turkish).
- Halıcı, E., & Aydın, C.C. (2019). Eğik fotoğraflar ile 3 boyutlu kent modeli üretimi ve kullanım alanları. *Türkiye Coğrafi Bilgi Sistemleri Dergisi*, 1 (1), 14-26.
- Jo, Y.H., & Hong, S. (2019). Three-dimensional digital documentation of cultural heritage site based on the convergence of terrestrial laser scanning and unmanned aerial vehicle photogrammetry. *ISPRS International Journal of Geo-Information*, 8(2), 53.
- Kun, M., & Güler, Ö. (2019). İnsansız görüntüleme sistemleri ile elde edilen sayısal yüzey modellerinin mermer madenciliğinde kullanımı. *Dokuz Eylül Üniversitesi Mühendislik Fakültesi Fen ve Mühendislik Dergisi*, 21(63), 1005-1013.
- Przybilla, H.J., Baumker, M., Luhmann, T., Hastedt, H., & Eilers, M. (2020). Interaction between direct georeferencing, control point configuration and camera self-calibration for RTK-Based UAV photogrammetry. *The International Archives of Photogrammetry, Remote Sensing and Spatial Information Sciences*, 43, 485-492.
- Rossi, P., Mancini, F., Dubbini, M., Mazzone, F., & Capra, A. (2017). Combining nadir and oblique UAV imagery to reconstruct quarry topography: methodology and feasibility analysis. *European Journal of Remote Sensing*, 50 (1), 211-221.
- Toprak, A.S., Polat, N., & Uysal, M. (2019). 3D modeling of lion tombstones with UAV photogrammetry: a case study in ancient Phrygia (Turkey). *Archaeological and Anthropological Sciences*, 11(5), 1973-1976.
- Tuncer, S., Çömert, R., & Avdan, U. (2018). Tarihi yapıların belgelenmesinde farklı yöntemlerle elde edilen verilerin entegrasyonu. *VII. Uzaktan Algılama-Cbs Sempozyumu (UZAL-CBS 2018), 18-21 Eylül 2018, Eskişehir*.
- Uysal, M., Toprak, A.S., & Polat, N. (2015). DEM generation with UAV Photogrammetry and accuracy analysis in Sahitler hill. *Measurement*, 73, 539-543.
- Vacca, G., Dessì, A., & Sacco, A. (2017). The use of nadir and oblique UAV images for building knowledge. *ISPRS International Journal of Geo-Information*, 6 (12), 393.
- Valenti, R., & Paternò, E. (2019). A comparison between TLS and UAV technologies for historical investigation. *ISPRS-International Archives of the Photogrammetry, Remote Sensing and Spatial Information Sciences*, 42(2), 739-745.
- Yastikli, N., & Özerdem Ö.Z. (2017). Architectural heritage documentation by using low cost UAV with fisheye lens: Otag-i Humayun in Istanbul as a case study. *ISPRS Annals of the Photogrammetry, Remote Sensing and Spatial Information Sciences*, 4, 415.
- Zeybek, M., & Kaya, A. (2020). Tarihi yağma kiliselerde hasarların fotogrametrik ölçme tekniğiyle incelenmesi: Artvin Tbeti kilisesi örneği. *Geomatik*, 5 (1), 47-57.
- Url-1:
<https://www.sony.com/en/SonyInfo/News/Press/201411/14-112E/> (last accessed 27 June 2021)



Monitoring of continuous GNSS stations in Central Anatolia region

Abdulmalek Redhwan ^{*1}, Hediye Erdoğan ¹, Osman Oktar ¹, Cemil Gezgin ¹

¹Aksaray University, Faculty of Engineering, Department of Geomatics Engineering, Aksaray, Turkey

Keywords

GNSS
ITRF
Central Anatolia Region
Time Series Analysis
Trend Component
Analysis

ABSTRACT

In this study, the linear behaviors in the North, East and Up directions of 30 CORS-TR stations in the Central Anatolian Region were obtained by the trend component analysis which is the time series component. The time series of the stations between 2017-2020 years were calculated in the Eurasia-fixed frame with the GAMIT/GLOBK software. As a result of the analysis, the average horizontal velocity of the stations in the east of the Central Anatolian Region is 17.59 mm/year in the northwest direction, and the average horizontal velocity of the stations in the west is 18.66 mm/year in the southwest direction. This movement shows the movement of the Anatolian plate in the southwest direction in terms of direction and velocity and is in agreement with other research results. In the linear changes in the up coordinates of the stations, the greatest linear change was detected at the KNY1 (-48.22 mm/year) station. It is thought that this change at station KNY1 is due to the decrease in groundwater level in this region (Konya Closed Basin). In addition, in the standard deviation (m_0) values of the time series that obtained as a result of the analysis, linear changes were approximately the same for the north and east directions, and about 2-3 times larger for the up values compared to the north or east directions.

1. INTRODUCTION

As one of the most tectonically active regions of the world, Turkey is located in an active earthquake zone. It is quite possible to encounter fault zones in engineering studies. Two of the most important (active) faults in Turkey are the North Anatolian and East Anatolian Fault Zones. The North Anatolian Fault (NAF), which extends from Karlıova in eastern Turkey to Saros Bay in the North Aegean Sea, is one of the longest active strike-slip faults in the world with a length of approximately 1500 km (Yavaşoğlu et al., 2011).

As it is known, due to the fact that Turkey is located at the intersection of the Arabian, Anatolian and Eurasian tectonic plates, annual changes (plate velocity) occur due to the movement of these plates in cm order at point locations. For this reason, it is important to determine the point location information accurately, continuously, quickly and economically with reliable methods and to present it to the relevant users who do both commercial and scientific studies in location-based studies.

Today, Global Navigation Satellite Systems (GNSS) are widely used to determine point locations. In particular, it has a wide range of uses such as tectonic movements, land subsidence, engineering services, scientific studies, aviation industry, navigation, vehicle tracking systems, military areas, and therefore has a large number of users (Uzel et al., 2013; Oktar and Erdoğan, 2018; Mutlu and Kahveci, 2019; Gezgin et al., 2020; Yalvaç, 2020; Orhan, 2021).

There are also many error sources that GNSS systems with reliable location services are exposed to. These are satellite-related such as satellite clock error, satellite orbital errors; errors originating from the receiver such as receiver clock error, antenna phase center error, and atmospheric errors such as tropospheric effect, ionospheric effect, signal reflection effect. The effect of these error sources on the results can be neglected according to the sensitivity of the work being done. However, in applications where precision is required such as geodetic studies, tectonic studies, continental deformations, it is important to create a

* Corresponding Author

*(abdulmalekredhwan2017@gmail.com) ORCID ID 0000-0003-3921-0315
(hediye.erdogan@aksaray.edu.tr) ORCID ID 0000-0002-6470-5857
(osmanoktar@aksaray.edu.tr) ORCID ID 0000-0001-6764-0561
(cemilgezgin.jfm@gmail.com) ORCID ID 0000-0002-5951-0107

Cite this article

Redhwan A., Erdoğan H., Oktar O., & Gezgin C. (2021). Monitoring of continuous GNSS stations in Central Anatolia region. Turkish Journal of Geosciences 2(2), 21-29.

mathematical model of these errors to eliminate the error sources (Mutlu and Kahveci, 2019).

In this study, the behaviors of 30 Continuously Operating Reference Stations-Turkey (TUSAGA-Aktif/CORS-TR) stations in the Central Anatolia Region were investigated with linear trend function. The coordinates of the stations were produced from the daily time series obtained between years of 2017-2020. The coordinates of the stations are the time series obtained daily between 2017 and 2020 for the Eurasia fixed-frame. The velocity values and directions of the region were estimated in the Eurasia fixed-frame by liner trend component of the time series analysis.

2. CENTRAL ANATOLIA EARTHQUAKE ZONE

Kırşehir, which is located in the great arc of Kızılırmak in Central Anatolia and consists of metamorphic and platonitic rocks, seems to have been divided into blocks from many parts by faults. The parts between the blocks were filled with Neogene sediments. These regions formed by faults are the main earthquake belts of Central Anatolia and 1938 Kırşehir earthquake occurred in this region. In this earthquake, 160 people lost their lives and 4066 buildings were destroyed or severely damaged. In addition to that 50 people died in the 1951 Kurşunlu (Çankırı) earthquake (Özdoğan, 1993).

Also, in the north of Ankara, faults in the northeast-southwest direction form parallel fracture zones in the direction of Kızılcahamam-Güdül-Ayaş and Çamlıdere-Bey pazarı. This shows that in the earthquakes in Central Anatolia, in addition to the "North Anatolian Earthquake Zone", the independent earthquake centers also have significant effects. Because the 1944 Bey pazarı and 1956 Eskişehir earthquakes are the results of an independent earthquake center. Another fault zone in Central Anatolia is located in the west of Tuz Gölü. Fractures running parallel to each other formed a belt. However, earthquakes causing massive damage were not detected either in Konya and its surroundings or in other settlements in this area (Özdoğan, 1993).

3. TIME SERIES ANALYSIS

Time series analysis provides useful information about the behavior of systems based on response or effect size. The sequential realization of the observed data over time is very important in terms of monitoring and analyzing the development of the data (Ostini, 2012).

In general, the $X(t_i)$ time series of measurements made at GNSS stations at times t_i ($i=1,2,3,\dots,N$) can be divided into three components, excluding artificial or co-seismic and seismic-induced deviations. These components are given in equation (1).

$$X(t_i) = Y(t_i)_{trend} + Y(t_i)_{periodic} + Y(t_i)_{stochastic} \quad (1)$$

In time series analysis, firstly the time axis of the series is plotted, unusual measurements (e.g. gross errors) in the series are eliminated and a general interpretation of the series can be made (Oktar, 2015).

3.1 Trend Component

Trend is the development or progress of a time series in a certain direction in the long run. The direction and intensity of the trend do not always remain constant. The trend can be linear or curvilinear (Equation 2).

$$Y(t_i) = \underbrace{a + bt}_{(1)Trend\ Component} \quad (2)$$

Here, "a" constant and "b" are the parameters that show the amount and direction of linear change with time. For GNSS stations, the increasing or decreasing linear changes (velocities) of the GNSS stations are determined with the "b" parameter. Considering the linear function given in Equation 2 for the estimation of the parameters in the time series $Y(t_i)$.

$$Y(t_i) = a + bt \quad (3)$$

$$= Ax + v(t_i) \quad (4)$$

$$A^T = \begin{bmatrix} 1 & 1 & 1, \dots, N \\ t_1 & t_2 & t_3, \dots, t_N \end{bmatrix}, X^T = [a \ b] \quad (5)$$

According to the least squares method, parameters "a", "b" and their standard deviations m_a and m_b are estimated. Test size values are calculated for each parameter.

$$t_a = \frac{a}{m_a}; t_b = \frac{b}{m_b} \quad (6)$$

The predicted $1-\alpha$ confidence level for the test sizes and the $t_{f,1-\alpha/2}$ confidence limit of the t distribution depending on the f degree of freedom are compared.

$$|t_a|; |t_b| < t_{f,1-\alpha/2} \quad (7)$$

If the situation is as seen in the equation given in 7, the parameters are insignificant,

$$|t_a|; |t_b| \geq t_{f,1-\alpha/2} \quad (8)$$

If the values above test size, parameters are significant at the estimated confidence level. If the parameters are statistically significant, it is decided that there is a trend component in the series.

In the process of determining the trend component in the time series, it is not possible to determine the existence of linear change and to accurately detect some periodic movements due to the long period of time for a full periodic movement to occur. For this reason, it is very important that the

measurements are made as long as necessary to reflect the changes in the monitored system, data or the existence of the trend must be interpreted correctly.

4. STUDY FINDINGS AND DISCUSSION

In this study, the linear behaviors of 30 TUSAGA-Aktif/CORS-TR stations in the Central Anatolia Region covering the years of 2017-2020 were investigated with the trend component function, which is the time series component. To this end; N (North), E (East) and U (Up) components of daily coordinate times series of the stations; AKD1, AKHR, AKSR, ANK2, ANRK, BEYS, BOG1, CANK, CIHA, CMLD, ESKS, GEME, GURU, HALP, KAMN, KAP1, KAYS, KIS1, KKAL, KLUU, KNY1, NAHA, NEV1, NIGD, SARV, SIH1, SIVS, SSE1, YOZ1 and YUN1 were used.

With the linear functions applied to the obtained time series, the linear changes (velocity values) of the stations in the determined time interval were calculated, and the linear behavior and functions of the stations were defined in the Eurasia Fixed system. General information about the IGS stations (14 sites) used in the processing is given in Table 1. GNSS data were evaluated with GAMIT/GLOBK software, an open-source software package developed by Massachusetts Institute of Technology (MIT) (Url-1). In the processing, for orbit information, Precise final orbits by the International Global Navigation Satellite Systems (GNSS) Service (IGS), for earth rotation parameters USNO_bull_b, for radiation and pressure effects 9-parameter Berne model was used. LC (L3), that is the ionosphere-free linear combination of the L1 and L2 carrier waves, and the FES2004 Ocean Tide Loading (OTL) grid was used. Time series of stations were obtained using

RINEX data that acquired from the web interface given in Url-2.

Table 1. IGS stations used in the processing

Station	City/ Country	Station	City / Country
ANKR	Ankara/ Turkey	MATE	Matera/ Italy
BAKU	Baku/ Azerbaijan	NICO	Nicosia/ South Cyprus
BUCU	Bucharest/ Romania	RAMO	MitzpeRamon/ Israel
CRAO	Simeiz/ Ukraine	SOFI	Sofia/ Bulgaria
GLSV	Kiev/ Ukraine	TEHN	Tehran/ Iran
GRAZ	Graz/Austria	TELA	Tel Aviv/ Israel
ISTA	İstanbul/ Turkey	TUBI	Gebze/ Turkey

4.1 The Field Study and Data

In this study, daily coordinate data of the 30 GNSS stations such as AKD1, AKHR, AKSR, ANK2, ANRK, BEYS, BOG1, CANK, CIHA, CMLD, ESKS, GEME, GURU, HALP, KAMN, KAP1, KAYS, KIS1, KKAL, KLUU, KNY1, NAHA, NEV1, NIGD, SARV, SIH1, SIVS, SSE1, YOZ1 and YUN1 were used in the analysis that located in the Central Anatolia Region. Location information of the stations are given in Figure 1 and Table 2. The GNSS data used in the study are the daily coordinate values between 01.01.2017 and 31.12.2020, and the data information of the stations are given in Table 3. In the evaluations and analyzes, there were data deficiencies and gaps between years in the daily coordinate data of GNSS stations between 01.01.2017-31.12.2020 due to reasons such as antenna defect, computer malfunction, etc.

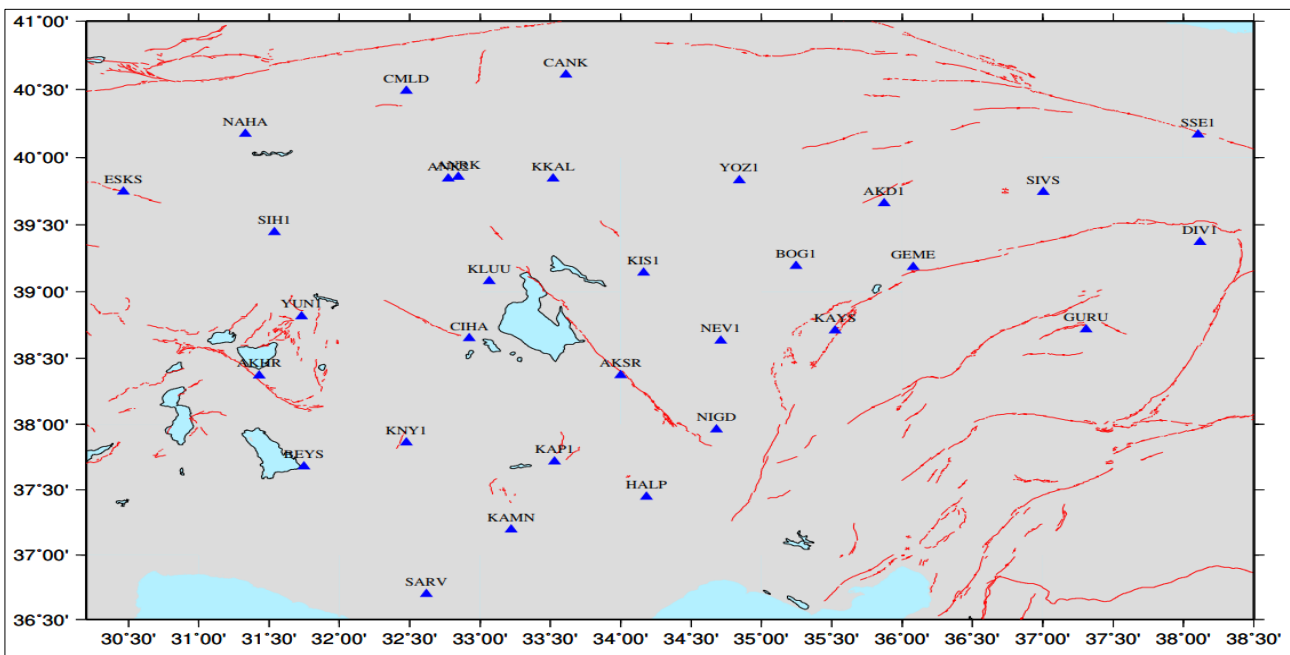


Figure 1. GNSS stations locations

Table 2. GNSS stations general information

Short Name	City/ Town	Latitude (Decimal Degree)	Longitude (Decimal Degree)	Short Name	City/ Town	Latitude (Decimal Degree)	Longitude (Decimal Degree)
AKD1	Yozgat/Akdağmadeni	39.6605	35.8711	KAP1	Konya/Karapınar	37.7144	33.5283
AKHR	Konya/Akşehir	38.3693	31.4297	KAYS	Kayseri/Melikgazi	38.7137	35.5031
AKSR	Aksaray/Merkez	38.3704	33.9982	KIS1	Kırşehir/Merkez	39.1434	34.1631
ANK2	Ankara/Çankaya	39.8428	32.7754	KKAL	Kırıkkale/Merkez	39.8433	33.5179
ANRK	Ankara/Çankaya	39.8560	32.8462	KLUU	Konya/Kulu	39.0791	33.0654
BEYS	Konya/Beyşehir	37.6773	31.7466	KNY1	Konya/Meram	37.8594	32.4764
BOG1	Yozgat/Boğazlıyan	39.1933	35.2471	NAHA	Ankara/Nallıhan	40.1733	31.3321
CANK	Çankırı/Merkez	40.6086	33.6104	NEV1	Nevşehir/Merkez	38.6315	34.7108
CIHA	Konya/Cihanbeyli	38.6504	32.9224	NIGD	Niğde/Merkez	37.9588	34.6794
CMLD	Ankara/Çamlidere	40.4910	32.4745	SARV	Karaman/Sarveliler	36.6967	32.6173
DIV1	Sivas/Divriği	39.3718	38.1194	SIH1	Eskişehir/Sivrihisar	39.4465	31.5363
ESKS	Eskişehir/Turgutlar	39.7457	30.4636	SIVS	Sivas/Merkez	39.7437	37.0025
GEME	Sivas/Gemerek	39.1851	36.0809	SSE1	Sivas/Suşehri	40.1691	38.1050
GURU	Sivas/Gürün	38.7174	37.3079	YOZ1	Yozgat/Merkez	39.8314	34.8447
HALP	Konya/Halkapınar	37.4451	34.1834	YUN1	Konya/Yunak	38.8162	31.7317
KAMN	Karaman/Merkez	37.1932	33.2203				

Data numbers and missing data percentages of these stations are given in Table 3. Data percentages of other stations are certain except AKD1, ANRK, BOG1, CANK, CMLD, KAP1, KAYS, KIS1, SARV, SIH1,

SIVS, YOZ1 and YUN1. In addition, since KIS1 and ANK2 stations are newly established, their data is used for 1 year, AKD1 station for 2 years, BOG1, NEV1 and SSE1 for 3 years.

Table 3. GNSS stations data and percentages

Station Name	Beginning	Finish	Number of Data	Missing Data(%)	Station Name	Beginning	Finish	Number of Data	Missing Data(%)
AKD1	01.01.2019	31.12.2020	620	0.8	KAP1	19.06.2017	31.12.2020	1268	0.9
AKHR	01.01.2017	31.12.2020	1460	0	KAYS	01.01.2017	31.12.2020	1436	1
AKSR	01.01.2017	31.12.2020	1455	0	KIS1	12.02.2020	31.12.2020	323	0.9
ANK2	01.01.2020	31.12.2020	365	0	KKAL	01.01.2017	31.12.2020	1460	0
ANRK	01.01.2017	31.12.2020	1435	1	KLUU	01.01.2017	31.12.2020	1460	0
BEYS	01.01.2017	31.12.2020	1460	0	KNY1	01.01.2017	31.12.2020	1460	0
BOG1	01.01.2018	31.12.2020	1095	0.7	NAHA	01.01.2017	31.12.2020	1460	0
CANK	01.01.2017	31.12.2020	1431	0.9	NEV1	01.01.2018	31.12.2020	1095	0
CIHA	01.01.2017	31.12.2020	1460	0	NIGD	01.01.2017	31.12.2020	1460	0
CMLD	01.01.2017	31.12.2020	1411	1	SARV	01.01.2017	31.12.2020	1263	0.9
ESKS	01.01.2017	31.12.2020	1460	0	SIH1	01.01.2017	25.06.2020	1047	0.7
GEME	01.01.2017	31.12.2020	1460	0	SIVS	01.01.2017	31.12.2020	1169	0.8
GURU	01.01.2017	31.12.2020	1460	0	SSE1	01.01.2018	31.12.2020	1095	0
HALP	01.01.2017	31.12.2020	1460	0	YOZ1	01.01.2017	31.12.2020	1405	1
KAMN	01.01.2017	31.12.2020	1460	0	YUN1	01.01.2017	31.12.2020	1397	1

4.2 GNSS Stations Time Series

For the time series analysis, BASK, SIVS, YAZ1, CANK, ANRK, CALM, AKD1 and YUN1 stations were considered as two data groups, and SARV and SIH1 stations as three data groups due to the large data gaps in some of the stations. The time interval of time series data obtained by taking Eurasia plate as constant is given in Table 3.

In this study, raw coordinate time series were created by subtracting the first coordinate value

from all coordinates in order to see the change of raw coordinates relative to the beginning.

In Figure 2, 3 and 4, it is clearly seen that the time series of KAP1 North (increase), East (decrease) and Up (decrease) raw coordinates contain a linear movement, and in addition, a one (1) year periodic movement is seen in the time series of the northing coordinates. Time series of the remaining stations are not given in this study due to the large number of data and figures.

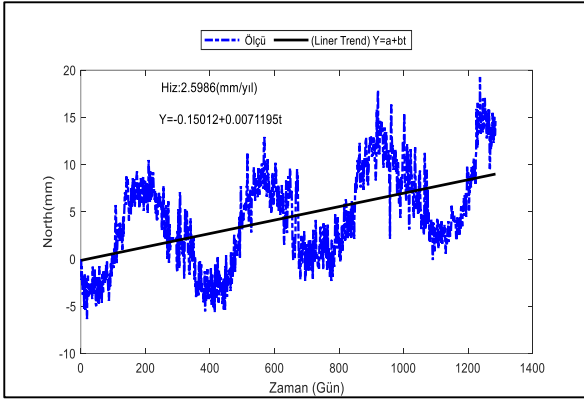


Figure 2. KAP1 North coordinate component linear model

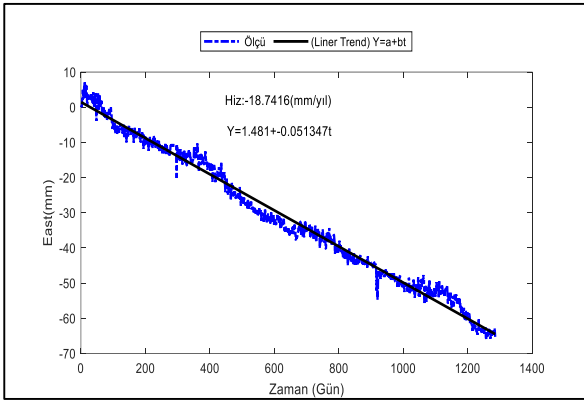


Figure 3. KAP1 East coordinate component linear model

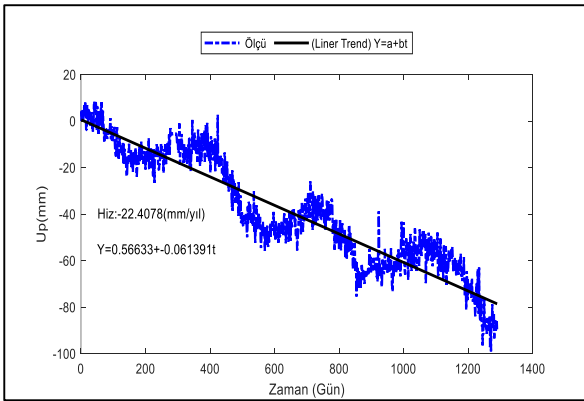


Figure 4. KAP1 Up coordinate component linear model

The linear trend component analysis of the time series was performed by calculating the “a” and “b” parameters and standard deviations given in Equation 3.2 according to the least squares method. The calculated test sizes were compared with the $\alpha=0.05$ significance level and the $t_{f,1-\alpha/2}$ confidence limit of the t distribution depending on the f degree of freedom, and statistically significant linear

movements were detected in the time series of all GNSS stations. Obtained results and functions are given in Table 4.

When Table 4 is examined, it is seen that CANK_1, CIHA, ANRK_1, ANKR, SERV_2, CALM_1, CALM_2, BEYS, YUN1_1, YUN1_2, SIH1_1, SIH1_2, SIH1_3, AKHR, NAHA, ESKS, BUCU and ANK2 stations have linear movements in the south direction, while the other stations have linear movements in the north direction.

The eastward movements were detected in stations; BASK_1, BASK_2, GURU, SIVS_1, SIVS_2, GEME, KAYS, YOZ1_1, YOZ1_2, NIGD, HALP, AKSR, CANK_1, CANK_2, KKAL, KAMN, KLUU, CIHA, ANRK_1, ANRK_2, ANKR, SARV1, SARV_2, SARV_3, CALM_1, CALM_2, BEYS, YUN1_1, YUN1_2, SIH1_1, SIH1_2, AKHR, NAHA, ESKS, BOR1, KAP1, BOG1, NIV1, AKD1_1, AKD1_2, ANK2, KIS1 and westward movements were detected at SIH1_3 and BUCU stations. The largest linear movement in the west direction (23.29 mm/year) was detected at ANKR station, and the smallest linear movement (0.36 mm/year) was detected at BUCU station.

In addition, the largest annual linear movement in the north direction of 15.51 mm was observed at BASK_1 station, and the smallest annual linear movement in the south direction of 0.06 mm was observed at ANRK_1 station. Considering the linear movements in the time series of the Up coordinates of the stations; (Table 4) BASK_1, BASK_2, SIVS_1, SIVS_2, GEME, KAYS, YOZ1_1, YOZ1_2, NIGD, HALP, KKAL, KLUU, ANRK_1, ANRK_2, SARV_2, SARV_3, CALM_1, CALM_2, BEYS, YUN1_1, YUN1_2, KSSI, BUCU, SSE1, AKD1_2 and ANK2 linear movements in the direction were observed in the positive direction, it was seen that the up values of the stations listed above are increased.

The highest linear motion was calculated at the SARV_3 station with a value of 29.75 mm/year and the lowest linear motion was calculated at the YOZ1_2 station with a value of 0.10 mm/year. Linear movements in up coordinates of GURU, AKSR, CANK_1, CANK_2, KAMN, CIHA, ANKR, SARV_1, KNY1, SIH1_3, AKHR, KAP1, BOG1, NIV1, and AKD1_1 stations are in (-) negative direction. In the up time series, the largest linear movement was detected at KNY1 station with a value of -48.22 mm/year and the smallest linear movement was determined at station NEV1 with a value of -0.15 mm/year. In addition, a change of approximately -22.41 mm/year is observed at KAP1 station (Table 4). It is thought that the KNY1 and KAP1 stations are located in the areas where the groundwater level decreases in the Konya Closed Basin, and the negative (-) change in these stations is related with the decrease in the water level. Many studies have been carried out on the decrease in groundwater level in this region. See for detailed information; Üstün et al. 2007; Üstün et al. 2015; Özdemir, 2014; Orhan et al. 2020; Orhan 2021.

Table 4. Linear models and annual rates of GNSS stations (Eurasian-fixed frame)

Station Name	$y(t) = a+bt$ NORTH Linear Model	Speed = $365*b$ (mm/year)	$y(t) = a+bt$ EAST Linear Model	Speed = $365*b$ (mm/year)	Resultant Speed (mm/year)		$y(t) = a+bt$ Up Linear Model	Speed = $365*b$ (mm/year)
BASK_1	$y(t) = 1.341+0.0425t$	15.51	$y(t) = -2.5443-0.0133t$	-4.84	16.25	Northwest	$y(t) = -5.1855+0.0193t$	7.04
BASK_2	$y(t) = 0.0217+0.0419t$	15.29	$y(t) = -1.7058-0.0126t$	-4.61	15.97	Northwest	$y(t) = 8.6337+0.0138t$	5.02
GURU	$y(t) = 0.7210+0.0252t$	9.19	$y(t) = -0.1948-0.0438t$	-15.99	18.44	Northwest	$y(t) = 1.6579-0.0006t$	-0.22
SIVS_1	$y(t) = 0.3337+0.0194t$	7.08	$y(t) = -0.3377-0.0439t$	-16.01	17.50	Northwest	$y(t) = -3.1008+0.0163t$	5.97
SIVS_2	$y(t) = -2.1542+0.0236t$	8.63	$y(t) = -4.4541-0.0497t$	-18.13	20.08	Northwest	$y(t) = -21.3763+0.0042t$	1.52
GEME	$y(t) = -7.7208+0.0247t$	9.01	$y(t) = -2.3107-0.0418t$	-15.25	17.71	Northwest	$y(t) = -0.9210+0.0033t$	1.22
KAYS	$y(t) = -0.1221+0.0181t$	6.61	$y(t) = 0.0131-0.0442t$	-16.14	17.44	Northwest	$y(t) = 3.6273+0.0003t$	0.11
YOZ1_1	$y(t) = 0.8331+0.0103t$	3.75	$y(t) = 3.2804-0.0480t$	-17.53	17.92	Northwest	$y(t) = -5.2383+0.0119t$	4.35
YOZ1_2	$y(t) = 3.2809+0.0130t$	4.76	$y(t) = -0.3345-0.0511t$	-18.64	19.24	Northwest	$y(t) = -6.5517+0.0003t$	0.10
NIGD	$y(t) = -0.0879+0.0146t$	5.31	$y(t) = -1.6882-0.0408t$	-14.89	15.81	Northwest	$y(t) = -23.8459+0.0016t$	0.59
HALP	$y(t) = 1.1983+0.0151t$	5.53	$y(t) = -0.8474-0.0387t$	-13.41	14.50	Northwest	$y(t) = -6.7455+0.0028t$	1.04
AKSR	$y(t) = -1.3001+0.0085t$	3.10	$y(t) = 2.8935-0.0516t$	-18.82	19.07	Northwest	$y(t) = -14.5906-0.0205t$	-7.48
CANK_1	$y(t) = 1.9777-0.0017t$	-0.63	$y(t) = -2.5724-0.0482t$	-17.59	17.60	Southwest	$y(t) = -0.8255-0.0009t$	-0.33
CANK_2	$y(t) = -1.8853+0.0180t$	6.56	$y(t) = -1.0364-0.0439t$	-16.01	17.31	Northwest	$y(t) = 5.6662-0.0141t$	-5.15
KKAL	$y(t) = -0.4284+0.0038t$	1.39	$y(t) = 1.5088-0.0578t$	-21.11	21.16	Northwest	$y(t) = -12.8039+0.0030t$	1.08
KAMN	$y(t) = -1.4761+0.0119t$	4.36	$y(t) = 0.1776-0.0336t$	-12.28	13.03	Northwest	$y(t) = -19.9852-0.0137t$	-5.00
KLUU	$y(t) = -1.1815+0.0074t$	2.70	$y(t) = -1.3936-0.0522t$	-19.04	19.23	Northwest	$y(t) = -0.5096+0.0032t$	1.19
CIHA	$y(t) = 0.9653-0.0012t$	-0.45	$y(t) = 1.4483-0.0563t$	-20.55	20.55	Southwest	$y(t) = 1.0117-0.0079t$	-2.89
ANRK_1	$y(t) = 2.0997-0.0002t$	-0.06	$y(t) = 0.4200-0.0621t$	-22.66	22.66	Southwest	$y(t) = -5.7743+0.0111t$	4.06
ANRK_2	$y(t) = -0.7142+0.0006t$	0.23	$y(t) = 0.5205-0.0565t$	-20.64	20.64	Northwest	$y(t) = -4.8296+0.0135t$	4.93
ANKR	$y(t) = -0.1372-0.0023t$	-0.82	$y(t) = -2.1792-0.0638t$	-23.29	23.31	Southwest	$y(t) = -13.43-0.0124t$	-4.54
SARV_1	$y(t) = 1.8299+0.0077t$	2.81	$y(t) = -1.4094-0.0421t$	-15.36	15.61	Northwest	$y(t) = -12.3092-0.0047t$	-1.72
SARV_2	$y(t) = 4.1808-0.0233t$	-8.49	$y(t) = -6.1333-0.0213t$	-7.76	11.50	Southwest	$y(t) = -12.0975+0.0706t$	25.76
SARV_3	$y(t) = 4.5048+0.0149t$	5.45	$y(t) = -0.2086-0.0600t$	-21.90	22.57	Northwest	$y(t) = 7.528+0.0815t$	29.75
KNY1	$y(t) = 5.7047+0.0217t$	7.93	$y(t) = -5.6043-0.0505t$	-18.42	20.06	Northwest	$y(t) = -42.4959-0.1321t$	-48.22
CALM_1	$y(t) = 1.6803-0.0046t$	-1.66	$y(t) = 1.4626-0.0540t$	-19.71	19.78	Southwest	$y(t) = -3.4678+0.0065t$	2.38
CALM_2	$y(t) = 0.5128-0.0043t$	-1.58	$y(t) = 1.3307-0.0524t$	-19.14	19.21	Southwest	$y(t) = -4.3832+0.0011t$	0.39
BEYS	$y(t) = 0.4754-0.0076t$	-2.77	$y(t) = -0.4252-0.0436t$	-15.92	16.15	Southwest	$y(t) = -9.6745+0.0047t$	1.70
YUN1_1	$y(t) = -0.7425-0.0068t$	-2.48	$y(t) = 1.006-0.0575t$	-20.99	21.13	Southwest	$y(t) = 0.1629+0.0139t$	5.08
YUN1_2	$y(t) = -0.3143-0.0084t$	-3.07	$y(t) = 5.7488-0.0545t$	-19.89	20.13	Southwest	$y(t) = 3.9402+0.0155t$	5.65
SIH1_1	$y(t) = -0.9776-0.0085t$	-3.10	$y(t) = 0.1050-0.0603t$	-22.01	22.23	Southwest	$y(t) = 1.5454+0.0105t$	3.83
SIH1_2	$y(t) = 0.6935-0.0193t$	-7.06	$y(t) = 0.6006-0.0602t$	-21.98	23.08	Southwest	$y(t) = -2.7725+0.0125t$	4.57
SIH1_3	$y(t) = 2.1295-0.0230t$	-8.40	$y(t) = 1.6909-0.0569t$	0.81	8.44	Southeast	$y(t) = -1.4834-0.0171t$	-6.26
AKHR	$y(t) = 12.1708-0.0121t$	-4.42	$y(t) = -5.1438-0.0575t$	-20.97	21.43	Southwest	$y(t) = 4.2996-0.0096t$	-3.49
NAHA	$y(t) = 2.3182-0.0069t$	-2.52	$y(t) = -0.3622-0.0592t$	-21.61	21.76	Southwest	$y(t) = -1.085+0.0068t$	2.50
ESKS	$y(t) = 0.0218-0.0090t$	-3.28	$y(t) = 2.7517-0.0586t$	-21.23	21.48	Southwest	$y(t) = -2.5633+0.0053t$	1.85
BUCU	$y(t) = -0.1475-0.0030t$	-1.11	$y(t) = -0.3426+0.0010t$	0.36	1.17	Southeast	$y(t) = -1.6873+0.0059t$	2.17
KAP1	$y(t) = -0.1501+0.0071t$	2.60	$y(t) = 1.481-0.0513t$	-18.74	18.92	Northwest	$y(t) = 0.5663-0.0614t$	-22.41
SSE1	$y(t) = 0.6549+0.0164t$	5.98	$y(t) = 0.3114-0.0289t$	-10.54	12.12	Northwest	$y(t) = -2.0701+0.0046t$	1.67
BOG1	$y(t) = -1.6183+0.0161t$	5.88	$y(t) = 4.8055-0.0530t$	-19.34	20.21	Northwest	$y(t) = -6.6115-0.0096t$	-3.51
NIV1	$y(t) = 2.7078+0.0187t$	6.84	$y(t) = 2.2719-0.0471t$	-17.21	18.52	Northwest	$y(t) = 2.5191-0.0004t$	-0.15
AKD1_1	$y(t) = -3.6114+0.0371t$	13.53	$y(t) = -4.554-0.0439t$	-16.01	20.96	Northwest	$y(t) = -21.0493-0.0254t$	-9.28
AKD1_2	$y(t) = 3.1354+0.0192t$	7.01	$y(t) = 9.3971-0.0552t$	-20.16	21.35	Northwest	$y(t) = -2.2247+0.0043t$	1.56
ANK2	$y(t) = 2.1425-0.0012t$	-0.44	$y(t) = 0.5857-0.0664t$	-24.25	24.26	Southwest	$y(t) = -0.8576+0.0148t$	5.41
KIS1	$y(t) = -2.1063+0.0155t$	5.64	$y(t) = -1.9041-0.0548t$	-20.01	20.79	Northwest	$y(t) = 3.4692+0.0183t$	6.69

In Table 4, the average horizontal movement (resultant velocity) was found to be 18.24 mm/year in the northwest direction and 18.66 mm/year in the southwest direction. When the results obtained for

the horizontal component from this study compared with other studies that given in Figure 5, such as, the velocity value of 20 mm/year in the southwest direction obtained from Cingöz et al. (2013), and

value of 21.72 mm/year obtained by Gülal et al. 2013 and the velocity of 20.52 mm/year by Güçlü 2021, around Kırıkkale, it is seen that the velocity values obtained from this study is in agreement with these studies.

In addition, it has been shown that the Anatolian Plate has a westward linear movement with a velocity of 13-27 mm/year (Şentürk, 2019) and the North Anatolian Fault Zone has a westward movement of approximately 25 mm/year relative to the Eurasian Plate (Aktuğ, 2006). In the study conducted by Tiryakioğlu (2012), it was determined that the velocities parallel to the fault was approximately 22 mm/year at the points in Southwest Anatolia and the north of the Fethiye-Burdur Fault Zone.

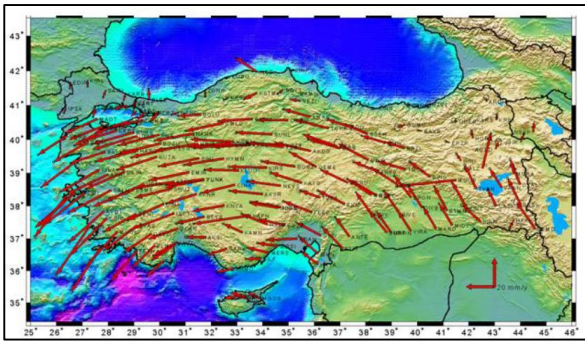


Figure 5. Point velocities (Eurasia fixed) (Cingöz et al., 2013)

It has also been determined that the results obtained from this study in the vertical component are in agreement with the vertical velocity values given in Figure 6.



Figure 6. Point velocities (vertical) (Özdemir et al., 2011)

Additionally, the standard deviation values (m_0) of the linear changes in the time series were also calculated. The m_0 values calculated for each station as a result of the adjustment in the north, east and Up directions, are given in Figure 7, 8 and 9. As it is seen (Figure 7, 8, 9), for the north direction of the stations, the m_0 values are in the range of approximately 1-4 mm, excluding SARV_1 ($m_0=4.89\text{mm}$), and KAP1 ($m_0=4.25\text{mm}$) stations, for the east direction, SARV_3 ($m_0=4.72\text{ mm}$) station. It is seen that the m_0

values are in the range of 0.8-3.5 mm except for the up direction, the biggest standard deviation is KNY1 ($m_0=18.01\text{ mm}$) station and the other stations m_0 values are in the range of 3-13 mm. Due to the insufficient number of data (data gap), the m_0 values of the SARV station, which were examined in three parts, were found to be higher than the other stations.

While the obtained m_0 values are approximately same for the north and east directions, it can be stated that the Up values are approximately 2-3 times greater than the north or east directions. As it is known, the fact that the sensitivity of the up component determined by GNSS is 2-3 times worse than the horizontal position sensitivity is also seen in the results obtained here.

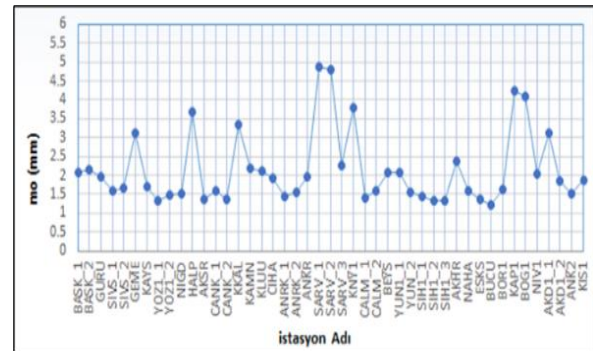


Figure 7. North direction linear variations standard deviations (m_0)

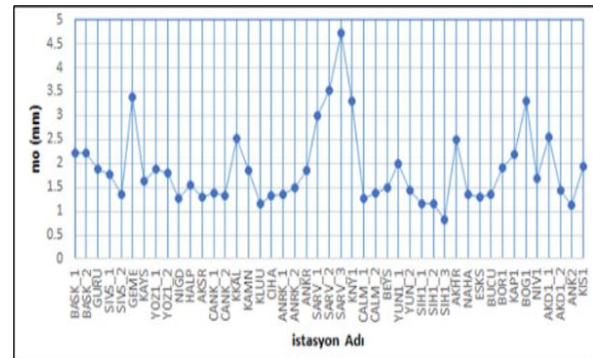


Figure 8. East direction linear variations standard deviations (m_0)

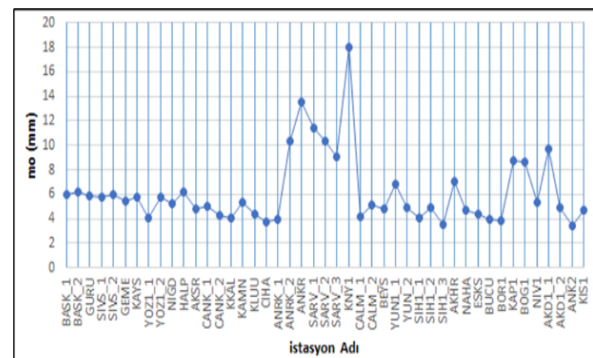


Figure 9. Up direction linear variations standard deviations (m_0)

5. RESULTS

Since Turkey is located at the intersection of Arabian, Anatolian and Eurasian tectonic plates, annual changes occur in point positions at the rank of cm due to the movement of these plates. For this reason, obtaining, evaluating, analyzing (time series analysis) and calculating the velocity values of GNSS stations at certain time intervals (daily, monthly, etc.) are important in terms of determining the position accuracy of the GNSS sites and ensuring their continuity.

In this study; The linear behaviors in the North, East and Up directions of 30 CORS-TR GNSS stations located in the Central Anatolian Region were obtained with the trend component analysis, which is the time series analysis component. The time series of the stations between the years of 2017 - 2020 were calculated with the GAMIT/GLOBK software, taking Eurasia plate as constant.

In the result of the analysis, it is obtained that the BASK_1, BASK_2, GURU, SIVS_1, SIVS_2, GEME, KAYS, YOZ1_1, YOZ1_2, NIGD, HALP, AKSR, CANK_2, KKAL, KAMN, KLUU, ANRK_2, SARV_1, SARV_3, KNY1, KAP1, SSE1, BOG1, NIV1, AKD1_1, AKD1_2 and KIS1 stations have an average horizontal velocity of 17.59 mm/year in the northwest direction and CANK_1, CIHA, ANRK_1, ANKR, SARV_2, CALM_1, CALM_2, BEYS, YUN1_1, YUN_2, SIH1_1, SIH1_2, AKHRSI, ESKS, BUCU and ANK2 stations have an average horizontal velocity of 18.66 mm/year in the southwest direction. This shows the movement of the Anatolian plate in the southwest direction in terms of movement direction and velocity value and is consistent with other research results.

In the linear changes in the Up coordinates of the stations, the largest linear movement in the (+) positive direction was determined at the SARV_3 station with 29.75 mm/year values, and the largest linear movement in the negative (-) direction was determined at the KNY1 station with the values of -48.22 mm/year. Also, 22.41 mm/year change was observed in the Up coordinate in negative direction at the KAP1 station. It is thought that the negative (-) change in these station is occurred due to the decrease in the groundwater level in this region (Konya Closed Basin).

In addition, standard deviation values (m_0) were calculated as a result of the analysis of the linear changes of time series, and due to the high number of data loss, the m_0 values of the SARV station, which were examined in three separate parts, were found to be large than the other stations. While the obtained m_0 values are approximately the same for the north and east directions, it can be stated that the Up values are approximately 2-3 times larger than the north or east directions. As it is known, the sensitivity of the Up values determined by GNSS is 2-3 times worse than the horizontal position sensitivity, is also seen in the results obtained from this study.

Acknowledgement

This article was produced from Abdulmalek REDHWAN's master thesis.

Author Contributions

Abdulmalek Redhwan: Methodology, Software, Validation, Formal analysis, Writing-Original Draft, Visualization. **Hediye Erdoğan:** Supervision, Writing-Original Draft. **Osman Otkar:** Methodology, Software, Formal analysis. **Cemil Gezgin:** Writing-Review & Editing, Visualization.

Conflicts of Interest

The authors declare no conflict of interest

REFERENCES

- Aktuğ, B. (2006). Determination of earthquake source parameters through geodetic observations (PhD thesis). Istanbul Technical University, Istanbul, Turkey (in Turkish).
- Cingöz, A., Erkan, Y., Kurt, Y.A., & Peker, S. (2013). Turkey national fixed gnss network-active (TUSAGA-Active) system. *TMMOB Chamber of Surveying and Cadastre Engineers, 14. Turkey Map Scientific and Technical Congress*, Ankara.
- Gezgin, C., Tiryakioğlu, İ., Ekercin, S., & Gürbüz, E. (2020). Monitoring of tectonic movements of the southern section of the Tuz Gölü fault zone (TGFZ) with GNSS observations. *Afyon Kocatepe University Journal of Science and Engineering*, 20(3), 456-464.
- Güçlü, A.T. (2021). Definition of behavior of GNSS stations in Kırıkkale and surrounding (MSc thesis). Aksaray University, Aksaray, Turkey (in Turkish).
- Gülal, E., Aykut, N.O., Akpınar, B., Tiryakioğlu, İ., Dindar, A.A., & Erdoğan, H. (2013). Establishment of Yildiz Technical University fixed GNSS station, analysis and presentation of data, 14. *Turkey Map Scientific Technical Congress*, Ankara.
- Mutlu, İ., & Kahveci, M. (2019). The importance of GNSS satellite distribution in Real-Time Kinematics GNSS and Network-RTK measurements. *Geomatics*, 4(3), 179-189.
- Otkar, O. (2015). Identification of behavior of stationary GNSS stations with wavelet transform (MSc thesis). Aksaray University, Aksaray, Turkey (in Turkish).
- Otkar, O., & Erdogan, H. (2018). Research of behaviours of continuous GNSS stations by

- signal. *Earth Sciences Research Journal*, 22(1), 19-27.
- Orhan, O., Yakar, M., & Ekercin, S. (2020). An application on sinkhole susceptibility mapping by integrating remote sensing and geographic information systems. *Arabian Journal of Geosciences*, 13,17, 1-17.
- Orhan, O. (2021). Monitoring of land subsidence due to excessive groundwater extraction using small baseline subset technique in Konya, Turkey. *Environmental Monitoring and Assessment*, 193(4), 1-17.
- Orhan, O., Oliver-Cabrera, T., Wdowinski, S., Yalvac, S., & Yakar, M. (2021). Land subsidence and its relations with sinkhole activity in Karapınar region, Turkey: a multi-sensor InSAR time series study. *Sensors*, 21(3), 774.
- Ostini, L. (2012). Analysis and quality assessment of GNSS-derived parameter time series (PhD thesis). Bern University, Bern, Switzerland.
- Özdemir, S. (2014). Analysis of GNSS time series obtained from Turkish national permanent GNSS stations network-active system using Hilbert-Huang transform (MSc thesis). Middle East Technical University, Ankara Turkey.
- Özdemir, S., Cingöz, A., Aktuğ, B., Lenk, O., Kurt, M., & Parmaksız, E. (2011). Analysis of fixed station data. *TMMOB Chamber of Surveying and Cadastre Engineers 13th Turkish Scientific and Technical Mapping Congress*, 18-22.
- Özdoğan, S. (1993). Turkey's earthquake zones. *Journal of Turkish Geography Research and Application Center*, 2, 53-68.
- Şentürk, M.D. (2019). Optimal filtering of strong motion records with GPS (MSc thesis). Ankara University, Ankara, Turkey (in Turkish).
- Tiryakioğlu, İ. (2012). identification of the block movements and stress zones in southwestern anatolia with GNSS measurements (PhD thesis). Yıldız Technical University, İstanbul, Turkey (in Turkish).
- Uzel, T., Eren, K., Gulal, E., Tiryakioğlu, I., Dindar, A. A., & Yılmaz, H. (2013). Monitoring the tectonic plate movements in Turkey based on the national continuous GNSS network. *Arabian Journal of Geosciences*, 6(9), 3573-3580.
- Üstün, A., Tuşat, E., & Abbak, R.A. (2007). Groundwater withdrawal in Konya Closed Basin and geodetic monitoring of possible consequences. *3. Engineering Symposium*, 24-26.
- Üstün, A., Tuşat, E., Yalvaç, S., Özkan, İ., Eren, Y., Özdemir, A., & Doğanalp, S. (2015). Land subsidence in Konya Closed Basin and its spatio-temporal detection by GPS and DInSAR. *Environmental earth sciences*, 73,10, 6691-6703.
- Yalvaç, S. (2020). Determining the effects of the 2020 Elazığ-Sivrice/Turkey (Mw 6.7) earthquake from the surrounding CORS-TR GNSS stations. *Turkish Journal of Geosciences*, 1(1), 15-21.
- Yavaşoğlu, H., Tarı, E., Tüysüz, O., Çakır, Z., & Ergintav, S. (2011). Determining and modeling tectonic movements along the central part of the North Anatolian Fault (Turkey) using geodetic measurements. *Journal of Geodynamics*, 51,5, 339-343.
- Url-1: http://geoweb.mit.edu/gg/GAMIT_Ref.pdf, (last accessed 10 July 2020)
- Url-2: <http://tusaga.Aktif.gov.tr/Sayfalar/Rinex/30snRinex.aspx>, (last accessed 4 July 2020)



© Author(s) 2021. This work is distributed under <https://creativecommons.org/licenses/by-sa/4.0/>

Classification and generation of the enclaves in Karapınar-Karacadağ volcanic rocks (Central Anatolia)

Gülin Gençoğlu Korkmaz *¹, Hüseyin Kurt ¹, Kürşad Asan ¹

¹ Konya Technical University, Faculty of Engineering and Natural Sciences, Department of Geological Engineering, Konya, Turkey

Keywords

Magma mixing enclave
Magma segregation
enclave
Volcanic rocks
Xenolith

ABSTRACT

Karapınar-Karacadağ Volcanic Rocks (KKVR) have very complex magmatic history and outcropped the southwestern part of the Cappadocia Volcanic Province (Central Anatolia). Here we present the petrography and whole-rock chemistry of the enclave-bearing rocks to constrain their source and evolution history. These petrographic observation and geochemical data reveal that the enclaves in the Karapınar-Karacadağ volcanic rocks are magma mixing/mingling enclaves (MME), magma segregation enclaves (MSE), and xenoliths. Here we discriminated these enclaves into eight different types according to their mineral composition and textural features. The magma mixing/mingling enclaves (Type 1, 7, 8) are the mixing products of coeval more felsic and mafic magmas. They show hypocrystalline porphyritic, holocrystalline granular, and intergranular textures, and rich in mafic minerals, and have characteristic petrographic features such as quenched amphibole, bladed biotite, ocelli-quartz, sieved and cellular plagioclases. In andesites they range from basalt to andesite in composition. However, in basalts, they are in basaltic composition. The magma segregation enclaves (Type 2, 4, 5, 6), which are observed in almost all the KKVRs, are cognate xenolith because of plucking from the different parts of the magma chamber. They are holocrystalline and granular in texture. The magma segregation enclaves contained in the andesitic host rocks are hornblende gabbro and pyroxene gabbro in composition, whereas in the basaltic host rocks they are dunite, lherzolite, and basalt in composition. The xenolithic enclaves (Type 3) are observed in the basalts as quartz, plagioclase, biotite, and amphibole xenocrysts. Major oxides and trace element data of the studied rocks indicate that the MSEs are more primitive than their host rocks, and all of the enclaves (MME-MSE) are in accordance with their hosts. According to petrographic observations and geochemical data we propose that fractional crystallization, magma mixing and assimilation processes have a key role in the evolution of the KKVRs and their enclaves.

1. INTRODUCTION

Generally, enclave means crystal clots (clusters) in the rock and they differ from the host rock in which it is located, disrupting the homogeneous appearance of the host-rock (Barbarin and Didier, 1992). Enclaves may be distinguished from the host-rock in terms of color, shape, size, texture, and mineralogical composition macroscopically and/or microscopically. The sizes of enclaves can vary from microscopic scale to several hundred meters. They can be composed of several different minerals or only one mineral (Cantagrel et al., 1984). Enclaves contain important information about the genesis and

evolution of magma and magma chamber processes. Based on formation, origins, and relationships with felsic host rocks, the enclaves in granitoid rocks have been classified as (1) Xenolite, (2) Restite, (3) Cognate enclave (4) Microgranular enclave (Barbarin and Didier, 1991; Best, 2003; Cantagrel et al., 1984; Dahlquist, 2002; Didier, 1991; Ilbeyli and Pearce, 2005; Kadioglu and Gülec, 1996; Kadioğlu and Güleç, 1999; Kocak et al., 2011; Kumar, 2010; Kumar et al., 2004; Kumar and Singh, 2014; Noyes et al., 1983; Özdamar et al., 2021; Winter, 2014; Zhang and Zhao, 2017). Xenoliths are known as foreign rock fragments assimilated from the wall-rock during ascending (Maury and Didier, 1991; Tindle and

* Corresponding Author

(ggkorkmaz@ktun.edu.tr) ORCID ID 0000-0003-0185-2806
(hkurt@ktun.edu.tr) ORCID ID 0000-0001-7991-2085
(kasan@ktun.edu.tr) ORCID ID 0000-0003-4244-1747

Cite this article

Korkmaz G.G., Kurt H., & Asan K. (2021). Classification and generation of the enclaves in Karapınar-Karacadağ volcanic rocks (Central Anatolia). Turkish Journal of Geosciences 2(2), 30- 46.

Pearce, 1983), and generally seem like a metamorphic rock. Due to their metamorphic textures and the sharp contacts with their hosts, they could be easily separated from the cognate enclaves (Cantagrel et al., 1984; Didier, 1991; Shelley, 1993). Restites are known as the residual material after partial melting (Chappell et al., 1987; Chen et al., 1991). Cognate enclaves are early-crystallized mineral clots or segregation of mafic phases, or products of earlier solidified phases which were wall and border rock in the magma chamber (Dahlquist, 2002; Kadioğlu and Güleç, 1999; Kocak et al., 2011; Noyes et al., 1983). They have cogenetic affiliation with their hosts, and have a coarse-grained appearance. If early-formed minerals assemblages seemed as cumulate textures, such as adcumulate, intercumulate, orthocumulate etc. they are called cumulate enclaves. Cumulates are generally present mafic magmas rather than the felsic magmas because of the different viscosity of the residual melts (Kumar and Singh, 2014). Magma segregation enclaves (MSE) as a kind of cognate enclave are formed by segregation and accumulation of the early-crystallized minerals, are also known monomineralic or polimineralic crystal clots displaying glomeroporphyritic textures. Phenocrysts are liable to aggregate into clusters as glomerocrysts, showing glomeroporphyritic texture in basalts (Gill, 2010). Microgranular enclaves are common in granitoids and they are rarely divided into subgroups as mafic and felsic microgranular enclaves. They are formed as a result of the reaction of coeval mafic and felsic magmas and are actually the products of the magma mingling process (Barbarin and Didier, 1991; Best, 2003; Cantagrel et al., 1984; Dahlquist, 2002; Didier, 1991; Ilbeyli and Pearce, 2005; Kadioğlu and Güleç, 1996; Kadioğlu and Güleç, 1999; Kocak et al., 2011; Kumar, 2010; Kumar et al., 2004; Kumar and Singh, 2014; Noyes et al., 1983; Winter, 2014). They are the products of hybridization process. While a homogeneous mixing takes place in the magma mixing process, the mingling process generates partial mixing. MMEs are liable to be cogenetic with their host rocks. They generally have a fine-grained appearance, and are equigranular to porphyritic in nature (Kumar, 2010). Some researchers (Winter, 2014) suggest that schlieren and chilled margins might be accepted as microgranular enclaves. Since volcanic rocks show textures ranging from holocrystalline granular to vitrophyric porphyritic, and they may have a groundmass composed of volcanic glass and/or microlite, and their minerals are generally small in size and acicular in shape, the definition of magma mixing/mingling enclaves (MME) is more convenient for volcanic units rather than the definition microgranular enclave. Therefore, considering their formation, origins and transportation of the host rock, enclaves can generally be divided into four groups: (1) Xenolite, (2) Restite, (3) Magma segregation enclave (4) Magma mixing/mingling enclave (Kadioğlu and

Güleç, 1999). In addition, MME may also contain another enclaves termed as double enclaves (Didier, 1973), or composite enclaves (Kumar, 2010).

Here, we present for the first time, field and petrographic features (textural, mineralogical) and whole-rock major oxide-trace element characteristics of the enclaves and their host rocks from the Neogene-Quaternary aged Karapınar-Karacadağ Volcanic Rocks. With this scope, we aim to determine the enclaves' occurrence, origins, relationships, and their importance in the Cenozoic Central Anatolian Volcanism.

2. GEOLOGICAL SETTING

The Karapınar-Karacadağ Volcanic Units are the southwestern extension of the Cappadocia Volcanic Province (CVP), and these post-collisional products commonly outcrop in the Kırşehir and Anatolide blocks in Central Anatolia (Gençoğlu Korkmaz et al., 2022) (Figure 1). Neogene aged calc-alkaline volcanites are mostly represented by lava flows/domes and pyroclastics, which are called "Karacadağ Volcanics". However Quaternary aged calc-alkaline-mildly alkaline volcanics outcropping as lava flows, maar pyroclastics and cinder cones, are called "Karapınar volcanics" (Gençoğlu Korkmaz et al., 2022). Keller (1974) argues that the geological and genetic understanding of Karacadağ was hindered by the arrival of much younger basaltic scoria cones (Karapınar volcanics) that do not have a direct genetic relationship to the northeast of Karacadağ. In recent studies, the age of Karapınar volcanics is <2.5 Ma (Dogan-Kulahci et al., 2018; Reid et al., 2017) as a result of ^{40}Ar - ^{39}Ar geochronology, while Platzman et al. (1998), (K-Ar; 4.7-5.98 Ma) and Gençoğlu Korkmaz et al. (2022), (^{40}Ar - ^{39}Ar ; 5.65-5.45 Ma) suggest that Karacadağ volcanics are Mio-Pliocene. The Karacadağ volcanics consist of lava flows and pyroclastics with in calcalkaline character, they are rarely basaltic and trachytic and mainly andesitic-dacitic in composition. Moreover, andesitic and dacitic rocks contain two types of enclaves as magma segregation enclaves and magma mixing enclaves. Karapınar volcanics, on the other hand, have mildly alkaline-calcalkaline (transitional) character, and are mostly basaltic and rarely andesitic products, and include three types of enclaves: magma segregation enclaves, magma mixing enclaves and xenoliths (Gençoğlu Korkmaz et al., 2018). The calc-alkaline rocks of the CVP are characterized by LILE/HFSE enrichments showing negative Nb, Ta and Ti anomalies. However, Na-alkaline volcanics from CVP are quite similar to calc-alkaline rocks in terms of LILE and REE patterns, although they have some OIB-like basaltic rock features (Aydar et al., 1994; Dogan-Kulahci et al., 2018; Ercan, 1987; Ercan et al., 1990; Güllü and Kadioğlu, 2019; Notsu et al., 1995; Reid et al., 2017; Uslular and Gençalioğlu-Kuşcu, 2019). Di Giuseppe et al. (2018) suggest that a mixing process between calc-alkaline and intraplate magmas during magma

uplift resulted in the formation of Ne normative basalts in Central Anatolia. Gençoğlu Korkmaz et al. (2022) report that not only temporally but also spatially crustal contamination has a critical role in the evolution of the rocks. Furthermore, from Neogene to Quaternary the effect of the crustal contamination process has decreased, but it has increased again spatially in Quaternary. Moreover, they report that all geochemical data and petrological models reveal that Karapınar mildly

alkaline basalts obtained an orogenic character via contamination with Karacadağ volcanites. In addition, Gençoğlu Korkmaz and Kurt (2021) suggested that magma recharging processes and convection in the magma chamber are effective in the formation of the rocks and their enclaves. Also they stated that these (multiple) recharging processes gave rise to the triggering of the Karapınar-Karacadağ volcanism.

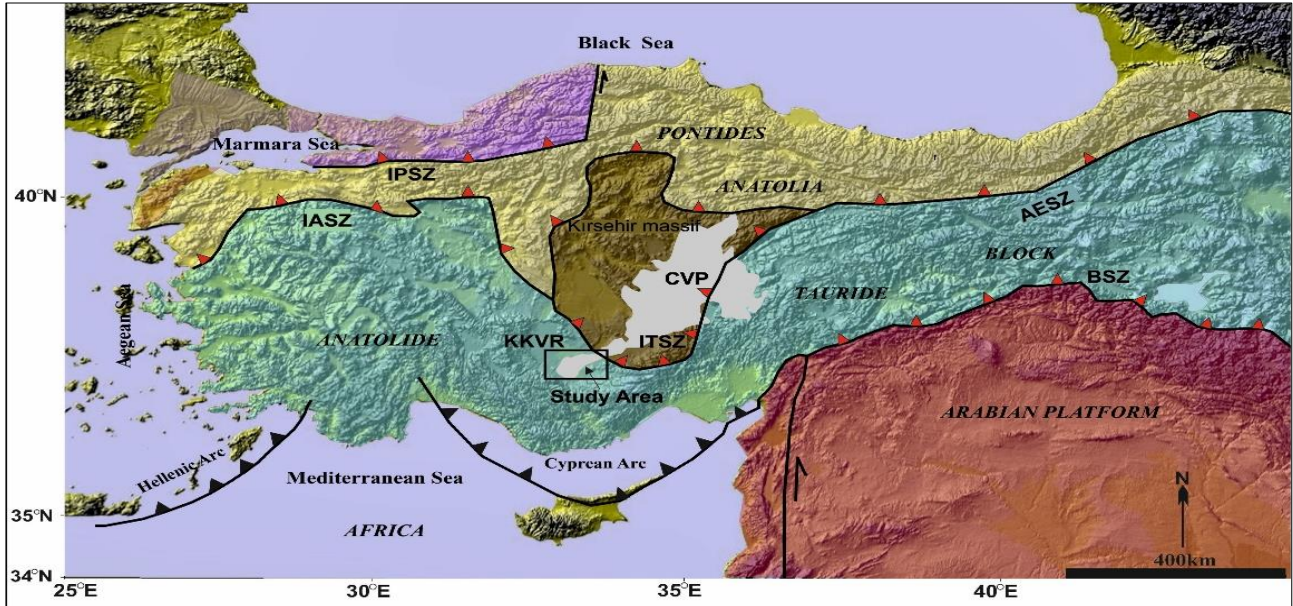


Figure 1. Location of the investigated area in the map showing the main tectonic units of Turkey (Okay and Tüysüz, 1999). The map shows also the position of the, Hellenic arc, and Cyprus arc. CVP: Cappadocian Volcanic Province, IASZ: İzmir-Ankara-Suture Zone, AESZ: Ankara-Erzincan Suture Zone, IPSZ: Intra-Pontide Suture Zone, ITSZ: Inner Tauride Suture Zone, BSZ: Bitlis Suture Zone. Solid lines stand for major suture zones (black lines with red triangles) separating continental blocks and arc systems (black lines with black triangles) The map is taken from Gençoğlu Korkmaz et al. (2022)

3. METHOD

Within the scope of this study, 180 thin sections were made from the most representative 700 samples collected from the Karapınar-Karacadağ area. Some of the basaltic and andesitic rocks from the KKVR contain enclaves with different textures and compositions varying in size from μm -dm. Approximately fifty of the collected samples contain enclaves in mm-dm size. Among them, twenty most representative and freshest enclaves and their hosts were used for this study.

In this study, some enclaves were carefully separated from the host-rock thus facilitating chemical analyses. Detailed petrographic examinations (modal mineralogical composition, texture, classification, alteration) of the samples, whose thin sections were obtained at the Thin Section Laboratory of Ankara University Earth Sciences Application and Research Center (YEBİM), were carried out with the help of polarizing microscopy in Konya Technical University Geological Engineering Department. Besides,

microphotographs were taken to highlight important mineralogical and petrographic features.

Among these samples, the most representative and determinant host-rock (eight) and enclave (nine) samples were analyzed in Spectro X-Lab 2000 model PED-XRF (Polarized Energy Dispersive XRF) device at YEBİM. The samples were first crushed in Retsch brand automatic stone crusher, then they were ground in a Tungsten Carbide mill in Fritsch brand automatic grinder. 4 grams of sample was mixed with 0.9 grams of binding material (wax-polyvinyl alcohol) and made ready for analysis in pellet form by compressing under a hydraulic press. Results of whole-rock analyses of the samples are available from Supplementary Material 1.

4. RESULTS

4.1. Types of Enclaves: Petrography and classification of the enclaves

KKVRs were classified as Basalt-1 (B1), Andesite-1(A1), Andesite-2(A2), Andesite-3(A3),

Andesite-4(A4), Dacite(D), Trachyte (T) (Karacadağ volcanic units) and Basalt-2(B2) and Basalt-3(B3) (Karapınar volcanic units) based on their petrographical and chemical properties as reported in Gençoğlu Korkmaz et al. (2022). Karacadağ volcanites are calc-alkaline, however Karapınar volcanites are mildly alkaline (B2) to calc-alkaline (B3) (Gençoğlu Korkmaz et al., 2022).

Karacadağ stratovolcano is dominantly composed of andesitic lava units contained both macroscale (Figure 2 a-d and g-m) and microscale enclaves (Figure 4 a-s). They are generally ellipsoidal in shape (Figure 2 c, d) and rarely contain chilled margins (Figure 2 i) In the investigated area they rarely exhibit banding texture (Figure 2 a, b, l, and m). However, Karapınar Quaternary volcanism has produced dominantly basaltic scoria cones and lava flows, having mainly microscopic enclaves (Figure 2 e, f, n, o and Figure 3 a-o). Investigated enclave types, their main mineralogical contents, and their textural characteristics are summarized in Table 1 and 2. Eight types of enclaves were distinguished on the basis of petrographic characteristics, mineral composition, and textural-structural features.

Karapınar basaltic host rocks generally exhibit a texture varying from holocrystalline porphyritic to hypocrySTALLINE porphyritic texture. They rarely display also vesicular and amygdaloidal textures. Some of the basaltic host rocks (B2) are olivine-dominated, whereas others (B3) are pyroxene-

dominated. Investigated basaltic hosts have Type-1 (MMEs; Figure 3 a-c, and Figure 3 k, l), Type-2 (MSEs; Figure 3 d, h-l, n, o) and Type-3 (Xenoliths; Figure 3 m) enclaves. Along with that, they include composite enclaves (enclave in enclave; Figure 3 i-l).

Type-1 enclaves (Figure 3 a-c, k, l) are observed both in macroscale and in microscale in the Karapınar basalts (generally B2) as magma mixing enclaves (MME). They are angular to semi-rounded shaped enclaves in the field (Figure 2 e, f, n, o). The groundmass of the Type-1 enclaves is rich in microlites. The appearance of the enclaves is formed by elongated plagioclase crystals, short prismatic micro-phenocrysts of pyroxene, and rarely fractured olivine phenocrysts with minor Fe-Ti oxides.

The magma segregation enclaves (MSE) in the basalts (B2-B3) called Type-2 enclaves are holocrystalline and granular in texture and are monomineralic to polymineralic in composition. They occur as independent aggregates and rarely within Type-1 enclaves (enclave in enclave-composite enclave), and they are in microscale. They don't display any cumulate or metamorphic rock texture as cumulate enclaves. They seem like typical igneous rocks and they are coarse-grained rocks showing glomeroporphyritic textures. They are often observed as crystal clots formed by segregation of the early solidified phases (olivine, pyroxene, plagioclase crystals).



Figure 2. Macro-scale enclaves and their structural and textural properties (a)-(b) enclave swarms showing relative magmatic flow structure with host magma, (c)-(d) ellipsoidal-rounded enclaves in Karacadağ volcanic rocks (e)-(f) semi- rounded-angular enclaves in Karapınar volcanic rocks

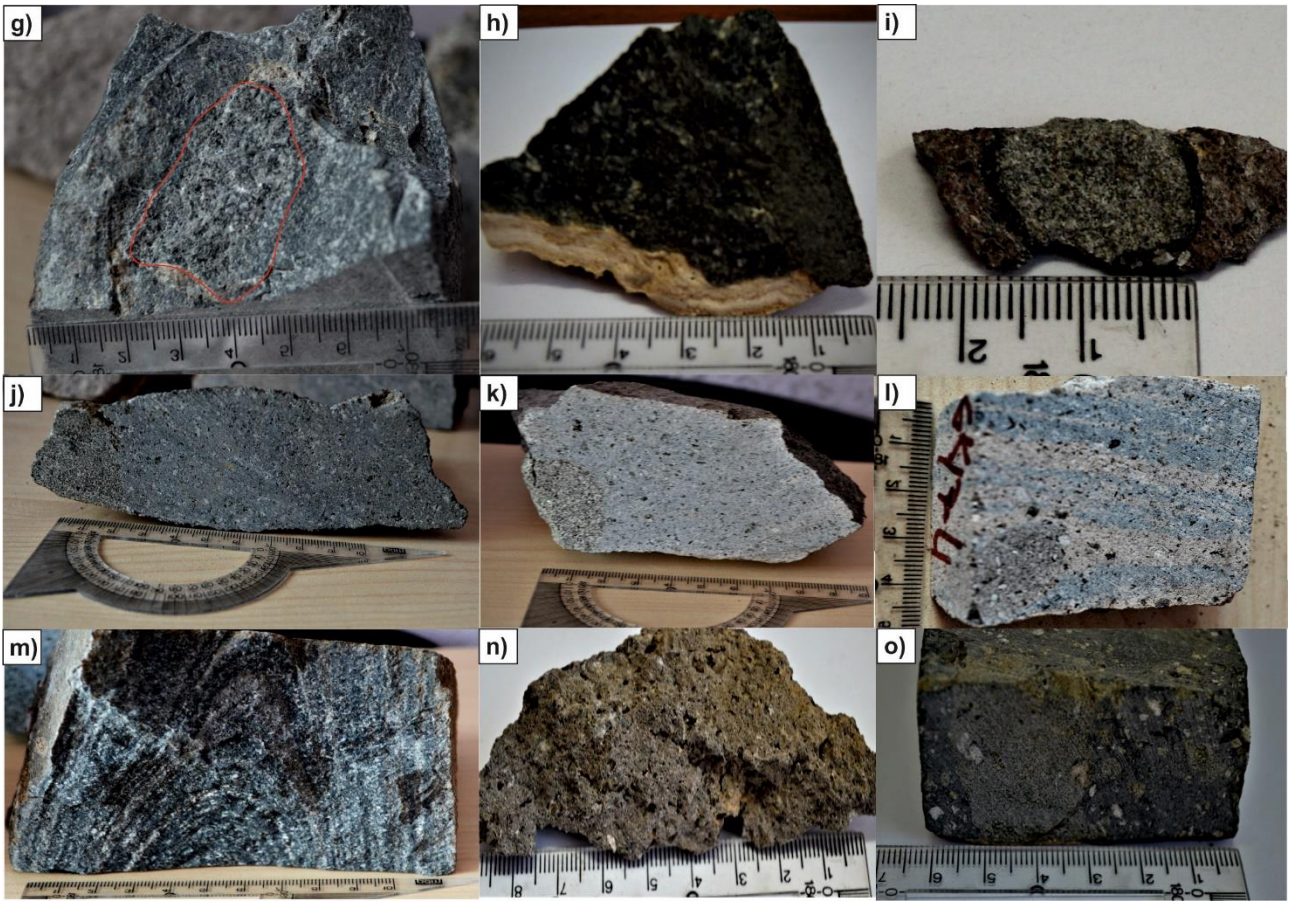


Figure 2. (continued) Macro-scale enclaves and their structural and textural properties (g)-(m) ellipsoidal-rounded enclaves in the Karacadağ volcanic rocks, (n)-(o) semi- rounded-angular enclaves in the Karapınar volcanic rocks

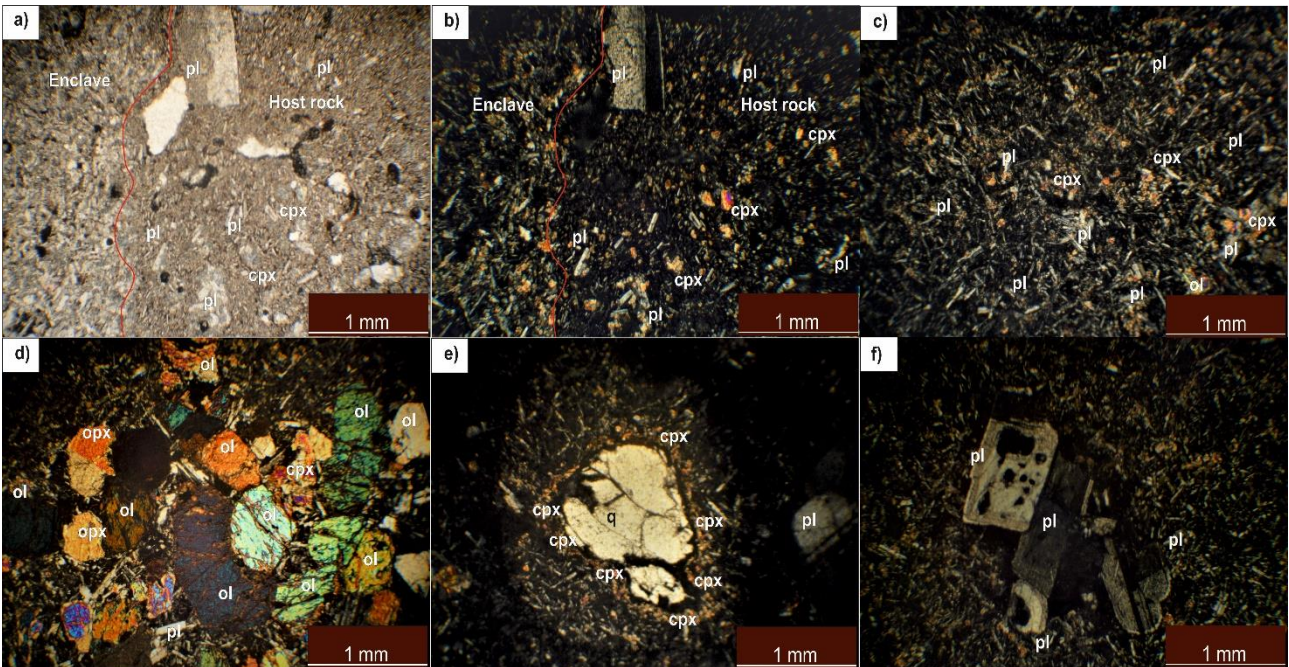


Figure 3. (a)-(b) Boundary of the Basalt-2 and Type-1 enclave (MME), (c) Type-1 enclave (MME in basaltic composition) in Basalt-2, (d) Type-2 enclave (MSE-in lherzolite composition) in Basalt-3, (e) ocelli quartz xenocryst in Basalt-3, (f) sieved plagioclase glomerocrysts (composite enclave) in Type-1 enclave. cpx: Clinopyroxene; ol: Olivine; opx: Orthopyroxene; ox: Fe-Ti oxides; pl: Plagioclase; q: Quartz (Kretz, 1983)

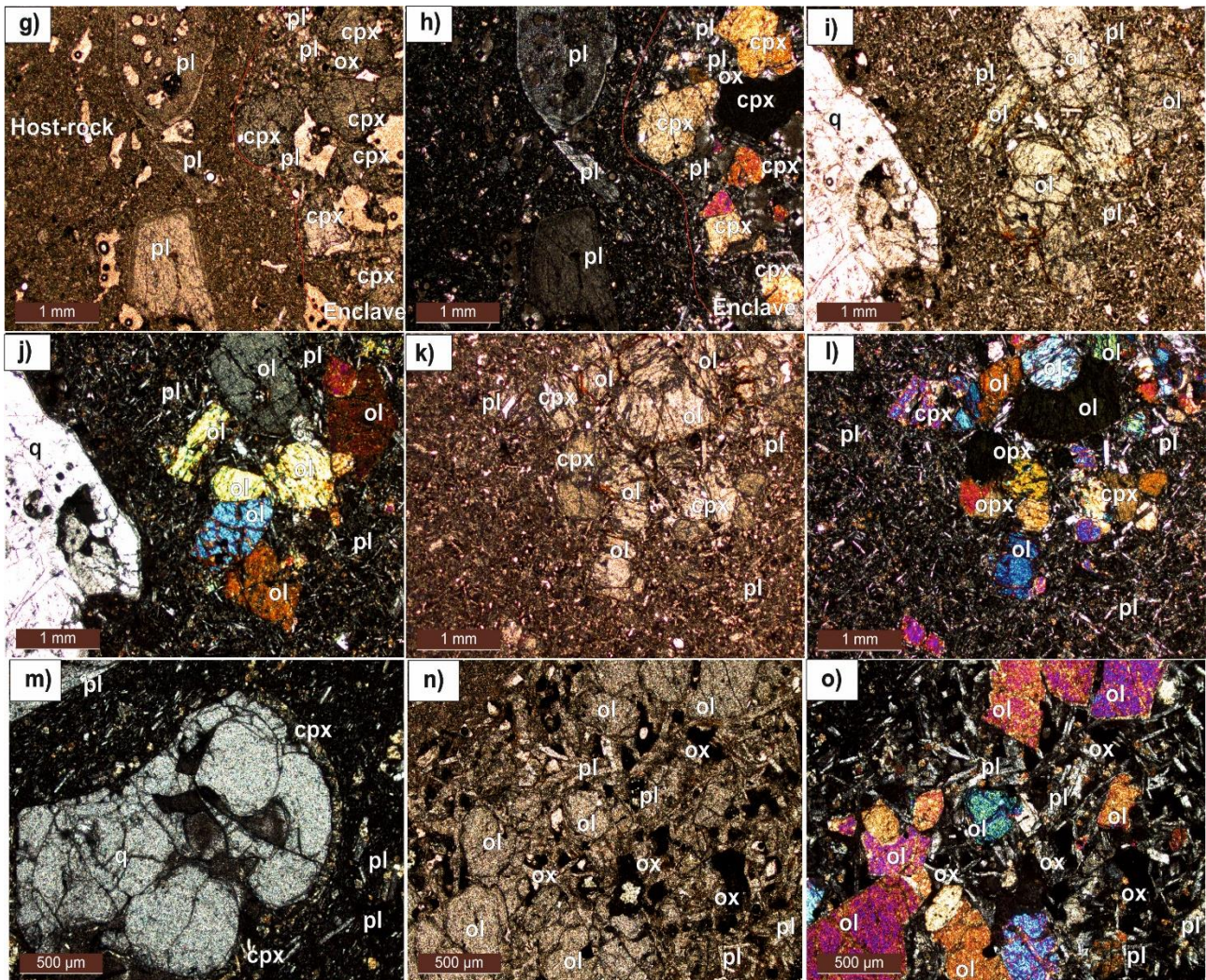


Figure 3. (continued) (g)-(h) Boundary of the in Basalt-2 and Type-1 enclave (MME), (i)-(j) Type-2 enclave (MSE-in dunite composition) and (k)-(l) Type-2 enclave (MSE-in lherzolite composition) in Basalt-2, (j)-(l) composite enclaves, (m) embayed and ocelli quartz xenocryst and (n)-(o) Type-1 enclave (MME in basaltic composition) in Basalt-3

The xenolithic enclaves (Figure 3 e, f, g, j, m) classified as Type-3 enclaves are observed in the basalts (generally in the B3) and rarely Type-1 enclaves (composite enclave) as quartz, plagioclase, biotite, and amphibole xenocrysts and also seemed a piece of quartzite rock. A composite enclave formed when one enclave is enclosed in another enclave are detected in some of the investigated rocks as demonstrated in Figure 3 e, f, j-l. Embayed and ocelli-quartz minerals and spongy cellular, coarse and/or fine sieved-plagioclase minerals are observed in both enclaves and their hosts as xenocrysts.

Karacadağ andesitic-dacitic host rocks have generally hypocrySTALLINE porphyritic rarely vesicular textures. Some of the andesitic host rocks include amphibole and pyroxene as major mafic mineral phases. Investigated intermediate host rocks generally contain pl+cpx± amph± bi± opx+ Fe-Ti oxides plus volcanic glass. They have Type-4 (MSEs; Figure 4b), Type-5 (MSEs; Figure 4d) Type-6 (MSEs; Figure 4f), Type-7 (MMEs; Figure 4 n, p) and Type-8 (MMEs; Figure 4 l, s) enclaves.

The magma segregation enclaves (MSE), which are observed in almost all of the Karapınar-Karacadağ Volcanic Rocks, are cognate xenolith due to their textural properties, and are best observed under the microscope because of their small sizes. MSEs in the andesitic host rocks are in amphibole gabbro, pyroxene gabbro and micro-gabbro composition with holocrystalline granular texture. Plagioclases generally exhibit dusty sieve, fine sieve and spongy sieve textures, and pyroxenes and amphiboles are rarely fractured and anhedral in host rocks relative to in MSEs. In addition, some of the plagioclases, pyroxenes, and amphiboles exhibit both textural and chemical zoning (Gençoğlu Korkmaz and Kurt, 2021). MMEs in andesites range from basalt to andesite in composition. They show hypocrySTALLINE porphyritic, holocrystalline granular, and intergranular textures, and rich in mafic minerals, and have characteristic petrographic features such as quenched amphibole, bladed biotite, sieved and cellular plagioclases. Along with that, some of the plagioclases display both textural and

chemical zoning in both enclaves and their hosts as in MSEs. Composite enclaves that appeared like basaltic/gabbroic rocks are also detected in the andesitic host rocks. Figure 4.s demonstrates that the basaltic MME from the andesitic host rock includes gabbroic MSE.

Type-4 enclaves (Figure 4b) are in the andesitic host rocks (A1) as MSEs in amphibole-gabbro composition and they are holocrystalline and equigranular in texture. They contain mainly prismatic amphibole and plagioclases and rarely clinopyroxene and opaque minerals. Amphibole and clinopyroxenes are often zoned, and plagioclases show generally sieve textures. The enclave mineralogy is the same as in the host, however, the host rock contains biotite and amphibole as major mafic phases rather than clinopyroxene (Figure 4 a). Accessory minerals contain zircon and Fe-Ti oxides.

Type-5 enclaves (Figure 4 d, h, i, k) are MSE in the andesitic (A1-A2-A3) and dacitic host rocks containing cpx+ pl +Fe-Ti ox, and rare biotite. The mineralogy of the enclaves is similar to that of their host rocks, but the enclaves contain abundant dusty sieved-plagioclases, and also have abundant clinopyroxenes as mafic phases. Some of the Type-5 enclaves are observed in two-pyroxene andesites as cpx+opx+pl+Fe-Ti oxide crystal cargoes (Figure 4 h).

Although having the same mineral composition as their enclaves (Type-6), some of the andesitic host rocks (A1) are porous and have a glassy groundmass (Figure 4 e). Type-6 enclaves (Figure 4 f) are classified as MSE and they have chilled margin through the host rock-enclave boundary. Type 6 enclaves are in the micro-gabbro composition and contain cpx+pl+ox±amph minerals. They show holocrystalline and equigranular texture. However, the chilled margins (Figure 4 g) seem as magma mixing enclave and are composed of quenched and elongated amphiboles, sieved plagioclases, rarely fractured and short prismatic clinopyroxenes and Fe-Ti oxides. Also, the grains in the chilled margins are larger than those in the enclave.

Type-7 enclaves (Figure 4n, p) are andesitic MMEs in the andesitic host (A1). They are rounded shaped and have no chilled margins. The mineralogy of the enclaves is similar to that of the andesitic host rocks. They show hypocrySTALLINE porphyritic and intergranular textures, and rich in mafic minerals. They are composed of mainly amphibole and plagioclase, rarely clinopyroxene, biotite, Fe-Ti oxide, and volcanic glass. Along with that, they have characteristic petrographic features such as quenched amphibole, bladed biotite, sieved and cellular plagioclases. Also, some of the plagioclases display both textural and chemical zoning both in enclaves and their hosts as in MSEs (Gençoğlu Korkmaz and Kurt, 2021).

Type-8 enclaves (Figure 4 l, r, s) are basaltic MMEs in the andesitic host rocks (A2). They have flow banding structure and show marble cake

textures in the field (Figure 2 a, b, m). Along with that, they are rounded shaped. They show holocrystalline and intergranular textures, and rich in mafic minerals, and have characteristic petrographic features such as sieved, cellular and zoned plagioclases, acicular plagioclases, fractured olivines. However, host rock show hypocrySTALLINE porphyritic texture and include clinopyroxene, amphibole, biotite, plagioclase, and Fe-Ti oxide minerals. Some of the plagioclase microphenocrysts in both enclaves and their hosts exhibit textural and chemical zoning (Gençoğlu Korkmaz and Kurt, 2021). Type-8 enclaves also contain crystal clots including cpx+pl+ol+ox as composite enclaves in which basaltic MME have enclosed gabbroic magma segregation enclaves (Figure 4 s).

4.2 Whole-Rock Composition of the Host Rocks and Their Enclaves

Here, only enclaves, which could be separated from their hosts due to their large size and whose geochemistry could be examined, and their hosts are classified and discriminated from each other, based on total alkali-silica diagram TAS (Le Bas et al., 1986; Middlemost, 1994). While the Karapınar basalts containing enclaves fall into the basaltic andesite-andesite areas, the enclave-bearing Karacadağ volcanic rocks include compositions varying from andesite to dacite (Figure 5 a). Type-1 enclaves are basaltic-andesite, Type-4 enclave plots in the basalt field (mineralogically, they are amphibole gabbro), Type-5 enclaves plot in the basaltic-andesite, andesite area (mineralogically, they are pyroxene gabbro), Type-7 enclave is andesite and Type-8 enclave is basaltic andesite (Figure 5 a). Since MSEs (Type 4-6) exhibit holocrystalline texture as in the plutonic rocks, the TAS classification diagram generated by Middlemost (1994) was utilized to discriminate the MSEs. Accordingly, MSE enclaves have a composition ranging from gabbro to diorite (Figure 5 b). Moreover, studied rocks include calc-alkaline and high-K calc-alkaline series in the K₂O-SiO₂ diagram. According to TAS diagrams, and SiO₂ versus K₂O classification diagram (Figure 5 d), magma segregation enclaves appear more primitive than their host rocks.

Investigated rocks and their enclaves exhibit different trends in MgO versus major oxide and trace element diagrams (Figures 6a-f, 7a-f). Karapınar enclave bearing basalts contain MgO 3-9 wt.%, SiO₂ 53-62 wt.%, CaO 5-9 wt.%, TiO₂ 0.68-0.94 wt.%. However, their enclaves include MgO 6-8 wt.%, SiO₂ 53-56 wt.%, CaO 8.16-8.85 wt.%, TiO₂ 0.85-1wt.%. Karacadağ enclave bearing andesites and dacites have MgO 1.9-4 wt.%, SiO₂ 58-64 wt.%, CaO 6-8 wt.%, TiO₂ 0.53-0.65 wt.%. In their enclaves, MgO contents range between 4-9 wt.%, SiO₂ values range between 51-59 wt.%, CaO contents are 9-14 wt.%, and TiO₂ values range between 0.56-0.83%wt.%.

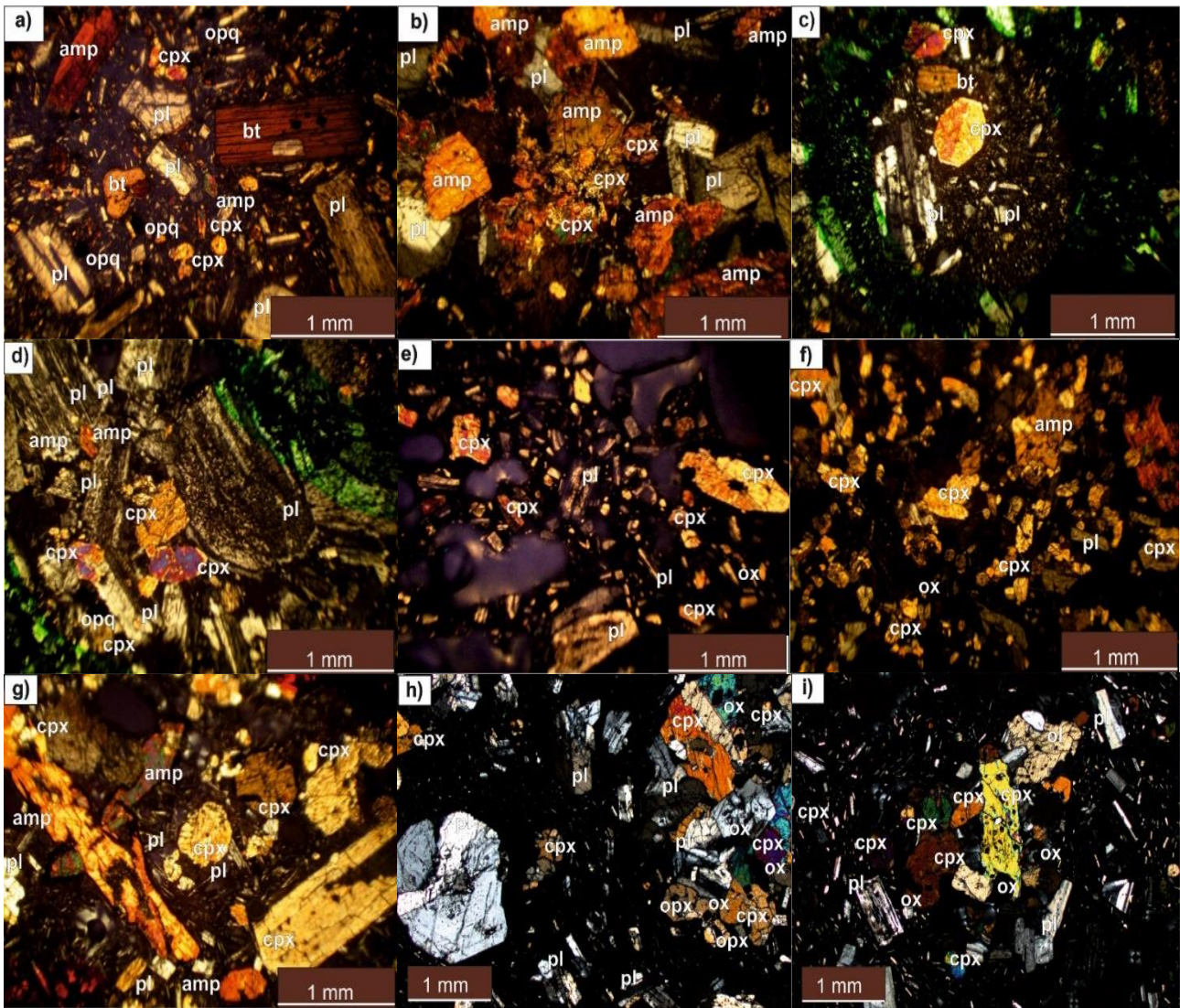


Figure 4. (a) Andesite-1 host rock and (b) its hornblende-gabbro magma segregation enclave with holocrystalline granular texture (Coarse-grained), (c) Andesite-1 host rock and (d) its pyroxene-gabbro magma segregation enclave with holocrystalline granular texture (Coarse-grained), (e) Andesite-1 host rock (vesicular) and (f) its micro-gabbro magma segregation enclave with holocrystalline equigranular texture, and (g) its chilled margins with intersertial texture (fine-grained, also porphyritic), (h) Andesite-3 host rock and (i) its pyroxene-gabbro magma segregation enclave. amph: Amphibole; bi: Biotite; cpx: Clinopyroxene; opx: Orthopyroxene; ox: Fe-Ti oxides; pl: Plagioclase; q: Quartz (Kretz, 1983)

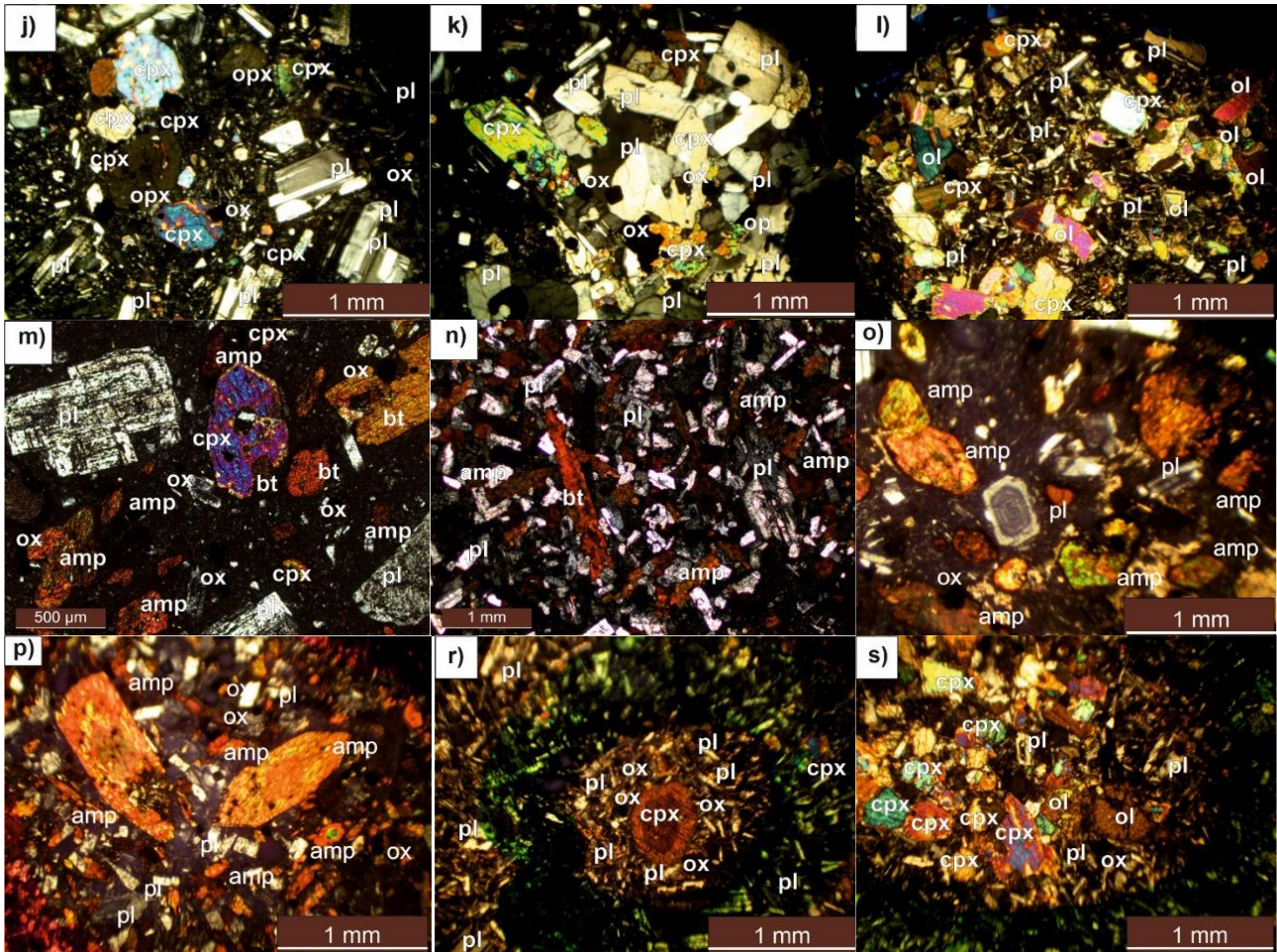


Figure 4.(continued) (j) Andesite-3 host rock (k) pyroxene-gabbro MSE (in Andesite- 3), (l) basaltic MME in the Andesite- 2, (m),(o) Andesite-1 host rock (n), (p) magma mixing enclave with elongated minerals (bladed biotites, quenched amphiboles) in the Andesit-1, (n) magma mixing enclave with elongated minerals and intersertal texture with basaltic composition, (r) basaltic magma mixing enclave in Andesite-2, (s) pyroxene gabbro magma segregation enclave/composite enclave: basaltic MME have enclosed gabbroic magma segregation enclaves

Table 1. Enclaves from the Karapınar-Karacadağ Volcanic Rocks, their main mineralogical contents, and their abundance

KKVR	Enclave Type	Classification	Rock Type (Petrographically)	Composition (Enclave)	Abundance
Karapınar Volcanic Rocks	Type-1	MME	Basalt	ol+cpx+pl+ox	%30
	Type-2	MSE	Basalt, Dunite, Clinopyroxenite, Lherzolite	ol+cpx+pl+ox ol+ox cpx+(rare)ol+pl ol+opx+cpx+ox	%60
	Type-3	Xenolith / Xenocrysts	Xenocrysts of Quartz, Plagioclase, Biotite, Amphibole	q/pl/bi/amph	%10
Karacadağ Volcanic Rocks	Type-4	MSE	Amphibole Gabbro	amph+(rare)cpx+pl+ox	%10
	Type-5	MSE	Pyroxene Gabbro	cpx+pl+ox ±amph±ol	%40
	Type-6	MSE	Micro Gabbro	cpx+pl+ox±amph	%10
	Type-7	MME	Andesite	amph+bi+pl+ox	%25
	Type-8	MME	Basalt	ol+cpx+pl+ox	%15

Table 2. The compositional and textural characteristics of the enclaves and their host rocks from the Karapınar-Karacadağ Volcanic Rocks

Host rock/ Symbole	Mineral composition (Host rock)	Texture	Enclave Type/Symbole	Rock type (Enclave)	Enclave Texture	Boundary/Shape
Dacite/ D	Pl+amph+ox+bi+q ±cpx	Hypocrystalline porphyric, glomeroporphyritic texture, cellular and sieve texture (pl)	1. Magma Segregation Enclaves /MSE	1. Pyroxene Gabbro	1. Holocrystalline granular texture-Coarse grained	1. Sharp contact/ elliptical
Andesite-1/ A1	Pl+cpx+amph+ox±bi ±q±ap±zr	Hypocrystalline porphyric, glomeroporphyritic texture, cellular and sieve texture (pl)	1. Magma Segregation Enclaves /MSE 2.Magma Mixing Enclaves /MME	1.a. Amphibole Gabbro 1.b. Pyroxene Gabbro 1.c. Micro Gabbro 2.Andesite	1. Holocrystalline granular texture-Coarse grained 2. Hypocrystalline porphyric, sieve (pl), quenching (amph)- Fine grained	1.a.b. Sharp contact/ elliptical 1.c. Chilled margin/ elliptical 2. Sharp contact/ elliptical
Andesite-2/ A2	Pl+cpx+opx+amph+ bi+olxe+ox±ap±zr	Hypocrystalline porphyric, spongy cellular and sieve texture (pl)	1. Magma Segregation Enclaves /MSE 2.Magma Mixing Enclaves /MME 3. Composite Enclave /C (in 2)	1.Pyroxene Gabbro 2.Basalt 3. Pyroxene Gabbro	1. Holocrystalline granular texture-Coarse grained 2. Holocrystalline porphyric, intersertal, sieve-cellular texture (plg), quenching (amph)-Fine grained 3. Holocrystalline granular texture	1. Sharp contact /elliptical 2. Sharp contact /elliptical 3. Micro-size enclave
Andesite-3/ A3	Pl+cpx+opx+ox±ap ±zr	Hypocrystalline porphyric, glomeroporphyritic texture, cellular and sieve texture (pl)	1. Magma Segregation Enclaves /MSE	1.Pyroxene Gabbro	1. Holocrystalline granular and Holocrystalline porphyritic texture-Coarse grained	1. Micro-size enclave
Basalt-2/ B2	Ol +cpx +pl +ox (±q xe)	Holocrystalline porphyric, texture- hypocrystalline porphyric, glomeroporphyritic, vesicular, cellular and sieve (pl),ocellar (Q)	1. Magma Segregation Enclaves /MSE 2. Xenocrysts and Xenolith /Xe	1.a. Basalt 2.a. q Xenocrysts 2.b. Quartzite Xenolith fragments	1. Holocrystalline granular texture-Coarse grained 2. Ocellar and embayed (q), sieve-cellular (pl)	1a. Sharp contact/ elliptical 1b. Micro-size enclave 2a. Sharp contact 2b. Micro-size enclave
Basalt-3/ B3	cpx+pl+ol+ox (amp±bi±q±plxe)	Hypocrystalline porphyric, glomeroporphyritic, vesicular, amygdaloidal, cellular and sieve (pl), ocellar (Q)	1. Magma Segregation Enclaves 2.Magma Mixing Enclaves /MME 3.Xenocrysts/Xe 4.Composite Enclave/C (in 2)	1.a. Dunite, lherzolite 1.b. Basalt 2.Basalt 3. Q, pl, bi, amph Xenocrysts 4.a. Dunite 4.b. Q, pl, bi, amph Xenocrysts	1.a Holocrystalline granular texture -Coarse grained 1.b. Holocrystalline granular texture-Coarse grained 2. Hypocrystalline porphyric, intersertal -Fine grained 3. Ocellar and embayed (q), sieve-cellular (pl) 4.a Holocrystalline granular texture 4.b Ocellar and embayed (q), sieve-cellular (pl)	1-3-4. Micro-size enclave 2. Sharp contact/ semi- rounded-angular

amph: Amphibole; ap:Apatite; bi: Biotite; cpx: Clinopyroxene; ol:Olivine; opx: Orthopyroxene; ox: Fe-Ti oxides; pl: Plagioclase; q: Quartz; zr: Zircon (Kretz, 1983)

While, some of the Type-1 (MME) enclaves in the Karapınar basalts appear to be primitive with MgO, CaO, Al₂O₃, TiO₂, Hf, V, Ce, others are more evolved than their hosts. It may be elucidated by the effect of crustal contamination on the evolution of the host rocks. MSE enclaves (Type 4-6) from the Karacadağ andesite and dacites generally contain higher Fe₂O₃, MgO, CaO, Cr, Ni, and lower SiO₂, Al₂O₃, TiO₂, Na₂O, K₂O, Ba, Sr, Pb compared to their host rocks (Supplementary Material 1). Some MMEs (Type-7) from the A1 type rocks include higher SiO₂, Al₂O₃, Fe₂O₃, CaO, TiO₂, La, Ce, Pb, Zr, Y and lower MgO Ni Th, Cr, Nb compared to their hosts. Furthermore, Type-8 enclaves from the marble cake textured A2 type host rocks contain higher Fe₂O₃, MgO, CaO, TiO₂, Cr, Ni, Sr, V lower Ba, La, Ce, Th, Pb,

Zr, Y, Nb than their hosts, and so they are more primitive than their hosts (Supplementary Material 1).

Generally, investigated rocks show enrichment in large ion lithophile elements-LILE (K, Rb and Th) relative to high field strength elements-HFSE (Ta, Nb, Zr, and Hf). Moreover, the Karapınar basalts and the Type-1 enclaves (MME) are in accordance with each other in terms of trace element contents. Although MSEs display much more primitive chemical characteristics than their host rocks, the investigated Karacadağ dacite-andesites and their MSE (Type 4-6) enclaves are in a harmony with each other in MORB normalized (Pearce, 1983) trace element diagrams (Figure 8a, b).

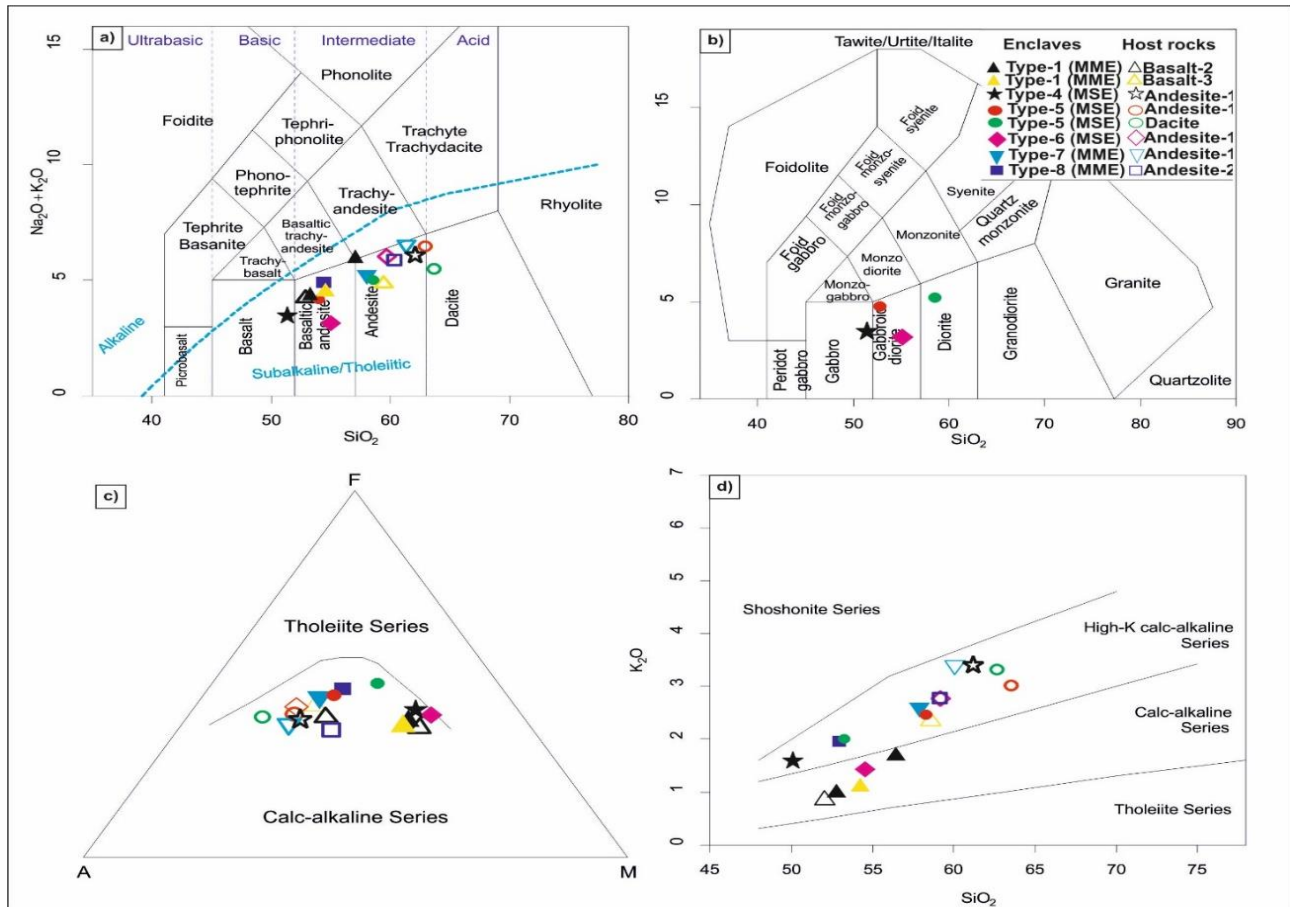


Figure 5. (a) Total alkali-silica (TAS) diagram (Le Bas et al., 1986) of the investigated enclaves and their host rocks, (b) classification of the plutonic rocks (magma segregation enclaves) using the total alkali versus silica (TAS) diagram (Middlemost, 1994), (c) AFM diagram (Irvine and Baragar, 1971) and (d) SiO₂ versus K₂O diagram of the investigated rocks

5. DISCUSSION AND CONCLUSION

Enclaves in the Karapınar volcanites are semi-rounded and angular in shape. However, in the Karacadağ volcanites they are generally ellipsoidal to rounded in shape and rarely display chilled margins, revealing that they were incorporated into their host magmas when they were still in a molten state (Pecerillo, 2005; Poli, 1992).

Bladed biotites, quenched amphiboles, acicular apatites, reverse zoned and sieved plagioclases are widely accepted as evidence of magma mixing processes (Browne et al., 2006; Chappell, 1996; Hibbard, 1991; Kadioğlu and Gülec, 1996). Furthermore, a superheating phenomenon (magma mixing/self-mixing/magma replenishment) may bring about the occurrence of the embayed and ocelli-quartz minerals (Kadioğlu and Zoroğlu, 2008; Kumar and Singh, 2014). Investigated Type-1, 7, and

8 enclaves are fine-grained, and contain elongated, bladed, acicular microphenocrysts of mostly plagioclase, biotite and hornblende crystals like porphyritic enclaves in Unzen (Japan) lavas (Browne et al., 2006). Also some of the Karapınar enclave-bearing basalts include embayed-ocelli quartz minerals. They may be probably the product of rapid cooling due to the temperature differences between the more mafic magma intrusions and more evolved host magma (Browne et al., 2006; Kadioglu and Gülec, 1996; Kumar et al., 2004). Combined with similar mineral contents and mineral chemistry data between the MMEs and their host rocks, we report that the MMEs from the Karapınar Karacadağ Volcanic Rocks were formed by mixing of coeval mafic and more evolved magmas (Zhang et al., 2020). However, Type 2, 4, 5, and 6 enclaves are MSEs and equigranular textured enclaves that stemmed from the more prolonged intrusion of the mafic magma within the host magma (Browne et al., 2006). Some of MSEs have chilled margins at the host rock boundary, and contain some vesicles between microphenocrysts, implying rapid quenching as in Type-6 enclave (Figure 4 g) (Browne et al., 2006). The MSEs, which are observed in almost all of the KKVR, are cognate xenolith due to their textural, mineralogical, and chemical properties. Generally investigated MSEs from the Karacadağ andesites are more primitive than their host rock based on their major oxides and minor- trace elements (Figures 5, 6, 7, 8). It supports that MSEs formed by more primitive magma relative to their hosts, and/or were

early crystallized phases of the same magmatic system. Similar mineralogical and chemical composition between the MSEs and their host rocks indicate that the host rocks and MSEs were derived from a cognate magma related to earlier phases of the volcanism (Özdamar et al., 2020). Hence, they were probably generated by accumulation and segregation of the early crystallized minerals, and then they were transported by plucking from the different parts of the magma chamber. In recent studies, based on the mineral chemistry data of the plagioclase phenocrysts, it was stated that Karapınar basalts contain a significant amount of plagioclase xenocrysts (Gençoğlu Korkmaz and Kurt, 2021).

In addition, petrographical observations reveal that especially Karapınar calc-alkaline basalts include quartz, plagioclase, amphibole, and biotite xenocrysts (Gençoğlu Korkmaz et al., 2022). Therefore, Type-3 enclaves represented by the sieved-plagioclase, ocelli-embayed quartz, biotite and amphibole xenocrysts in the Karapınar basalts are the xenoliths that were plucked from the wall rock during magma arising.

The coexistence of different types and compositions of enclaves in the same host rock may be probably an evidence of repeated/multiple replenishment processes in the magma chamber. Petrographic observations and major-trace element composition of the rocks suggests that the evolution of the Karapınar and Karacadağ volcanic rocks was dominated by fractional crystallization, with magma mixing and assimilation of the wall rocks.

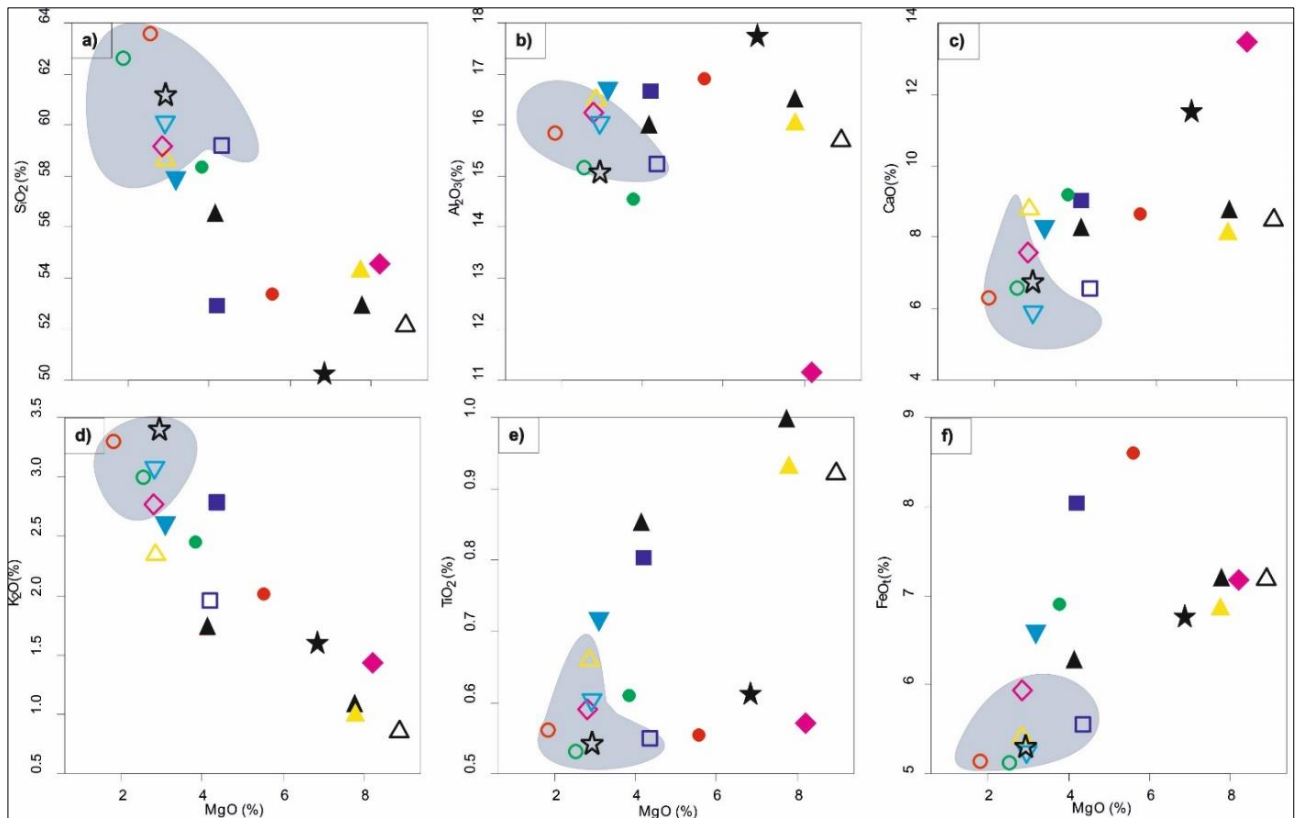


Figure 6. MgO (%wt.) vs. the selected major oxide (%wt.) distribution diagrams of the investigated rocks and their enclaves. The symbols are the same as in Figure 5. Grey-shaded areas represent the general trend of the host rocks

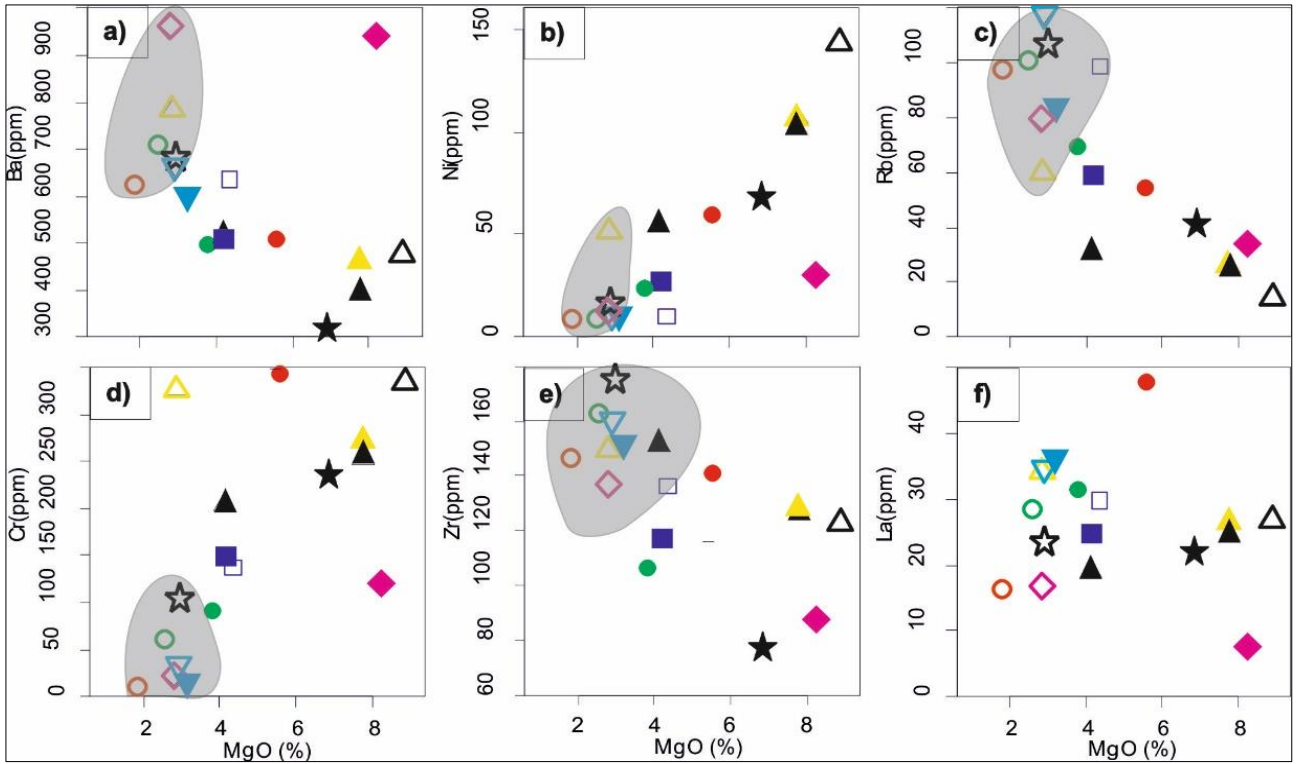


Figure 7. MgO (%wt.) vs. the selected trace element (ppm) distribution diagrams of the investigated rocks and their enclaves. The symbols are the same as in Figure 5. Grey-shaded areas represent the general trend of the host rocks

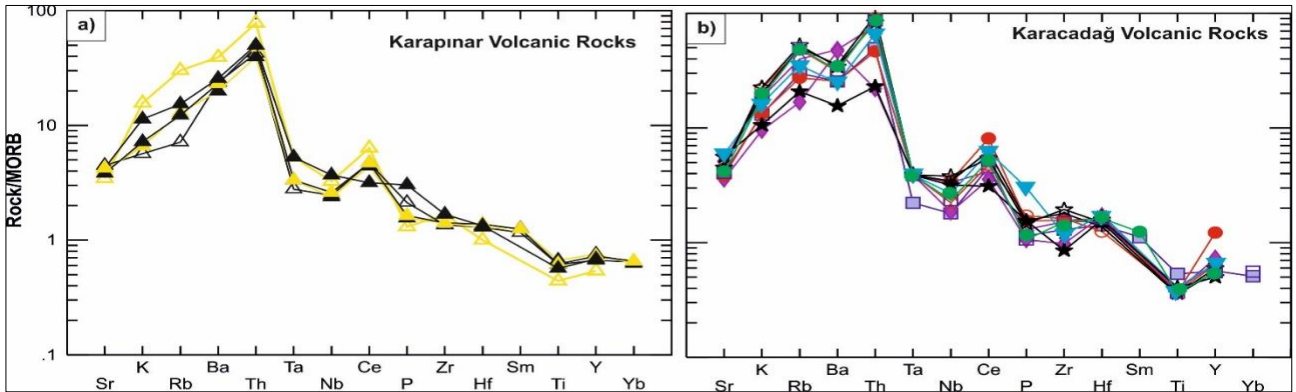


Figure 8. (a)-(b) MORB-normalized (Pearce, 1983) and diagrams of the studied rocks and their enclaves from Karapınar-Karacadağ Volcanic Rocks

Acknowledgement

This study is part of the Ph.D. thesis of the first author and funded by Selçuk University ÖYP project number 2016-ÖYP-041. We thank Prof. Dr. Yusuf Kağan Kadıoğlu and Dr. Kıymet Deniz for realizing the XRF analyses. The authors thank to the Editor Dr. Mustafa Haydar Terzi, and two anonymous reviewers for their critical and constructive comments that improved the quality of this paper.

Author Contributions

The authors conceived all parts of the article together. **Gülin Gençoğlu Korkmaz** and **Kürşad Asan** realized the field study and petrographic

observation, and **Gülin Gençoğlu Korkmaz**, **Hüseyin Kurt** and **Kürşad Asan** evaluated the geochemical analyses results together.

Conflicts of Interest

The authors declare no conflict of interest.

REFERENCES

- Aydar, E., Gündoğdu, N., Bayhan, H., & Gourgau, A. (1994). Kapadokya bölgesinin Kuvaterner yaşlı volkanizmasının volkanik-yapısal ve petrolojik incelenmesi. *TÜBİTAK Yerbilimleri Dergisi*, 3, 25-42.

- Barbarin, B., & Didier, J. (1991). Review of the main hypotheses proposed for the genesis and evolution of mafic microgranular enclaves. In *Enclaves and granite petrology*.
- Barbarin, B., & Didier, J. (1992). Genesis and evolution of mafic microgranular enclaves through various types of interaction between coexisting felsic and mafic magmas. *Earth and Environmental Science Transactions of the Royal Society of Edinburgh*, 83(1-2), 145-153.
- Best, M.G. (2003). *Igneous and metamorphic petrology* (2 ed.): John Wiley & Sons.
- Browne, B. L., Eichelberger, J. C., Patino, L. C., Vogel, T. A., Uto, K., & Hoshizumi, H. (2006). Magma mingling as indicated by texture and Sr/Ba ratios of plagioclase phenocrysts from Unzen volcano, SW Japan. *Journal of Volcanology and Geothermal Research*, 154(1), 103-116.
- Cantagrel, J.M., Didier, J., & Gourgau, A. (1984). Magma mixing: origin of intermediate rocks and "enclaves" from volcanism to plutonism. *Physics of the Earth and Planetary Interiors*, 35(1), 63-76.
- Chappell, B.W. (1996). Magma mixing and the production of compositional variation within granite suites: evidence from the granites of southeastern Australia. *Journal of Petrology*, 37(3), 449-470.
- Chappell, B.W., White, A.J.R., & Wyborn, D. (1987). The importance of residual source material (restite) in granite petrogenesis. *Journal of Petrology*, 28(6), 1111-1138.
- Chen, Y., Chappell, B.W., & White, A.J.R. (1991). Mafic enclaves of some I-type granites of the Palaeozoic Lachlan Fold Belt, southeastern Australia. In *Enclaves and granite petrology* (pp. 113-124).
- Dahlquist, J.A. (2002). Mafic microgranular enclaves: early segregation from metaluminous magma (Sierra de Chepes), Pampean Ranges, NW Argentina. *Journal of South American Earth Sciences*, 15(6), 643-655.
- Di Giuseppe, P., Agostini, S., Manetti, P., Savaşçın, M.Y., & Conticelli, S. (2018). Sub-lithospheric origin of Na-alkaline and calc-alkaline magmas in a post-collisional tectonic regime: Sr-Nd-Pb isotopes in recent monogenetic volcanism of Cappadocia, Central Turkey. *Lithos*, 316-317, 304-322.
- Didier, J. (1973). *Granites and their enclaves: the bearing of enclaves on the origin of granites*.
- Didier, J. (1991). The different types of enclaves in granites-Nomenclature. *Enclaves and granite petrology*, 19-23.
- Dogan-Kulahci, G.D., Temel, A., Gourgau, A., Varol, E., Guillou, H., & Deniel, C. (2018). Contemporaneous alkaline and calc-alkaline series in Central Anatolia (Turkey): Spatio-temporal evolution of a post-collisional Quaternary basaltic volcanism. *Journal of Volcanology and Geothermal Research*, 356, 56-74.
- Ercan, T. (1987). Orta Anadolu'daki senozoyik volkanizması. *Maden Tetkik ve Arama Dergisi*, 107, 119-140.
- Ercan, T., Fujitami, T., Matsuda, J., Tokel, S., & Notsu, K. (1990). Hasandagi-Karacadağ (Orta Anadolu) dolaylarındaki senozoyik yaşlı volkanizmanın kökeni ve evrimi. *Jeomorfoloji Dergisi*, 18, 39-54.
- Gençoğlu Korkmaz, G., & Kurt, H. (2021). Interpretation of the magma chamber processes with the help of Textural Stratigraphy of the Plagioclases (Konya-Central Anatolia). *Avrupa Bilim ve Teknoloji Dergisi* (25), 222-237.
- Gençoğlu Korkmaz, G., Kurt, H., Asan, K., & Leybourne, M. (2022). Ar-Ar Geochronology and Sr-Nd-Pb-O isotopic systematics of the post-collisional Karapınar-Karacadağı volcanic complex (Central Anatolia, Turkey): An alternative model for orogenic geochemical signature in sodic alkali basalts. *Journal of Geosciences* (In press).
- Gençoğlu Korkmaz, G., Kurt, H., Asan, K., & Kadioğlu, Y. (2018). *The first mineralogical and petrographical investigations of enclaves and their host rocks from the Karapınar-Karacadağ area (SE Konya, Turkey)*. Paper presented at the 36th National and the 3rd International Geosciences Congress
- Gill, R. (2010). Igneous rocks and processes: A practical guide. *The Geographical Journal*, 176(4), 375-376.
- Güllü, B., & Kadioğlu, Y.K. (2019). The Petro-chemical properties of Meke and Acigol (Karapınar-Konya) volcanites. *PAU Journal of Engineering Sciences*, 25(3), 325-335.
- Hibbard, M. (1991). Textural anatomy of twelve magma-mixed granitoid systems. *Enclaves and granite petrology*, 431-444.
- İlbeyli, N., & Pearce, J. (2005). Petrogenesis of Igneous Enclaves in Plutonic Rocks of the Central Anatolian Crystalline Complex, Turkey.

- International Geology Review*, 47(10), 1011-1034.
- Irvine, T., & Baragar, W.R.A. (1971). A Guide to the Chemical Classification of the Common Volcanic Rocks. *Canadian Journal of Earth Sciences*, 8(5), 523-548.
- Kadioğlu, Y.K., & Zoroğlu, O. (2008). Nature of Bey pazari Granitoid: Geology and geochemistry, Northwest Anatolia, Turkey. *In IOP Conference Series: Earth and Environmental Science* 2(1), 12-14.
- Kadioglu, Y.K., & Gülec, N. (1996). Mafic microgranular enclaves and interaction between felsic and mafic magmas in the agacoren intrusive suite: evidence from petrographic features and mineral chemistry. *International Geology Review*, 38(9), 854-867.
- Kadioglu, Y.K., & Gülec, N. (1999). Types and genesis of the enclaves in Central Anatolian granitoids. *Geological Journal*, 34, 243-256.
- Keller, J. (1974). Quaternary Maar Volcanism near Karapinar in Central Anatolia. *Symposium on Volcanism and Associated Metallogenesis, Bucharest*.
- Kocak, K., Zedef, V., & Kansun, G. (2011). Magma mixing/mingling in the Eocene Horoz (Nigde) granitoids, Central southern Turkey: evidence from mafic microgranular enclaves. *Mineralogy and Petrology*, 103(1), 149-167.
- Kretz, R. (1983). Symbols for rock-forming minerals. *American Mineralogist*, 68(1-2), 277-279.
- Kumar, S. (2010). Mafic to hybrid microgranular enclaves in the Ladakh batholith, northwest Himalaya: Implications on calc-alkaline magma chamber processes. *Journal of the Geological Society of India*, 76(1), 5-25.
- Kumar, S., Rino, V., & Pal, A.B. (2004). Field Evidence of Magma Mixing from Microgranular Enclaves Hosted in Palaeoproterozoic Malanjkhand Granitoids, Central India. *Gondwana Research*, 7(2), 539-548.
- Kumar, S., & Singh, R.N. (2014). Modelling of magmatic and allied processes. *Springer International Publishing*.
- Le Bas, M.J., Le Maitre, R.W., Streckeisen, A., & Zanettin, B.A. (1986). A Chemical classification of volcanic rocks based on the total alkali-silica diagram. *Journal of petrology*, 27(3), 745-750.
- Maury, R., & Didier, J. (1991). Xenoliths and the role of assimilation. *In Enclaves and granite petrology*.
- Middlemost, E.A. (1994). Naming materials in the magma/igneous rock system. *Earth-Science Reviews*, 37(3-4), 215-224.
- Notsu, K., Fujitani, T., Ui, T., Matsuda, J., & Ercan, T. (1995). Geochemical Features of Collision-Related Volcanic-Rocks in Central and Eastern Anatolia, Turkey. *Journal of Volcanology and Geothermal Research*, 64(3-4), 171-191.
- Noyes, H.J., Frey, F.A., & Wones, D.R. (1983). A tale of two plutons: geochemical evidence bearing on the origin and differentiation of the Red Lake and Eagle Peak plutons, central Sierra Nevada, California. *The Journal of Geology*, 91(5), 487-509.
- Okay, A.I., & Tüysüz, O. (1999). Tethyan sutures of northern Turkey. *Geological Society, London, Special Publications*, 156(1), 475-515.
- Özdamar, Ş., Zou, H., Billor, M.Z., & Hames, W.E. (2021). Petrogenesis of mafic microgranular enclaves (MMEs) in the oligocene-miocene granitoid plutons from northwest Anatolia, Turkey. *Geochemistry*, 81(2).
- Pearce, J. (1983). Role of the sub-continental lithosphere in magma genesis at active continental margin. *Continental Basalts and Mantle Xenoliths*, 230-249.
- Peccerillo, A. (2005). Plio-quaternary volcanism in Italy. New York: Springer-Verlag Berlin Heidelberg.
- Platzman, E.S., Tapirdamaz, C., & Sanver, M. (1998). Neogene anticlockwise rotation of central Anatolia (Turkey): preliminary palaeomagnetic and geochronological results. *Tectonophysics*, 299(1-3), 175-189.
- Poli, G. (1992). Geochemistry of Tuscan Archipelago granitoids, central Italy: the role of hybridization processes in their genesis. *The Journal of Geology*, 100(1), 41-56.
- Reid, M.R., Schleiffarth, W.K., Cosca, M.A., Delph, J.R., Blichert-Toft, J., & Cooper, K.M. (2017). Shallow melting of MORB-like mantle under hot continental lithosphere, Central Anatolia. *Geochemistry, Geophysics, Geosystems*, 18(5), 1866-1888.
- Shelley, D. (1993). *Igneous and Metamorphic Rocks Under the Microscope. Classification, Textures, Microstructures and Mineral Preferred Orientations* (Vol. 130).

Tindle, A.G., & Pearce, J.A. (1983). Assimilation and partial melting of continental crust: evidence from the mineralogy and geochemistry of autoliths and xenoliths. *Lithos*, 16(3), 185-202.

Uslular, G., & Gençaliolu-Kuşcu, G. (2019). Mantle source heterogeneity in monogenetic basaltic systems: A case study of Eğrikuyu monogenetic field (Central Anatolia, Turkey). *Geosphere*, 15(2), 29.

Winter, J.D. (2014). *Principles of Igneous and Metamorphic Petrology*, Pearson New International Edition.

Zhang, G., Peng, R., Qiu, H., Wen, H., Feng, Y., Chen, B., Zhang, L., Liu, S., & Liu T. (2020). Origin of Northeast Fujian Basalts and limitations on the heterogeneity of mantle sources for Cenozoic Alkaline Magmatism across SE China: Evidence from Zircon U-Pb Dating, Petrological, Whole-Rock Geochemical, and Isotopic Studies. *Minerals*, 10(9), 770.

Zhang, S.H., & Zhao, Y. (2017). Cogenetic origin of mafic microgranular enclaves in calc-alkaline granitoids: The Permian plutons in the northern North China Block. *Geosphere*, 13(2), 482-517.



© Author(s) 2021. This work is distributed under <https://creativecommons.org/licenses/by-sa/4.0/>

Supplementary Material 1. Major and trace element contents of the some of the enclaves and their hosts from KKV

Sample	Karapınar Volcanics					Karacadağ Volcanics										GK108H.	GK108E.
	KR28H.	KR28E.	KR21H.	KR21E.	KR21E.2	GK139H.	GK139E.	GK144H.	GK144E.	GK161H.	GK161E.	GK35H.	GK35E.	GK15H.	GK15E.		
Major oxides (%wt.)																	
SiO ₂	58.58	54.24	52.06	52.85	56.49	59.19	54.55	62.65	53.36	63.58	58.33	61.18	50.04	59.15	52.96	60.08	57.9
Al ₂ O ₃	16.48	16.01	15.66	16.49	15.97	16.23	11.07	15.84	16.88	15.16	14.56	15.02	17.73	15.24	16.68	16.07	16.77
Fe ₂ O ₃	5.86	7.49	7.79	7.84	6.8	6.51	7.84	5.63	9.39	5.64	7.59	5.77	7.3	6	8.63	5.69	7.29
MgO	2.86	7.77	8.89	7.78	4.14	2.82	8.23	1.87	5.59	2.55	3.84	2.93	6.85	4.36	4.2	2.91	3.15
CaO	8.75	8.09	8.46	8.72	8.15	7.57	13.48	6.29	8.58	6.55	9.16	6.78	11.59	6.56	9.03	5.89	8.36
Na ₂ O	2.45	3.4	3.34	3.26	4.2	3.21	1.69	3.15	2.06	2.49	2.57	2.62	1.75	2.94	2.86	3.04	2.55
K ₂ O	2.35	1.08	0.85	0.99	1.7	2.77	1.43	3.3	2	2.99	2.45	3.38	1.59	2.78	1.96	3.4	2.62
TiO ₂	0.66	0.93	0.92	1	0.85	0.59	0.57	0.56	0.55	0.53	0.61	0.54	0.61	0.55	0.8	0.6	0.72
P ₂ O ₅	0.16	0.2	0.26	0.19	0.37	0.16	0.13	0.21	0.19	0.19	0.37	0.18	0.19	0.13	0.14	0.17	0.24
MnO	0.1	0.13	0.13	0.13	0.11	0.12	0.17	0.11	0.22	0.11	0.14	0.1	0.11	0.11	0.14	0.11	0.12
Cr ₂ O ₃	0.05	0.04	0.05	0.04	0.03	0	0.02	0	0.05	0.01	0.01	0.02	0.03	0.02	0.02	0.01	0
FeO _t	5.39	6.83	7.17	7.16	6.23	5.94	7.16	5.11	8.62	5.11	6.9	5.3	6.76	5.55	8.04	5.25	6.62
V ₂ O ₅	0.02				0.02	0.03	0.04	0.02	0.02	0.02	0.03	0.03	0.03				
SO ₃	0.27				1.41	0.21	0.16	0.08	0.06	0.07	0.07	0.82	0.33				
Cl	0.03				0.29	0.03	0.02	0.01	0.01	0.04	0.06	0.05	0.06				
Total	98.62	99.38	98.41	99.29	100.52	99.43	99.39	99.73	98.96	99.93	99.8	99.41	98.21	97.84	97.42	97.97	99.71
LOI	1.73	0.3	1.2	0.4	0.33	0.73	0.33	0.32	0.83	0.52	0.42	0.72	0.93	1.9	2.3	1.8	0.63
Trace elements (ppm)																	
Ba	784.7	462	475	397	511.9	964.3	939	620.6	510	707.7	496.9	682.5	311.5	636	508	669	604.6
Ni	51.4	107	143	102	54.5	12.2	30.1	7.1	58	8.4	22.2	16.7	67.9	<20	27	<20	11.6
Co	46.8	33.4	37.8	34.9	72.5	38.4	117	49.4	46.4	56.8	54.1	51.4	46.4	19.5	29	14.7	72.9
Cs	3.9	0.9	0.5	0.7	3.7	3.7	3.8	3.5	5.5	3.8	3.6	3.8	3.5	5.2	2	5.7	
Ga	16	15.9	14.6	15.2	16.3	17.2	15.4	19.8	17.1	19.2	17.1	20.1	19.5	16.6	16.9	16.6	19
Hf	2.4	3.3	3.1	3.1	3.2	3.7	4.1	3	3.9	3.3	4.2	3.6	3.8	3.9	3.4	4.5	5.4
Nb	11.4	9.1	8.6	8.3	12.9	11.7	6.5	7.8	12.1	12	9.4	13.3	11.1	8.2	6.3	9.5	6.5
Rb	60.3	24.5	14.3	25.7	30.7	79.8	33.6	96.6	54.7	100	70.1	105.2	41.6	98.7	60	118.4	84.7
Sn	1.3	<1	<1	<1	1	1.7	1	0.9	1.8	2	3.9	1.8	3.2	<1	<1	<1	1.6
Sr	413.5	457.7	536.6	478.6	508.9	613.3	429.8	532.3	459.9	548.4	707.2	542.4	672.1	485.8	484.1	490.3	641.3
Ta	0.95	0.6	0.5	0.6	0.95	0.7	0.7	0.7	0.7	0.7	0.7	0.7	0.7	0.7	0.4	0.9	1
Th	15.6	9.6	8.5	7.9	10	15.6	4.4	18.2	9.3	19.1	13.2	16.6	4.6	17.3	9.9	20.1	14
U	10.8	2.5	2.3	2	23.2	21.3	15.1	18.3	18	9	20.8	9	13.2	5	3.1	6.3	26.5
V	104.97	125	135	153	10.58	14.05	20.43	13.72	11.87	10.36	19.03	14.39	16.07	152	245	159	17.41
W	31.1	<0.5	<0.5	<0.5	321.8	417.7	672.4	119.2	123.7	235.2	206.6	372	144.3	2.1	1.2	1.9	282.1
Zr	149.6	127.3	122.2	126.3	151	136.9	88.1	145.9	141	162.3	105.4	175.3	76.9	136.3	117.2	160.4	152
Y	16.2	21.7	20	22.6	20.5	19.8	21.9	19.2	36.7	16.7	19.7	17.9	15	16.6	17	18.8	20
La	34.2	26.6	26.8	24.7	19.1	16.8	7.5	16.5	47.8	28.4	31.4	23.1	22	29.8	24.8	34.5	36.5
Ce	63.3	47	47.1	44.1	31.6	41.7	35.6	47.6	81	62.9	62.1	54	31.1	52.1	45.4	62.4	76
Mo	3.1	0.2	1.2	0.3	5.4	12.1	4.3	3.1	6.6	4.2	4	4.2	2.9	0.2	0.7	0.2	6.4
Cu	14.8	24.9	34.3	35.4	35.2	52.2	59.9	30.6	51.7	41.1	69.7	53.6	54.5	44.9	58.4	31.3	127.9
Pb	14.6	2.1	5.9	2.9	9.9	23	12.3	18.4	13.4	23.7	20.6	25.1	12.2	3.1	4	2.5	18.6
Zn	45.2	15	22	23	53.1	56	50.8	44.9	82.3	50.9	56.5	55.3	45.1	26	30	26	60.9
As	0.6	<0.5	1.9	0.8	0.7	2.1	1.3	1.2	0.7	2.6	2.3	3.3	1.9	<0.5	1.4	<0.5	3.6
Cd	0.9	<0.1	<0.1	<0.1	1.7	0.7	0.9	0.8	1.4	0.9	2.8	0.9	0.9	<0.1	<0.1	<0.1	3.3
Sb	0.8	1.1	3.1	2.3	1	0.9	0.9	0.9	1.5	0.9	1	0.9	0.8	1.1	1.4	0.9	1.5
Cr	326.94	253.15	335.25	273.67	205.25	24.29	122.47	7.53	341.41	61.58	90.24	105.36	236.73	136.84	150.52	34.21	8.21

Modelling and assessing the impact of illegal water abstractions by upstream farmers on reservoir performance

Nura Jafar Shanono^{*1,2} , John Ndiritu¹ 

¹University of the Witwatersrand, Faculty of Engineering, Civil and Environmental Engineering, Johannesburg, South Africa

²Bayero University Kano, Faculty of Engineering, Agricultural and Environmental Engineering, Kano, Nigeria

Keywords

Farmers
Illegal water abstraction
Reservoir performance
Reservoir upstream

ABSTRACT

This study proposes a reservoir yield analysis that incorporates the realities of upstream illegal human activities relating to water abstraction. The study assesses the impact of such unlawful human activities on reservoir storage and yields quantitatively. A reservoir operation water balance model was simulated and coupled with upstream irrigation users' propensity to unauthorized water abstraction and set to co-evolve for the entire simulation period. The model was developed using four-state drivers (hydrological state, users' compliance, management competence and reservoir performance). The impact of human behaviour (users' and management) was assessed using 9 plausible human behaviour scenarios. The model was applied to a system of 5 reservoirs using the 90-year historical hydrologic dataset. The trajectories of the storage, yield-demand and storage-yield ratios were analyzed under different human behaviour scenarios. Both storage and yield were found to substantially decrease as users' compliance and management competence deteriorated for the same reservoir hydrological state. Depending on the scenario, the annual yield (%) was observed to reduce from 100 to 80 or 50 or even 30 of the annual demand due to changing behaviour. Also, most of the years in which the yield differs significantly from one scenario to the other are years with shallow storage due to drought. A yield difference of about 23% was recorded between the scenarios without and with the highest unauthorized abstractions. The study, therefore, revealed how human behaviour can significantly affect reservoir storage and yield performances. This highlighted the need to be incorporating the impact of unlawful human activities into yield analysis models to quantitatively assess the impact of human behaviour on reservoir performance.

1. INTRODUCTION

Reservoir storage (Dam) is traditionally considered to be affected by climatic erraticism such as drought (low runoff) and evaporation losses only. These are what have been incorporated in the reservoir analysis to determine system yield capability under climatic uncertainties. However, the impact of human activities that can affect yield, though significant, are typically not explicitly incorporated into reservoir yield analysis. For example, the practice of water abstraction at reservoir upstream has been reportedly linked to the low storage and poor yield performance (van Oel et al., 2008; Shanono, 2019). Van Oel et al. (2008),

revealed a water-scarcity probability of 10% as a result of reservoir upstream water abstraction. In a water-stressed country like South Africa, a water loss of even 1% should not be ignored as stressed by Bhagwan et al. (2014). Therefore, this paper reported the developed reservoir yield analysis model that can evaluate yield due to not only the estimated streamflow data as typically assumed in the yield analysis but the actual flows into the reservoirs. Thus, a socio-hydrological model for quantifying water users' propensity to compliant or unlawful behaviour relating to water use was developed and reported herein. The aim was to account for the water abstractions along the waterways at the reservoir upstream. The vital part

* Corresponding Author

^{*}(njshanono.age@buk.edu.ng) ORCID ID 0000-0002-1731-145X
(john.ndiritu@wits.ac.za) ORCID ID 0000-0001-9092-3172

of this study is, therefore, not just the abstraction, but the ethical questions surrounding the abstraction (lawful or unlawful).

Since lawful water use is usually incorporated in yield analysis (Joshi and Gupta, 2009), this modelling framework captures the causes of the water users' propensity to abstract water illegally. This is a novel approach to yield analysis that incorporated the ethics of water use and management as stressed by Groenfeldt (2013). Such an attempt to incorporate the impact of unlawful water use in the reservoir yield analysis is regarded as a real analysis that considerably minimises unnecessary needless assumptions (Ndiritu, 2005; Shanono et al., 2019). Besides, the outcomes can add value to the reservoir operational decision-making.

The study perceived to incorporate the impact of human behaviour on yield using plausible human behaviour scenarios that assimilated the tendencies for society's norms and values to change. According to Walker et al. (2001), plausible future scenarios that incorporate societal responses dynamically led to robust policies. These scenarios should incorporate the realities of the causes and effects of societal norms and values (behaviour) (Rittel and Webber, 1973; Groenfeldt, 2010). Moreover, it was suggested that reservoir planning and operational decisions should consider the uncertainties of changing water users behaviour (Muller, 2017). Thus, it is crucial to develop a yield analysis model that incorporates the co-evolutionary dynamics between users' behaviour and reservoir operation using the concept of socio-hydrology (Sivapalan et al., 2012). Socio-hydrology is an interdisciplinary area of studying human-water interactions (Montanari, et al., 2013), and recently attracted much attention (Di Baldassarre et al., 2013a, b, 2017; Viglione et al., 2014; Elshafei et al., 2014; Liu et al., 2015). However, studies relating reservoir operation to human behaviour are limited in the socio-hydrological literature. Also, reservoir operation is an essential aspect of South Africa's water management and the impact of unlawful water abstraction cases are significant. Thus, a socio-hydrological model that simulates and couple's reservoir operation and human behaviour using plausible scenarios to assess the impact of users' behaviour on reservoir yield could inform operational decisions. The study was therefore inspired by the need to quantitatively incorporate the impact of illegal water use into reservoir analysis thereby assessing their impact on yield. Such a novel approach to yield analysis is in line with the quest of changing water governance towards the inclusion of the reality of human behavioural impact (Montanari et al., 2013; Muller, 2017). The modelling framework in this study was built such that the level of human behaviour will vary dynamically with the reservoir hydrological state (Shanono, 2020, 2021), thereby estimating the amount of water that could be abstracted illegally at a different level of human behaviour scenarios.

The perceived factors to affect users' risk perception (RP) and water utilization pattern are reservoir hydro-climatic conditions (hydrological state). The model was thus developed using the concept of a stimuli-response system to predict water users' propensity to unlawful water use (users compliance) as explained in the theory of resilience (Forbes et al., 2013). Water managers' expertise and system facilities (management competence) are also conceived to affect the overall system yield (reservoir performance). The model quantitatively and stochastically relates these four-state drivers: i) hydrological state to users' compliance; ii) users' compliance to reservoir performance; iii) reservoir performance to management competence; and iv) management competence to reservoir hydrologic state as shown in Figure 1. This paper does not cover the detailed description and mathematical quantification of the model. It only briefly covers the conceptual basis with which the model was assembled (section 2), model application (section 3), results (section 4) and conclusions (section 5).

2. MODEL DEVELOPMENT

As state earlier, the reservoir operation-human behaviour socio-hydrological model was developed using four-state drivers using a stimuli-response model (black-box). The four building blocks of the coupled socio-hydrological model are briefly described below.

The first model's building block is the hydrological state (HS) which is made up of variables that can affect the storage state of the reservoir (streamflows, rainfall and evaporation). A decrease in reservoir HS is expected to generate concern and increase water users' level of risk perception (RP). According to Kinzig et al. (2013), RP can interrupt and change society's established norms and values (behaviour). Studies revealed RP due to drought increase the rate at which farmers abstract water (Elshafei et al., 2014; Firoz et al., 2017). An increase in RP can therefore drive users to disobey the water allocation rules by abstracting water without authorization. Thus, reservoir HS can affect users' propensity to lawful or unlawful activities. The causal relationships of the state drivers of the coupled model are as presented in Shanono (2021). The study therefore conceived annual relative change of rainfall P , temperature T , and storage S to serve as a surrogate to reservoir HS. Whenever reservoir HS decreases, the users' level of RP will increase and the higher the propensity to illegal water abstraction. The relative annual change in reservoir HS for a long period was computed as the difference between the mean annual value and the annual value and normalized through dividing by the mean annual value of rainfall and temperature. For the storage, the annual value is the storage state at annual decision time (April), and the mean was replaced with a given storage-state-threshold value above which no restrictions are imposed. Also, the

negative sign was, however, assigned to temperature since an increase in temperature is not favourable to the reservoir HS. Also, these 3 variables can have a varied impact, and weights w_p , w_T and w_S are introduced to enable this variability to be effected as shown below. The modelling also further conceived and proposed two situational factors each for users and management which can affect users' level of RP (users' compliance and management competence).

$$HS_t = f([\Delta P].w_p + [\Delta S].w_S - [\Delta T].w_T) \quad (1)$$

The users' compliance (UC) factor is the 2nd building block of the model and was introduced to represent the level of users' willingness and propensity to compliance. Willingness to comply depends on the individual's motives (self-interest or fairness), shaped by some inherent factors (Tenbrunsel and Smith-Crowe, 2008). These factors include trust, knowledge, culture, religion, social well-being and other values that shape individuals moral thinking (Treviño et al., 2006). Studies revealed a positive relationship between society's well-being and ethical practices as in accepting resource sharing policies (Tiliouine et al., 2006). More concern is expected in a less prosperous society due to a perceived threat to their quality of life, and the higher the tendency to illegal activities. The UC was also modelled to change with time in a random fashion due to the erratic nature of human behavior.

The management competence (MC) factor is the 3rd building block of the model and comprised many other factors that affect water managers' performance. It represents the reservoir system's infrastructural development and water managers' expertise, monitoring and law enforcement unit for tackling unlawful activities. This factor aims to represent the water users' perceptions of the level of water allocation effectiveness and water managers' (Url-1). This factor can thus be affected by employees' job satisfaction. When users perceived that the water managers and supply facilities are good enough, the level of RP will reduce. Measurable parameters related to water allocation efficiency can be used as surrogates for this factor. In this study, MC was incorporated into the model dynamically and modelled using the probability density function (PDF). The moment of the distribution was varied to obtain different levels of MC. The annual users' RP was expressed as the function of reservoir HS, users' compliance (UC) and management competence (MC) as shown below. At the beginning of every water year, when $RP \leq 0$; the users' propensity to compliance increases. However, if $RP > 0$; propensity to compliance decreases.

$$RP_t = f(HS, UC, MC) \quad (2)$$

The modelling conceived how users' RP can change users' behavioural intention (BI). The BI is the individual's perceived likelihood to engage in a

particular manner (Ajzen, 1991). A study revealed RP affect individuals' BI thereby eroding compliance behaviour (Gonzalez and Sawicka, 2003). The users' RP-BI was modelled as a stimuli-response system using the logistic (sigmoidal) regression function. Logistic functions are non-linear classification algorithms commonly used to classify and discriminate between two or more probable events (Komarek and Moore, 2005). The BI is therefore referred to as the probability estimate for predicting whether an action will occur. The users' RP function is the input to the logistic function, and hence users' BI is a function of RP using the logistic function as shown below.

$$Users' BI_t = f(Users' RP) \quad (3)$$

The users' BI could lead to unlawful actions, and this depends on two possibilities. Firstly, the range on which the BI fall ($0 \leq BI \leq 1$). If $BI \geq 0.5$, unlawful action may not occur, while if $BI < 0.5$, unlawful action may likely occur. The users' BI is thus a threshold and binary classifier that creates a decision boundary at 0.5 such that lawful and unlawful activities are a set of 0 and 1 respectively. The second possibility for unlawful water use to occur depends on the random factor as it is not certain when the action will occur, and was used as a surrogate to the users' compliance ($0 \leq UC \leq 1.0$). This was reflected using probability distribution and the moment of the distribution was varied to obtain different levels of users' willingness to act ethically. Hence, the occurrence or non-occurrence of illegal water use depending on the users' level of compliance (UC). The UC was also used to change the time step of the model from yearly to monthly. For a year (i) in which the BI_i predicted unlawful water use could occur, then the random variable (UC) was used to randomly specify the month (j) within that year when the unlawful water use occur. Since it is unrealistic to assume that the unlawful abstraction occurs every month as summarized below.

$$If \begin{cases} BI_i \geq 0.5; & \text{Unlawful water abstraction not occur} \\ BI_i < 0.5 \begin{cases} If UC_{i,j} > 2 * BI_i; & \text{Unlawful water abstraction not occur} \\ If UC_{i,j} < 2 * BI_i; & \text{Unlawful water abstraction occur} \end{cases} \end{cases} \quad (4)$$

The users' BI was modelled to determine the possibilities for illegal water use to occur. However, a variable behavioural effect (BE) was introduced to quantify the impact of these actions when they occur (proportion of water abstracted illegally). Also, the users' BE being perceived to vary with the users' RP, availability of the water at users' disposal and time, thus the response model was used to model users' response (BE) to RP and water availability. Response models are used to predict the desired behaviour to act in a specific manner. The widely used response models in ecology are the functional response models, usually used to study predator-prey interplay and are generally classified into Holling's types I, II, and III (Holling, 1959). These models are used to model the intake rate of a predator as a

function of the food density (prey), the rate of the prey-predator encounter and the time is taken before processing the food (Aljetlawi et al., 2004). The RP-BE response was therefore related to when a hungry predator is looking for food. Hence, the magnitude of users' BE due to unlawful water use was related to the level of users' RP, availability of water at users' disposal and time to use the illegally abstracted water. But, the time was simply considered as deterministic due to simulation time steps. The Hollings type II functional response model was found to be suitable to model BE as a function of RP, water availability and simulation time interval as shown below.

$$Users' BE_t = f(RP, Water Availability, Time Interval) \quad (5)$$

The modelling also created a link for assessing the impact of users' BE on reservoir performance by coupling users' BE with the reservoir mass balance variables. This aims to account for the unlawful water use along the streamflows and other waterways. Such a paradigm of yield analysis that accounts for the impact of human behaviour is expected to help minimize unnecessary assumptions in yield analysis. Reservoir storage determines the amount of water to be released, and releases are determined to satisfy demands. In reservoir operation, either the system is capable of satisfying the demand or can only satisfy a portion of the demand. In the latter case, restriction measures are normally implemented, and the extent of these restrictions depend on the storage state, operating rules and the set supply reliabilities. Depending on the level of reservoir hydrological state, users' compliance and management competence, the delivered supply (R_d) may be equal to or less than the allocated supply (R_a). When users' compliant was high and effective management, it is expected that the delivered supply will equal the allocated supply and streamflows into the reservoirs (Q_d) will be as expected (Q_e) without upstream illegal abstraction. Conversely, when the users' tendency to unlawful activities is high and ineffective management, the delivered supply can be less than the allocated supply and streamflows can also reduce due to unlawful abstraction along supply waterways and reservoir upstream respectively. The delivered supply and streamflows to the reservoir are respectively as expressed below.

$$R_d = \begin{cases} R_a & ; \text{If unlawful abstractions are negligible} \\ (1 - BE)R_a & ; \text{If unlawful abstractions are significant} \end{cases} \quad (6)$$

$$Q_d = \begin{cases} Q_e & ; \text{If unlawful abstractions are negligible} \\ (1 - BE)Q_e & ; \text{If unlawful abstractions are significant} \end{cases} \quad (7)$$

Management competence (MC) in rectifying users' BE was modelled and incorporated into the model to serve as feedback (intervention measures). Whenever reservoir performance deteriorates due to BE, the management usually responds using intervention measures. In the field of human

resource management, the normal distribution has been found to fit management performance data accurately (Sarkar et al., 2011). Depending on the employees' work engagement, the normal distribution can skew to right or left indicating ineffective or effective MC. The MC was thus modelled using probability density function (PDF), and the moment of this distribution was varied to obtain different levels of MC. Let MC and 1-MC be interpreted as the probabilities that the system is protected from, and vulnerable to the users' BE. For simplicity, a linear relationship was used to relate how MC suppresses the negative effect of BE on reservoir performance. The BE ($0 \leq BE_t \leq BE_{max}$) for a given level of MC at a particular time ($0 \leq MC_t < 1$) are linearly related as the product of the BE and the probability that the system is vulnerable to the BE ($1 - MC$) as shown below.

$$Actual Users' BE_t = f([BE] * [1 - MC]) \quad (8)$$

3. SIMULATION OF RESERVOIR OPERATION COUPLED WITH USER BEHAVIOURAL EFFECT (BE)

The reservoir operation-human behaviour model was simulated and applied to a hypothetical but realistic system of 5 reservoirs (Olifants River Reservoir System) using a 90-year historical monthly hydrological dataset. The hydrological aspect is thus real while the social aspect (users' tendency to illegally use water) was hypothetically incorporated using scenarios. The mass balance as affected by users' BE at reservoir upstream is described in equation. 1. Also, the total allocated and delivered supplies are as expressed in equations. 2 and 3 respectively.

$$S_{t+1} = \sum_{k=1}^N S_{t,k} + (1 - BE_{t,k})Q_{t,k} - R_{t,k} - NE_{t,k} - SP_{t,k} \quad (9)$$

$$R_a = \sum_{t=1}^T \sum_{k=1}^N R_{t,k} \quad (10)$$

$$R_d = \sum_{t=1}^T \sum_{k=1}^N (1 - BE_{t,k})R_{t,k} \quad (11)$$

Where: S_{t+1} , = total system storage, $S_{t,k}$ = initial storage of reservoir k ; $Q_{t,k}$ = inflow to reservoir k ; $R_{t,k}$ = allocated supply from reservoir k . $BE_{t,k}$ = users' behavioural effect at reservoir k . $NE_{t,k}$ and $SP_{t,k}$ = net evaporation losses and spills out of reservoir k ; R_a and R_d = total allocated and delivered supplies. t = monthly.

Reservoir yield (Y) performance is the 4th building block of the model which is the ratio of the total delivered supplies to the total streamflows into the system for the entire simulation period under various levels of human behaviour scenarios. This aims to identify the extent to which the system is affected for a long period of time due to co-evolving dynamics between unlawful water abstraction and system performance as expressed in equation. 4.

$$Y = \frac{\sum_{i=1}^T \sum_{j=1}^{12} \sum_{k=1}^N Rd_{i,j,k}}{TR} \quad (12)$$

Where: Y = yield, $Rd_{i,j,k}$ = delivered supply in month j of year i for reservoir k . N and T = number of reservoirs in the system and number of years of simulation. TR = total runoff for the entire simulation period.

The human behaviour scenarios were formulated to enable assessment of the impacts of changing users' compliance (UC), management

competence (MC) and hydrological state (HS) on reservoir yield. Nine scenarios are created from different combinations of 3 categories of UC and MC as shown in Table 1. Also, a 90-year historical monthly hydrological dataset was used to reflect the natural variability of HS. The system was also simulated without incorporating the human behaviour scenario as typically assume in yield analysis and used as a reference to the other scenarios.

Table1. Summary of the human behaviour scenarios

SC	3 Levels of Scenario Building-Blocks			Range of values		
	HS	UC	MC	HS	UC	MC
1	Favourable	Lawful	Effective	NV	$0.7 < UC \leq 1.0$	$0.7 < MC \leq 1.0$
2	Moderately favourable	Moderately lawful	Effective		$0.5 \leq UC \leq 0.7$	$0.7 < MC \leq 1.0$
3	Unfavourable	Unlawful	Effective		$UC \leq 0.5$	$0.7 < MC \leq 1.0$
4	Favourable	Lawful	Moderately effective	NV	$0.7 \leq UC \leq 1.0$	$0.5 \leq MC \leq 0.7$
5	Moderately favourable	Moderately lawful	Moderately effective		$0.5 \leq UC \leq 0.7$	$0.5 \leq MC \leq 0.7$
6	Unfavourable	Unlawful	Moderately effective		$UC \leq 0.5$	$0.5 \leq MC \leq 0.7$
7	Favourable	Lawful	Ineffective	NV	$0.7 < UC \leq 1.0$	$MC < 0.5$
8	Moderately favourable	Moderately lawful	Ineffective		$0.5 \leq UC \leq 0.7$	$MC < 0.5$
9	Unfavourable	Unlawful	Ineffective		$UC < 0.5$	$MC < 0.5$
0	Users' behavioural effects (BE) not incorporated					

HS: hydrological state **UC:** users' compliance **MC:** management competence **NV:** depends on natural variability of the hydrologic data **SC:** scenario

4. SIMULATION RESULTS

The result discussion was limited to 3 scenarios: scenario with no BE (nBE – scenario 0), least BE (lBE – scenario 1) and highest BE (hBE – scenario 9) as these provided the needed information on how unauthorized water abstractions at reservoir upstream impacted the reservoir performance. The nBE scenario result was used as a reference to the results of other scenarios with different levels of BE. The trajectories of the storage state, yield/demand ratio and storage-yield trade-off for the 90-year monthly simulated data were analysed. The aim was to dynamically assess the impact of unauthorized water abstractions on storage state and yield, thereby understanding the co-evolving dynamics between unauthorized water abstractions and reservoir performance for a long period. The analysis is presented on an annual basis since the reservoir operation socio-hydrological model incorporates hydrological variables annually. The analysis was also limited to the total storage since it was computed as the weighted linear average of all the 5 reservoirs and hence provides a real picture of the system. Besides, reservoir operating rules consider the state of the total storage before allocating water from any reservoir.

Figure 1 illustrates the trajectories of the annual storage state (%) of the total storage at the beginning of every water year (April). Storage state at the beginning of the water year was chosen as it provides a hint on the proportion of the annual

target draft to be released within that year and the amount of water loss due to illegal use can be traced at different behaviour scenarios. The total storage trajectories were found to differ due to the impact of unlawful abstraction along the streamflows for the nBE, lBE and hBE scenarios. The unlawful use effect was first shown in the 8th year (marked A) in which the total storage state for scenarios 1 and 9 was found to be slightly lower than that of scenario 0. There were about 12 major instances in which unlawful abstractions was found to significantly affect the total storage state (marked A to L). The impact of unlawful abstraction on the storage was found to lasts for 1 to 2 years in case A, B, H, J, K and L and 3 to 5 years in case C, D, E, F, G and I. A total of 25 years were observed to be affected by unlawful water abstraction. Since the simulation is for 90-year data, the major effect of unlawful abstraction on storage can be said to occur once every 8 years (90/12) with 1 year affected in every 4 years (90/25).

Since the reservoir operating rule considers the state of the total storage before allocating water from any reservoir, the overall system yield can therefore be affected by the total storage state. Although, depending on the storage state of a given reservoir and its location within the system, not all the identified incidents can lead to a substantial reduction of water supplies from that reservoir. For example, incidents A, B, C and J in which the difference in the storage state between the nBE and hBE scenarios was not significant, this may not likely

affect the amount of water to be allocated. However, in incident D, the storage state for the nBE and hBE scenarios differs significantly and the annual allocation could reduce from 50% to 30% of the annual target draft. Other similar cases can be spotted at incidents E, F and G in which the annual allocation could reduce from 80% to 50% or even to 30% of the annual target draft. Hence, reservoir yield can reduce whenever massive unlawful water abstraction occurs at the reservoir upstream. Most of the years in which the storage state differs due to changing human behaviour are the years with poor storage state (below 70%). Thus, the model reveals that unlawful abstractions are likely to occur during a poor hydrological state.

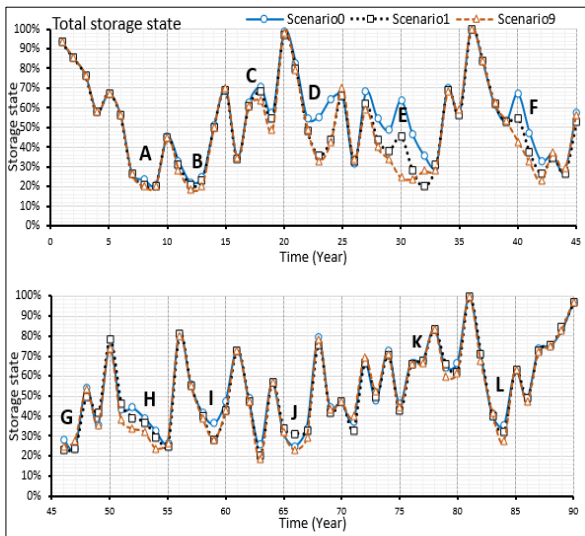


Figure 1 Annual total storage state trajectory for scenarios 0, 1 and 9

Figure 2 shows the trajectories of the total storage state on decision month (April) and the percentage of the annual demand that has been delivered (yield) for scenarios 0, 1 and 9. The aim was to relate annual storage to yield at different scenarios. Most of the years in which the yield found to significantly differ from one scenario to the other are the years with poor storage (droughts), and this agrees with the observation that drought increases water consumption due to perceived risk and threat to their quality of life (Elshafei et al., 2014; Firoz et al., 2017). An excellent example is in the 30th year marked X in which about 89%, 67% and 37% of the total annual target draft were found to be delivered in the nBE, lBE and hBE scenarios respectively. The result indicates that for a given year that experience massive unlawful water abstractions, water supply can drastically reduce to even less than half of the anticipated supply. Although there were very few years in which water supply reductions could occur, there are a considerable number of years in which illegal water abstraction affected the storage and yield substantially. It is therefore crucial for the management to ensure effective compliance by the

users particularly in the years of the poor hydrological state.

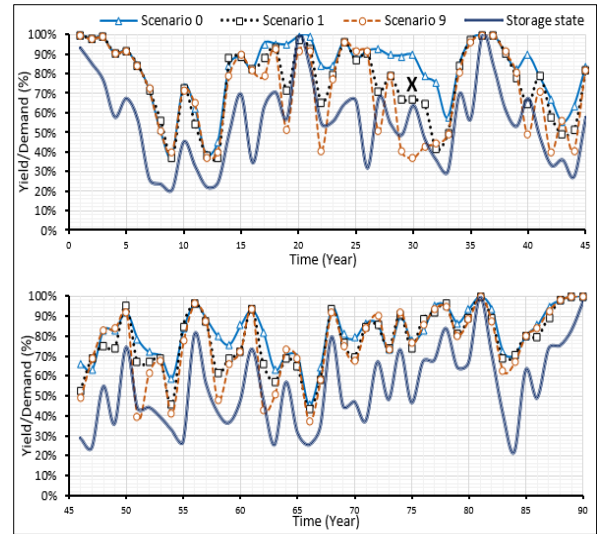


Figure 2: Yield/demand ratio and storage state trajectory for scenarios 0, 1 and 9

Figure 3 shows the total storage volume and yield trajectories of the results obtained from the simulation for scenarios 0, 1 and 9. The aim was to relate and assess how annual yield changes as the annual storage volume change under different human behaviour scenarios. Less water is lost through unlawful abstractions as the storage state improves as all the trend lines tend to join together as the storage volume improves.

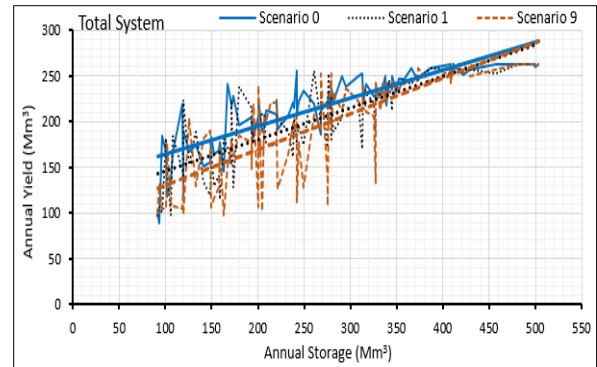


Figure 3: Storage-Yield trade-off as affected by human behaviour

For example, when the total annual storage volume was 150 Mm³, the total system yield for the scenarios with no, least and highest BE (scenario 0, 1 and 9) were 138 Mm³, 119 Mm³ and 106 Mm³ respectively. The calculated reduction in yield was 32 Mm³ (23%) between nBE and hBE scenarios. Whereas, when the total storage volume was 350 Mm³, the total system yield for all the three scenarios was nearly the same (240 Mm³). The total system yield and the storage volume can thus be affected substantially by human behaviour through illegal water use as previously observed.

5. CONCLUSIONS

The study developed a reservoir operation socio-hydrological simulation model that couples and dynamically co-evolves reservoir operation and water users' propensity to unlawful water use. The aim was to get insight into the co-evolving dynamics due to interactions between upstream unauthorized water use and reservoir performance. The trajectories of the storage were analysed at different human behaviour scenarios for 90-year simulated data. The storage was found to be decreasing as human behaviour deteriorated due to unlawful water abstractions. The study revealed that the effect of unlawful abstraction on storage occurred once every 8 years with 1 year affected every 4 years. Also, annual supplies were observed to reduce from 100% to 80% or 50% or even 30% of the annual target draft due to changing behaviour. The analysis revealed that most of the years in which the yield differs significantly from one scenario to the other are years with shallow storage (drought years). A yield difference of about 23% was recorded between the scenarios without and with the highest behavioural effects. Finally, the study demonstrated how human behaviour can significantly affect reservoir storage and yield performance. This stresses the need to be incorporating the realities of unlawful human activities relating to water abstraction into reservoir analysis to quantitatively assess the impact of human behaviour on yield.

Author Contributions

Nura Jafar Shanono: conceptualization, methodology, data generation from the model and writing. **John Ndiritu:** supervision, reviewing and editing.

Conflicts of Interest

The authors declare no conflict of interest.

REFERENCES

- Ajzen, I. (1991). The theory of planned behaviour. *Organizational Behavior and Human Decision Processes*, 50(2), 179–211.
- Aljetlawi, A.A., Sparrevik, E., & Leonardsson, K. (2004). Prey-predator size-dependent functional response: derivation and rescaling to the real world. *Journal of Animal Ecology*, 73(3), 239–252.
- Bhagwan, J., Wegelin, W., McKenzie, R., & Wensley, A. (2014). Counting the lost drops: South Africa's study into non-revenue water. *Water Practice and Technology*, 9(4), 502–508.
- Di Baldassarre, G., Kooy, M., Kemerink, J.S., & Brandimarte, L. (2013a). Towards understanding the dynamic behaviour of floodplains as human-water systems. *Hydrology and Earth System Sciences*, 17(8), 3235–3244.
- Di Baldassarre, G., Viglione, A., Carr, G., Kuil, L., & Salinas, J.L. (2013b). Socio-hydrology: conceptualising human-flood interactions. *Hydrology and Earth System Sciences*, 17(8), 3295–3303.
- Di Baldassarre, Giuliano, Martinez, F., Kalantari, Z., & Viglione, A. (2017). Drought and flood in the Anthropocene: feedback mechanisms in reservoir operation. *Earth System Dynamics*, 8(1), 225–233.
- Elshafei, Y., Sivapalan, M., Tonts, M., & Hipsey, M.R. (2014). A prototype framework for models of socio-hydrology: identification of key feedback loops and parameterisation approach. *Hydrology and Earth System Sciences*, 18(6), 2141–2166.
- Firoz, A.B.M., Nauditt, A., Fink, M., & Ribbe, L. (2017). Quantifying human impacts on hydrological drought using a combined modelling approach in a tropical river basin in Central Vietnam. *Hydrology and Earth System Sciences Discussion*, 22(1), 547–565.
- Forbes, B.C., Fresco, N., Shvidenko, A., Danell, K., & Stuart, F. (2013). Geographic Variations in Anthropogenic Drivers that Influence the Vulnerability and of Social-Ecological Resilience Systems. *AMBIO: A Journal of the Human Environment*, 33(6), 377–382.
- Gonzalez, J.J., & Sawicka, A. (2003). The role of learning and risk perception in compliance. *In Proceedings of the 21st International Conference of the System Dynamics Society*, New York.
- Groenfeldt, D. (2010). The next nexus: Environmental ethics, water management and climate change. *Water Alternatives*, 3(3), 575.
- Groenfeldt, D. (2013). *Water Ethics: A values approach to solving the water crisis* (First Edit). Routledge.
- Holling, C.S. (1959). The components of predation as revealed by a study of small-mammal predation of the European Pine Sawfly1. *The Canadian Entomologist*, 91(5), 293–320.
- Joshi, G.S., & Gupta, K. (2009). A simulation model for the operation of a multipurpose multi-reservoir system for River Narmada, India. *Journal of Hydro-Environment Research*, 3(2), 96–108.
- Kinzig, A.P., Ehrlich, P.R., Alston, L.J., Arrow, K., Barrett, S., Buchman, T.G., ... & Saari, D. (2013).

Social norms and global environmental challenges: the complex interaction of behaviors, values, and policy. *BioScience*, 63(3), 164-175.

- Komarek, P., & Moore, A.W. (2005). Making logistic regression a core data mining tool: A practical investigation of accuracy, speed, and simplicity. *In Institute, Carnegie Mellon University*.
- Liu, D., Tian, F., Lin, M., & Sivapalan, M. (2015). A conceptual socio-hydrological model of the co-evolution of humans and water: a case study of the Tarim River basin, western China. *Hydrology and Earth System Sciences*, 19(2), 1035-1054.
- Montanari, A., Young, G., Savenije, H.H.G., Hughes, D., Wagener, T., Ren, L.L., ... & Z. Balyaev, V. (2013). "Panta Rhei—Everything Flows": Change in hydrology and society-The IAHS Scientific Decade 2013-2022. *Hydrological Sciences Journal*, 58(6), 1256-1275.
- Muller, M. (2017). Understanding the origins of Cape Town's water crisis. *Civil Engineering= Siviele Ingenieurswese*, 2017(5), 11-16.
- Ndiritu, J.G. (2005). Maximising water supply system yield is subject to multiple reliability constraints via simulation-optimisation. *Water SA*, 31(4), 423-434.
- Rittel, H.W.J., & Webber, M.M. (1973). Dilemmas in a general theory of planning. *Policy Sciences*, 4(2), 155-169.
- Sarkar, A., Mukhopadhyay, A.R., & Ghosh, S.K. (2011). Comparison of performance appraisal score: A modified methodology. *Research and Practice in Human Resource Management*, 19(2), 92-100.
- Shanono, N.J. (2019). Assessing the Impact of Human Behaviour on Reservoir System Performance Using Dynamic Co-evolution, *A PhD Thesis Submitted to University of the Witwatersrand, Johannesburg*.
- Shanono, N.J. (2020). Applying the concept of socio-hydrology to assess the impact of human behaviour on water management sectors: A review. *Bayero J.of Eng & Tech*, 15(2), 105-116.
- Shanono, N.J. (2021). Co-evolutionary dynamics of human behaviour and water resource systems performance: a socio-hydrological framework. *Academia Letters*.
- Shanono, N.J., Nasidi, N.M., Maina, M.M., Bello, M.M., Ibrahim, A., Umar, S.I., ... & Putra, U. (2019). Socio-hydrological study of water users' perceptions on the management of irrigation schemes at Tomas irrigation project, Kano, Nigeria. *Nig J. Eng, Sci & TECH*, 5(2), 139-145.
- Sivapalan, M., Savenije, H.H.G., & Blöschl, G. (2012). Socio-hydrology: A new science of people and water. *Hydrological Processes*, 26(8), 1270-1276.
- Tenbrunsel, A.E., & Smith-Crowe, K. (2008). Ethical decision making: where we've been and where we're going. *The Academy of Management Annals*, 2(1), 545-607.
- Tiliouine, H., Cummins, R.A., & Davern, M. (2006). Measuring wellbeing in developing countries: The case of Algeria. *Social indicators research*, 75(1), 1-30.
- Treviño, L.K., Weaver, G.R., & Reynolds, S.J. (2006). Behavioural Ethics in Organizations: A Review. *Journal of Management*, 32(6), 951-990.
- Van Oel, P.R., Krol, M.S., Hoekstra, A.Y., & De Araújo, J.C. (2008). The impact of upstream water abstractions on reservoir yield: The case of the Orós Reservoir in Brazil. *Hydrological Sciences Journal*, 53(4), 857-867.
- Viglione, A., Di, G., Brandimarte, L., Kuil, L., Carr, G., Luis, J., Scolobig, A., & Blöschl, G. (2014). Insights from socio-hydrology modelling on dealing with flood risk-roles of collective memory, risk-taking attitude and trust. *Journal of Hydrology*, 518, 71-82.
- Walker, W.E., Rahman, S.A., & Cave, J. (2001). Adaptive policies, policy analysis, and policy-making. *European Journal of Operational Research*, 128(2), 282-289.
- Url-1:
<http://www.dwa.gov.za/Masibambane/documents/structures/wsslg/may10/WSLG TT Report Version 01.pdf> (last accessed 27 June 2021)

